Dosimetry of Auger Electron Emitters

By

Shahed Khan B.Sc. (Hons), M.Sc.

A Thesis Submitted for the Degree of Masters in Philosophy

At

The University of St. Andrews

St. Andrews

Scotland

September 2001

Contents

Declaration	**ii**
Certification	**iii**
List of Publications and Conferences Attended	**iv**
Acknowledgement	**vi**
Dedication	**vii**
Abstract	**viii**
Table of Contents	**xi**
List of Tables	**xv**
List of Figures	**xvi**
List of Appendices	**xviii**
Preface	**xix**

Declaration

I, Shahed Khan, hereby certify that this thesis, which is approximately 50,000 plus words in length, has been written by me, that it is the record of the work carried out by me that it has not been submitted in a previous application for a higher degree.

Date: 17th June 2003

Signed

Shahed Khan

I was admitted as a candidate for the degree of MPhil in January 1995.

Date: 17th June 2003

Signed

Shahed Khan

Certification

I hereby certify that the candidate has fulfilled the conditions of the Resolution and Regulations appropriate for the degree of M.Phil. at the University of St. Andrews and that the candidate is qualified to submit this thesis in application for that degree.

Date:

Signed

Supervisor

Dr David E Watt

List of Publications and Conferences Attended

Watt DE, Khan S,

'Cross section for the biological effectiveness of electrons in mammalian cells'

Presented at third international symposium on biophysical aspects of Auger processes University of Lund, Sweden. August 1995

Khan S, Watt DE,

'Physical specification of biological effectiveness of electrons from incorporated radionuclides'

Poster presentation P01-15 at 10th ICRR Wurzburg Germany. September 1995

Watt DE, Khan S,

'Cytotoxicity factors for some radiopharmaceutical nuclides'

Presented at 12th symposium on microdosimetry, 29th Oxford, U.K. September 1996

Watt DE, Khan S,

'Unified dosimetry: biological effectiveness of incorporated electron-emitting radionuclides'

Presented at 3rd international symposium of biophysical aspects of Auger processes, University of Lund, Sweden, October 1996

Meetings and Courses Attended

3rd Symposium on Biophysical Aspects of Auger Processes,

University of Lund,

Lund, Sweden. 24-25/8/95 (Funded by Symposium)

10th International Congress on Radiation Research,

Wurzburg,

Germany. 26-27/8/95 (Funded by Congress)

Dose descriptors and their Measurement in Diagnostic Radiology & Nuclear Medicine

British Institute of Radiology Congress,

Birmingham, U.K. 21-23/5/96

12th Symposium on Microdosimetry,

University of Oxford

Oxford. 30/9-4/10/ 96

Progress in Internal Dosimetry and Monitoring for Internal Contamination,

Society of Radiological Protection 22/1/97

Scientific sessions related to radiation physics

British Institute of Radiology Congress

Birmingham, U.K. 19-21/5/97

Nuclear Medicine Dosimetry and other topics

Radiological Society of North America,

Chicago, USA. 28/11-10/12/97

Current issues in radiation protection

Institute of Physics and Engineering in Medicine,

Sheffield Medical School. 22/1/98

Scientific sessions related to radiation physics

British Institute of Radiology Congress,

Birmingham, U.K. 1-3/6/98

Scientific sessions related to radiation physics

British Institute of Radiology Congress,

Birmingham, U.K. 20-23/6/99

Impact of new legislation on Radiation Protection

Society of Radiological Protection. 23/11/99

Acknowledgements

I am very grateful to my supervisor Dr David E Watt for his support, guidance and supervision. I am particularly thankful for his scientific advice and faith in my abilities.

Thanks are also due to my colleagues John, Ian and Juma at the Radiation Biophysics Laboratory for their encouragement.

Dedication

To my father

Abdul Hannan Khan

Abstract

Radionuclides, which decay by electron capture, have important application in nuclear medicine and in therapy by incorporation into cell nuclei. Special problems arise in the dosimetry because of the accompanying Auger electron cascades, which can deposit large specific energies in non-equilibrium conditions. The ability in radiobiological experiments to deliver simultaneously a complex distribution of soft electrons into cell nuclei provides a unique means of exploring radiation damage mechanisms. Guidance is obtained in elucidation of the mechanisms of cell damage by testing the feasibility of unifying the internal action of the Auger emitters with that already established for external irradiation's, for any radiation type.

There are a wide number of radionuclides used in medicine including ^{51}Cr, ^{64}Cu, ^{67}Ga, ^{75}Se, ^{77}Br, ^{99m}Tc, ^{114m}In, ^{124}I, ^{125}I, ^{195m}Pt, these nuclides decay with a shower of electrons, which produce highly localised energy deposition. The use of conventional dosimetry to classify these emitters has been shown to be inadequate see section 3.5. There are fundamental problems with the calculation of radiation doses from internal emitters see section 3.5 and 3.6.

The template model for inactivation of mammalian cells, based on lambda (λ) and the geometrical cross-sectional area (σ) of the deoxyribonucleic acid (DNA), is expressed in equation 2.9. The model is unique as it explicitly allows for many of the known features of cell inactivation: direct effects through, 'λ'; indirect effects due to radicals through the diffusion length (Λ); equilibrium and non-equilibrium charged

particle fluence (φ), important in soft electron irradiations, by use of a range cut-off; approximate repair corrections through the U(Z, t) unrepair function which determines the probability of survival of DNA double-strand breaks (dsb's); the effect of the multiplicity of targets at risk across a mean chord path length, 15 for heavy particles and about unity for Auger electrons; allowance for double track action in the same DNA segment, again of importance for soft electron cascades produced by the Auger emitters but of minor significance for protons and heavier particles; explicit determination of the saturation cross-sections and why these differ from the geometric and allowance for temperature-effects on the radiosensitivity of cell nuclei.

From the interpretation of experimental survival data the main mechanism of radiation damage for inactivation of mammalian cells is attributable to the spacing of physical and chemical interactions along single particle tracks. Optimum damage occurs if the spacing of interactions is 2nm and each interaction coincides with the spacing between the strands of the double-stranded DNA in a template-like action to produce a double-strand break.

The radiation quality is described by the mean free path for linear primary ionization (Lambda, λ) along single charged particle tracks of any type. As the reciprocal of lambda is simply the mean number of interactions per unit track length, each collision corresponds to the zeroth moment of energy transfer. The quality is therefore dependent on a number of events and is unrelated to the amount of energy transfer in the collisions. Consequently, in this type of damage mechanism, *there is no role for absorbed dose*. Two-track action is negligible for heavy charged particles but can be important for electrons.

Good prospects of a satisfactory model for dosimetry on the basis of the above. Data can be unified with external radiations. Bio-effect of Auger's is fundamentally the same as for any other electrons but the fluence is enhanced by the cascade aspect. The radiation quality is determined by the probability that the mean free path for interaction along single tracks is about 2nm. Absorbed dose is not valid. Further work is required, with specifically designed radiobiological experiments, to help decide on the roles of one and two track damage and of the target multiplicity for electrons.

Bismillah

Table of Contents

Preface

Chapter One

Status of Modelling the Effects of Ionising Radiations in Mammalian Cell Nuclei

1.1	Prelude and Objectives	1
1.2	Lambda (λ) the Mean Free Path for Linear Primary Ionisation of Tracks in the Equilibrium Slowing Down Spectra (SLD)	3
1.3	Review of Models	4
1.31	Radiation Damage Mechanisms	4
1.4	Conclusions and Implications from the Current Models of Radiation	15
1.5	Dose is Unnecessary	22
1.6	Dosimetry problems with Auger-electron emitter	25
1.6.1	Assigning Weighting Factors; Theoretical and Experimental Studies of Auger-electron Dosimetry	25
1.7	Deoxyribonucleic Acid (DNA) Damage	30
1.8	Biological Consequences	34
1.9	Therapeutic Potential	37
1.10	Biological Implications of Auger Electrons	39
1.11	Bio-Effectiveness of Radiopharmaceutical Nuclides: the 'Template' Model	40

Chapter Two

Semi-Empirical Modelling of Radiations Action: The 'Template' Model

2.1	**Philosophy of Approach**	**42**
2.2	**Development of the Template Model**	**44**
2.3	**Extraction of the Observed Charged Particle Fluence and Bio-Effect Cross-Sections**	**45**
2.4	**Calculations of Physical Track Structure Parameters: Computer Programs**	**48**
2.4.1	**Quality Parameters Calculated: Monoenergetic Electrons (30ev to 30 MeV); Characteristic Kα X-Rays (Carbon to Uranium); Medical X-rays (50kV to 300kV; 8MV and 26MV Bremsstrahlung); Some β Emitters and Electron-capture Nuclides (Auger electrons, etc. extended in this thesis); γ-ray Spectra (Am-241, Cs-137 and Co-60)**	**52**
2.4.2	**Heavy Charged Particles: 100eV/amu to 1GeV/amu**	**53**
2.4.3	**Neutrons: 100eV to 100MeV (monoenergetic). 2keV; 24keV; 144keV; Cf-252 Spontaneous fission and Am/BE Neutrons**	**53**
2.4.4	**Beta Ray Spectra**	**54**
2.5	**The Radiobiological Database**	**55**
2.6	**Cumulative Probability of Damage**	**59**
2.7	**Delta-Ray Effects and Target Multiplicity**	**62**
2.8	**The 'Template' Model of Radiation Bio-Effetiveness**	**63**
2.9	**Definition of Quantities Used in the 'Template' Model**	**64**
2.10	**For Synchnronised Cells**	**67**
2.11	**For Asynchronised Cells**	**66**

Chapter Three

Auger Electron Emitting Radionuclides and Dosimetry of Internal Emitters

3.1	**Auger Electron Emitting Radionuclides: A Background to the Auger Effect**	**68**
3.2	**The Auger Process**	**69**
3.3	**Auger and Coster Kronig (CK) Electron Energies**	**77**
3.4	**Auger Emitters Used in Medicine**	**79**
3.5	**Current Theory in Internal Dosimetry**	**81**
3.5.1	**Basis for Dosimetry**	**81**
3.5.2	**Structural Organisation of DNA**	**83**
3.5.3	**MIRD Internal Dose Methodology**	**86**
3.5.4	**ICRP Internal Dosimetry**	**88**
3.5.5	**Conventional Dosimetry**	**88**
3.6	**Dosimetry of Auger Emitters**	**90**
3.6.1	**Principles of Current Auger Dosimetry**	**92**
3.6.2	**The Energy Budget in the Auger Effect**	**93**
3.6.3	**Spatial Distribution of Energy Density**	**94**
3.6.4	**Tissue Localisation of Radionuclides**	**95**
3.6.5	**ICRP Quality Factor and Radiation Weighting Factor for Auger Electrons**	**100**

Chapter Four

Application of the Template Model for Auger Electron Emitters

4.0	**Dosimetry of Auger Electron Emitters: Need for Change?**	**105**
4.1	**Introduction**	**105**
4.2	**Probability of Damage by Internal Radio-Nuclides**	**106**
4.3	**Cyto-toxicity Factors**	**107**
4.4	**Determination of Cyto-toxicity Factors for Auger Electron Emitting Radionuclides Incorporated Into Soft Tissue in Equilibrium Concentrations**	**107**
4.5	**Assumptions**	**108**
4.6	**Testing of Validity of Model**	**112**
4.6.1	**Testing of the Model**	**112**
4.7	**Comments on the Available Data**	**120**
4.8	**Several Conclusions Can be Drawn From the Data Obtained**	**122**
4.9	**Limitations of Data**	**124**
4.9.1	**Analysis of Data**	**124**
4.10	**Parameters of Interest for the Model**	**125**
4.11	**Collected/Required Parameters**	**125**
4.12	**Derived Parameters**	**126**
4.13	**Evidence in Support of the Model**	**127**
4.14	**Determination of Slowing Down (SLD) Spectra for Beta Emitters and Characteristic X-Rays as a Preliminary Step in Calculating the Cross-Section and Fluence for Auger Electron Emitters**	**127**
4.15	**Fitting Experimental Data with the Template Model**	**137**
4.15.1	**Correlation Between Bio-Effect Cross-Section and Lambda for Calculated and Experimental Results**	**138**

4.15.2 Assessment of Radiation Quality of Different Radiations on Different Cell Lines from Sparsely Ionising Radiation 140

4.15.3 Hofer's Experimental Results 143

4.15.3.1 General Trends 143

4.15.3.2 Effect of Radioprotectors 145

Chapter Five

Bio-effectiveness of Auger Electron Emitters

5.0 Introduction 152

5.1 Bio-Effect of Auger Electron Emitters 152

5.2 Cyto-toxicity Factors for Collected Data and Specific Cases 154

5.3 Conclusions 163

References **174**

Appendix 1 Calculated Radionuclide Decay Data By Electron Capture for Conversion and Auger Electrons and Characteristic X-Ray and Gamma Ray Decay 183

CD ROM **Program to Calculate Model and Experimental Cross-Sections:**

1) xscel.for, for photons.

2) pelsld.for, for electrons.

3 hcplet.for, for heavy particles.

4) nysp.for; ntlet.for and nynalp.for, for neutrons.

5) bemic.for; betacon.for and betaspec.for; for β radiation.

6) fominc.for

7) Auglsq.for

List of Tables

1.0 Table showing the different intrinsic damage occurring in DNA.

1.1 Table showing the different stages in the processes of biological damage by ionising radiation.

1.2 Table of the historical development of models in predicting radiation damage.

1.3 A representation of the microscopic patterns of radiation tracks corresponding to macroscopic absorption of three different types of radiation.

1.4 Radiation weighting factors associated with different radiation types to show classification of Auger electron emitters.

1.5 The changes in dosimetric terminology over the years from ICRP 26 to 60

3.1 List of the decay modes and half lives of some of the Auger electron emitting radionuclides.

4.1 Table showing the collected and extrapolated survival curve data from various authors and publications related to Auger electron emitters.

5.1 Table of beta decay bio-effect cross-sections, and the bio-effectiveness for 19 beta radionuclides.

5.2 Table of the Bio-effect cross-section for the 16 electron emitting radionuclides.

5.3 Table for the Auger conversion electrons.

List of Figures

1.1 Diagrammatic representation of the various types of DNA damage.

2.1 Plot of the mean spacing of ionisations(nm) and the cumulative probability (ρ), illustrating the 2nm importance.

2.2 Plot of Lambda (λ) and the cross-section for activation, illustrating the importance of 2nm spacing.

2.3 Plot of lambda (λ) and the cross-section compared with the template model predictions.

3.1 Diagrammatic representation of the three types of Auger electron emission.

3.2 Diagrammatic representation of the Auger process in Tin Oxide (SnO_2).

3.3 Relationship between yield as a function of atomic number form different electron shells (K, L_1, L_2, and L_3).

3.4 Diagrammatic representation of the electron levels in an Auger electron emitters.

4.1 Graph showing the primary electron distributions from beta emitters in water, the results having been extended down to 30eV.

4.2 Graph showing the slowing down (SLD) spectra from 19 beta emitters, the results extended down to 30eV

4.3 Graph showing the SLD electron spectra for some of the photon decay EC nuclides. Results have been extended down to 30eV, for Pb-203, Pt-195m, I-125, In-114m, Pd-103, Br-77, Ga-67 and Fe-55.

4.4 Graph showing the SLD electron spectra for some of the photon decay EC nuclides. Results have been extended down to 30eV, for Tl-201, I-131, I-123, In-111, Tc-99m, Se75, Zn65, and Cr51.

4.5 Graph showing the SLD electron spectra for some Auger/conversion electrons from some Auger electron emitters. Results have been extended down to 30eV, for Se-75, Ga-67, Zn65, and Cr51.

4.6 Graph showing the electron spectra for some Auger/conversion electrons from some Auger electron emitters. Results extended down to 30eV, for In-114m, In-111, Pd-103, Tc-99m, Br-77

4.7 Graph showing the electron spectra for some Auger/conversion electrons from some Auger electron emitters. Results extended down to 30eV, for Pb-203, Tl-201, Pt195M, I-131, I-125 and I-12.

4.8 Graph showing the primary electron yield from photon and Compton electrons with the results extended down to 30eV, for Br77, Se75, Ga67, An65, Fe55, Cr51.

4.9 Graph showing the primary electron yield from photon and Compton electrons with the results extended down to 30eV, for I123, In114m, In111, Pd103, Tc99m.

4.10 Graph showing the primary electron yield from photon and Compton electrons with the results extended down to 30eV, for Pb203, Tl201, Pt195m, I131 and I125.

4.11 Graphs showing the photon induced primary electron spectra for I-125 and Br-77.

4.12 Graph showing the equilibrium spectra for I-125 and Br-77..

4.13 Plot of effective cross-section against lambda for V79 cells irradiated with heavy ions and the results of the Auger emitters. Compared to the beta emitters for experimental and calculated data.

4.14 Graph of bio-effect cross-section for the calculated sparsely ionizing radiation along with, the Auger electrons.

4.15 Plot of the effective cross-section against lambda including the experimental results on V79 cells and projected curves for the different ionizing radiations.

4.16 Plot of the effective cross-section against lambda for different sparsely ionizing radiations and the effect on human, hamster and mouse cells.

4.17 Plot of the available data on human, hamster and mouse cells irradiated with sparsely ionizing radiation, plotted for effective cross-section against mean free path (λ lambda).

4.18 Graph of inactivation probability of mammalian cells correlated to the mean free path (lambda) at 37C.

4.19 Graph of inactivation probability of mammalian cells correlated to the mean free path (lambda) at -196C, showing the effect of eliminating indirect action.

4.20 Graph of the surviving fraction and decays per cell showing the effects of radioprotectors compared with Hofer and calculated data for I-125.

4.21 Plot of the experimental (Hofer et al) and calculated survival fraction for I-125.

4.22 Graph of Hofer's experimental data with the model predicted curves for all exposure durations.

4.23 Plot of experimental mean number of double strand breaks (dsb's) in DNA per cell and the calculated mean number of dsb's.

4.24 Graph showing the relationship between the dsb's in DNA against lambda for a wide number of radiation sources including the 16 Auger electron emitters.

5.1 Graph showing the bio-effect cross-section as a function of primary ionization for the 19 beta emitters.

5.2 Graph showing the calculated Cyto-toxicity factors from the 19 beta emitters, C-11 positron and I-131 beta contribution.

5.3 Graph of the bio-effect cross-section as a function of primary ionization for the EC gamma, K, L, M X-rays of the beta emitters.

5.4 Composite graph od bio-effect cross-section for Auger and beta nuclides as a function o f lambda.

5.5 Plot of the calculated cyto-toxicity factors for the Auger electron emitters.

5.6 Graph of yield of lesions per decay as a function of lambda for Auger and conversion electrons.

5.7 Composite graph of the beta and Auger electron emitters for the yield of lesions per decay against lambda.

List of Appendices

Appendix 1 Calculated data for use with Fluence analysis program

Appendix 2 Programs:

1 AUGLSQ.FOR Program for the analysis of survival data including the Auger electron emitters.

2 RADNUC.FOR Program for the analysis of survival data to calculate the cross-section for model and experimental results

3 XCEL.FOR, for photons.

4 PELSLD.FOR, for electrons.

5 HCPLET.FOR, for heavy particles.

6 NYSP.FOR; NTLET.FOR and NYNALP.FOR, for neutrons.

7 BEMIC.FOR; BETACON.FOR and BETASPEC.FOR; for β radiation.

8 FOMINC.FOR Program for the calculation of Cyto-toxicity factors Auger electron emitters.

Preface

Radiopharmaceuticals are used in medicine for both diagnostic and therapy purposes. In the treatment of cancer cells a wide variety of radionuclides are used, the selection depending on; the method of delivery, clinical area of interest, protector in use and the desired dose delivery at the site of interest. The selection appears to be empirically based on experience rather than upon quantitative reasoning.

It is assumed that due to the nature of the decay of Auger electron emitting radionuclides, in particular the shower of electrons that is produced in the proximity of the decay site, there must be very highly localised energy deposition. This is further confirmed by the International Commission on Radiological Protection (ICRP) who allocate a high quality factor of 20 for Auger electron emitting radionuclides. This quality factor is the maximum, similar to that used for alpha particles. The assumptions of the electron shower and the stated quality factor, is assumed to provide a high dose to the cancer cells and in turn results in the high effectiveness for inactivation of these cells by Auger electron emitters.

The quality factor given by ICRP is based more on qualitative parameters. It is the aim here to find a method by which these radionuclides (Auger electron emitting) can be classified quantitatively in terms of merit/cytotoxicity factors, which evolve from a proposed unified scheme for quantifying radiation effectiveness. The latter involves new physical parameters, for expressing the mechanisms of cellular damage, in particular the mean free path and the observed inactivation cross sections for the biological targets of interest, which are demonstrated to be the

Deoxyribonuclease (DNA) molecule, taking into account the cell cycle, repair and efficiency of DNA double strand break (dsb) production.

The method will avoid the general assumption that because an Auger electron emitter produces a shower of electrons, these electrons will be effective in contributing to the inactivation of the cell, which may not be necessarily true. It will also deal with the limitations of conventional dosimetry as far as these radionuclides are concerned.

It is hoped that these merit/cytotoxicity factors will help in the understanding of these radionuclides both in terms of effectiveness for treatment of cancer cells as well as radioprotection requirements. The ultimate aim is to improve the effective use of Auger electron emitting radionuclides in clinical situations for the radiation treatment of cancer tumors.

CHAPTER ONE

Status of Modelling the Effects of Ionising Radiations in Mammalian Cell Nuclei

1.1 Prelude and Objectives.

Many attempts have been made to develop models for the specification of the biological effectiveness of ionising radiations but with only very limited success. Typically the end-points investigated are the survival fractions of irradiated mammalian cells. In the following sections, a critical overview is presented of the main damage models and their limitations, attributed mainly to the use of energy deposition parameters.

During the past decade, researchers in the Radiation Biophysics Group at the University of St. Andrews, have conducted an extensive programme aimed at investigating the relevance of all basic physical track quantities to measurement of the stated radio-biological endpoints of interest. The results lead to proposals in favour of a 'template' model of radiation action. It does not depend on energy deposition but does depend critically on the *spacing* between ionising interactions along single particle tracks and their correlation with radio-sensitive target sizes measured experimentally to be of ~ 2 nanometer dimensions, for external irradiation fields.

The proposed mechanism of radiation action permits absolute measurement of radiation effects to be unified into a single curve for any radiation type, and for the specified biological endpoint, obviating the need for a Relative Biological Effectiveness (RBE). Satisfactory results have already been obtained for

external irradiations with electrons, characteristic X-rays, bremsstrahlung, accelerated heavy charged particles, and neutrons, across the whole energy spectrum. During the past few years the model, designated for convenience as the 'template' model, has been extensively tested for external irradiations of mammalian cells. Based on the findings of the model, radically new instrumentation for *absolute* dosimetry, has been devised and proposed for testing in radiation fields of unknown type [1].

The main objectives of the research work reported in this thesis are:

(A) To confirm that energy based parameters currently used for modelling, cannot adequately describe radiobiological effects. However a fluence-based system of dosimetry (the 'template' model), dependent on the action of single charged particle tracks can be formed to produce a unified system of dosimetry which is independent of radiation type. The quality of the radiation is controlled by the bio-effect cross-section (σ_B) which comprises the geometrical cross-section area for the intrinsic DNA, and the mean free path lambda (λ) for linear primary ionisation, rather than the conventional Relative Biological Effectiveness (RBE) and Linear Energy Transfer (LET).

(B) To extend the 'template' model of radiation bio-effect to accommodate incorporated radionuclides with the objective of demonstrating that the model is a unified one for internal radiation fields of beta rays and incorporated Auger electron emitters and to compare the results where practicable with the results reported for internal and external radiation fields in conventional dosimetry.

(C) To determine cyto-toxicity factors (bio-effectiveness per unit decay concentration) for 19 beta-emitters and 16 electron capture nuclides, some of which pose an unsolved problem for conventional dosimetry, of current interest in nuclear medicine and radiological protection.

1.2 Lambda (λ) the Mean Free Path for Linear Primary Ionisation of Tracks in the Equilibrium Slowing Down Spectrum.

Lambda denotes the mean free path for linear primary ionisation (a zeroth moment of energy transfer). It represents the number and spacing of the initial energy transfer interactions per unit track of electrons in the relevant charged particle equilibrium spectrum. [It should not be confused with the linear primary ionization used by Lea [2] and which is really a specific primary ionization, as used also by Harder [3] and which are volume quantities.]. Therefore it is independent of the magnitude of the energy transfer and hence of the LET and absorbed dose. Use of lambda, avoids the problems associated with these two energy transfer parameters.

Lambda provides the best means of quantifying the quality of ionising radiations of any type into a unified scheme. It is a fundamental parameter, which ensures that Poisson statistics can be taken into account i.e. the stochastic nature of radiation action. There are benefits in the use of Lambda: (a) it allows the generalisation of the effects in terms of cell inactivation by unifying results for all types of ionizing radiation. (b) It allows the possibility of obtaining information on the nature of the radiosensitive targets. If the interaction spacing is correlated to the target size then the degree of damage associated with different lambda allows one to reach conclusions on the nature of the

radiosensitive target. (c) It enables deductions to be made about the critical lesion and its method of production. (d) The method allows the determination of the nature of the radiosensitive targets and whether they have 'single or multi-hit' response. This is related to the fact that the critical lesion separation can be identified by a unique lambda, i.e. for lambda that is greater than the lesion separation the inactivation will be less effective than for a lambda that matches the lesion separation. (e) It permits prediction of the mean number of targets at risk for the passage of radiation through the cell. (f) It can explain the effect of secondary radiation produced by the primary beam, and whether it makes a significant contribution to the damage mechanism. (g) An explanation is obtained as to why Auger-electron emitters may not be as effective as high LET particles (per unit fluence) in causing damage. The mean free path of the Auger electron emitting radionuclide related to the DNA dsb separation would determine the effectiveness of the radionuclide. (h) It can explain the observed onset of saturation of damage from radiation tracks, this being related to the radiosensitive target of interest and the lambda.

1.3 Review of Models.

1.3.1 Radiation Damage Mechanisms.

In trying to identify the mechanism(s) involved in the induction of deleterious biological effect by ionizing radiation, modelling in general has concentrated around the damage to Deoxyribonucleicacid (DNA). The intranuclear DNA of mammalian cells has been demonstrated to be the dominant radiosensitive sites and the key lesions are single and double-strand breaks in the DNA. There are several reasons for this. Some of these reasons include: (a) For simpler organisms, such as bacteriophages and viruses, a quantitative relationship

between the damage to DNA and biological function can be established. Direct measurement of single-strand breaks in organisms with single-stranded DNA and measurements of double-stranded DNA, precisely correlate with biological inactivation; (b) For higher organisms, the relationship between DNA damage and loss of biological function is not as easy to establish quantitatively due to the complexity. However, loss of function has been shown to correlate with double-strand breaks in DNA: (c) The repair of DNA damage has been shown in many organisms to relate closely to cell survival as measured by the ability of the cell to divide: (d) Cells that lack the ability to repair DNA as a result of an inherited genetic defect are found to be more sensitive to radiation exposure than the normal phenotypes: (e) Chemical agents that are known to block the repair of DNA damage increase the sensitivity of cells to irradiation: (f) DNA is the largest molecule in the cell. At doses which cause a cell line to lose its ability to further divide, it is highly unlikely that extensive or significant damage can be attributed to the smaller molecules in the cell.

The expressions of these molecular lesions at the biological level cause the cell to lose the ability to carry out normal DNA replication and cell division. There is no doubt that a single radiation track, traversing through one living cell, can cause an irreparable double strand break in a DNA molecule and hence initiate the development of cancer. However, we are all subject to environmental and naturally occurring internal radiation at all times and we are not all developing induced cancer. The naturally occurring changes in DNA are shown in Table 1.0. DNA damage of importance in radiogenic diseases occurs at a high rate naturally even in the absence of radiation exposure (Table 1.0). Small doses of radiation (10-100 mGy) increase the spontaneous background rate by a small

fraction of 1 %, essentially contributing an insignificant increase to the DNA damage which occurs naturally.

Table 1.0 Intrinsic DNA Damage

Type of Event	Rate of Spontaneous DNA Events Per Day Per Cell	DNA Damage Per 10 mGy Per Cell [4]	% of Daily Spontaneous Rate
Single-strand breaks	121,000	10	0.008
Double-strand breaks	36,000	0.4	0.001
Base lesions	30,000	9.5	0.03
Total events	187,000	20	0.01

Damage to mammalian cells by ionising radiation is generally considered to arise from two sources, the direct effect and indirect effect. The pre-cursors to biological damage by ionising radiation are shown in Table 1.1.

Table 1.1 Pre-cursor to biological damage by ionising radiation

Stage of Process	Time scale of Action	Relevant Phenomena
Physical absorption of particle tracks	10^{-13}s	Energy absorption directly and indirectly in bio-molecules.
Physico-chemical stage	10^{-10}s	Formation of primary lesions and diffusing radicals by re-arrangement of excited and ionised molecules.
Chemical stage	10^{-6}s	Intramolecular energy transfer; reaction with bio-molecules; production of bio-radicals; molecular alterations.
Biological stage	Seconds-Years-Next Generation	Can cause: cell death; chromosome aberrations; mutations; oncogenic transformation; acute radiation sickness; death or organism; hereditary consequences.

Damage by direct effect originates from energy deposited by ionising collisions in the Dioxyribonucleicacid (DNA) molecule, it being considered the critical target.

Damage by indirect effect arises from attack on the DNA by diffusing radical species generated in other molecules, e.g. water molecules, due to excitations in the vicinity of tracks of charged particles. The major source of the indirect effect is the free radicals produced from water. Within the cell are two classes of water to consider: bound water and solvent water. Ionisation of all water molecules forms H20+; however, such a species produced from a bound water molecule may react with the molecule to which it is bound before it can undergo the conversion to an off-radical - the reaction of salient water cation radicals. The reaction of a cation water radical with DNA could produce a cation DNA radical and it is possible that this could result in a different radiation product, although it is possible that products from cationic species and off-radicals are the same.

Reactions of radicals formed from bound water it may not be possible to prevent them from reacting with the DNA by the use of scavengers. This type of damage cannot properly be described as being caused by the indirect effect.
The importance of water in biological radiation damage was shown initially by Powers [5] who showed that water could markedly increase the radiation response of living systems, using the bacterial spore as a model. Powers and his co-workers showed that there are three water compartments that are significant in the radiosensitivity of the spore. These compartments interact with oxygen and with other sensitisors and protectors. In this system the ionisation of water

to radiosensitivity is found to be complex. Therefore the situation could be expected to be even more complex in mammalian cells because of the manner in which DNA is packaged.

There is very little evidence to indicate that indirect action is as significant as direct action and generally it is difficult to distinguish between the two for densely ionising radiations. It is possible that indirect effects dominate for low-LET radiation but the reverse is found.

There are many models of radiation action, based mainly on energy deposition quantities such as absorbed dose and RBE, but as yet there is no generally accepted mechanism of action that adequately explains the resulting damage. The methods employed so far have been to define suitable physical parameters to describe the 'radiation quality' which will enable the effectiveness of different radiation types to be additive. At the present time, RBE is used as a relative quality parameter.

Most radiobiological theory is based on the cell survival curve. The cell survival curve describes the relationship between the fractional survival of a population of radiated cells and the dose of radiation to which the cells are exposed. Biological cell survival data whether for micro-organisms or mammalian cells are generally describable by two types of relationship, either the exponential survival curve or the shouldered (sigmoid) survival curve.

The models in use today have all had only very limited success. Indeed, arguments can be made that there is something fundamentally wrong with the

use of energy deposition for quality specification. There are other indicators that this may be so e.g. the finding that particles of the same type, the same LET_w (on either side of the stopping power maximum, the low energy side has a significant component of quasi-elastic nuclear scattering) may induce damage which differ by factors of 2 or 3, Dertinger [6].

Typically models are derived from presumed quantities and then compared with experiment. None of these have had any real degree of success at predicting biological effects, except possibly the Katz [7] model which attempts to unify data for different radiation and target types but, again in common with many models, contains arbitrary fitting parameters which have unacceptable magnitudes.

Various models have been created to describe the action of radiation. The development of models for the classification of radiation damage is listed in Table 1.2 to serve as an introduction to a proposed new model for the bio-effectiveness of ionising radiations, including electron capture nuclides and which are discussed in detail in Chapter 2 of this thesis.

Table 1.2 Table of the history of approach to radiation damage modelling

Authors/ Appllication	Date	Formulation	Category	Principles/Comment
Dessaur, Shape of survival curves	1922 et seq.	$F = e^{-h}$; $h = V.D$	Statistical 'hit' theory	Poisson probability of surviving 'h' energy absorption events. Replicates shapes of some dose-effect curves
Crowther,	1924 et seq.	$F_{1,m} = 1 - (1-F_{1,1})^m$	Hit and target theory sensitive volume from dose-effect	Well-defined hit and target. Replicates shape of some survival curves.
Holweck and Lacassagne Kolweck, Target sizes via irradiation.	1930 1938.	$V = - \ln (F) / D$	Statistical ultra-micrometry.	Measures radiosensitive volume for single hit inactivation.
Lea. Cell survival.	1940	$N_h = \pi d^3 / 6F$ N_h is the mean hit number. F is an overlap factor and 1/F is the mean hits per target.	Target theory; track structure.	Utilises associated volume due to delta rays, treated as separate tracks; mean chord distribution through spheres. Quality is the mean free path for primary ionisation clusters. Corrects for saturation.

Table 1.2 continued.

Authors/ Appllication	Date	Formulation	Category	Principles/Comment
Dessaur, Shape of survival curves	1922 et seq.	$F = e^{-h}$; $h = V.D$	Statistical 'hit' theory	Poisson probability of surviving 'h' energy absorption events. Replicates shapes of some dose-effect curves
Lea. Chromosome aberrations.	1946	$N = \varsigma \cdot l \cdot \tau \cdot (1 - e^{-T/\tau}) \cdot (e^{-T/\tau})$ T is the irradiation time, τ is the mean repair time, $\varsigma \cdot l$ is the dose rate. The yield of lesions, $\propto$ n2, is: $Y = 0.5 \cdot \varsigma \cdot k \cdot \tau \cdot D2 \cdot G$ G is the repair term.	Target theory; track structure.	As above but allows for repair. Chromosome breaks are due to direct lesions and paired interactions of sub-lesions.
Neary Chromosome aberrations; RBE and (cell survival).	1965	$Y = f \cdot n$ Track properties; geometrical properties of chromosome structure	Dual action.	Primary damage to a macromolecule (DNA) is direct effect of a single energy-loss event. Chromosome damage is due to intratrack (high LET) or intertrack (low LET) action (primary lesion) in two separate sections of a chromosome.

Table 1.2 Continued

Authors/ Appllication	Date	Formulation	Category	Principles/Comment
Harder Chromosome aberrations.	1984	The generalised lesion interaction rate: $\varepsilon(t) = f \cdot n$ of the interaction efficiency, the relative variance of the primary ionisation density and the repair weighted dose rate in quadratic form.	Dual action. Pairwise lesion interaction in chromatin.	Advances Lea's model using principles of microdosimetry. Dose-rate dependent. Quality, the relative variance of primary ionisation density, is proportional to LD, 100.
Katz Cell survival	1972, 1987.	$F_D = e^{-hi} \cdot [1 - (1 - e^{hg})^m]$ $hi = \sigma \cdot \Phi;$ $hg = (1 - (1 - e^{-hl})^m) \cdot \varepsilon_D / \varepsilon_{\gamma,o}$ $hL = \varepsilon_L / \varepsilon_{\gamma,o}$	Two-component model for heavy ions.	Effects of the delta-ray penumbra, separated by a novel procedure from the primary ion track core, are allocated the radiosensitivity of Co^{60} gamma rays. They have single-hit, multi target action. Cross-sections are used to characterise the track core action.
Curtis Cell survival; DNA breaks	1986	$S = [-a \cdot D + \varepsilon \cdot \ln(1+bD)$ $A = -(\eta_L + \eta_{PL})$ $B = \eta_{PL} \cdot [1 - \exp(-\varepsilon_{PL} \cdot t_r)] / \varepsilon$	Repairable / irrepairable lesions.	Lethal-potentially lethal repairable damage depending on intitial severity. Fast and slow repair included. Model gives linear quadratic survival at low doses and low LET. Tends to exponential at high doses.

Table 1.2 continued

Authors/ Appllication	Date	Formulation	Category	Principles/Comment
Chaterjee and Holley DNA breaks.	1991	$\sigma_{ssb} = a \cdot L \cdot [(f_{core} / D^{core}_{37}) + (1 - f_{core}) / D^{pen}_{37}]$ f = fraction of energy deposited in core penumbra. L is LET.	Delta-ray track structure; structural chemistry; Monte-Carlo methods.	Double strand breaks in DNA are assumed to be the critical lesion relevant to cell death transformations and mutations. Damage is attributed to direct (excitation, ionisation) and indirect effects-diffusing water radicals.
Chadwick, Leenhouts DNA strand-breaks. Cell survival	1973 1981	$N_{dsb} = N_{1,1} + N_{1,2}$ Single track: $N_{1,1} = \alpha \cdot D$ Two track: $N_{1,2} = \beta \cdot D^2$ $N_{1,1} = 2 \cdot \mu \cdot k \cdot \Omega \cdot k \cdot D$ $N_{1,2} = 2 \cdot n \cdot \mu \cdot k \cdot (1-\Omega \cdot k) \cdot n_1 \cdot \mu_1 \cdot k_1 \cdot D^2 / 2$	Dual action model.	α Component is independent of particle type. β Component is quality dependent.
Kellerer and Rossi. Cell survival	1972 1978	$\varepsilon(D) = k \cdot (\zeta \cdot D + D^2)$ $k = f \cdot n (\int g(x) \cdot s(x) \cdot dx)$ ζ = dose average spectral energy density	Dual action microdosimetry.	Generalised 'distance' model. Intratrack action dominates at low doses and intertrack action at high doses.
Günther and Schultz. RBE	1983		Microdosimetry	

Table 1.2 continued

Authors/ Appllication	Date	Formulation	Category	Principles/Comment
Yamaguchi and Waker Cell survival	1982	$L_P = 2 \cdot k \cdot v \cdot L^2 / (L_0 - L)^2 + (2kL)^2$; $\varepsilon_p = l_P \cdot D$	Resonance action; microdosimetry	Resonance assumed between the spatial distribution of ionisation clusters (dose) and critical elements in the biological system.
Cannel and Watt Cell survival; lesion yield.	1984	$F = \exp [- (\alpha D + \beta D^2)]$ $\alpha = a \cdot (1 + c \cdot f(L))$ $\beta = [b \cdot (1-f(L))]^2$ $f(L) = \exp [- (1-L)^2 / \varepsilon^2] / \int \pi \cdot \varepsilon$ ε is the width of the distribution. L normalised to 180 keV/μm	Dual action; resonance in quality; sub-lesion interaction.	Resonance between spacing of linear primary ionisation and average distance between critical sites for sub-lesions. Quality dependence of f(L) is a delta function. Both α and β are quality dependent.
Sedlack Cell survival	1988		Dual action; microdosimetry	
Bond and Varma Cell survival	1981 1987		Hit theory, microdosimetry.	A 'hit-size effectiveness' theory dependent on cumulative damage, which is effective when it exceeds a defined threshold.

1.4 Conclusions and Implications from the Current Models of Radiation

There are several important assumptions, which form the basis for most mathematical models listed in Table 1.3 in describing loss of clonogenic potential from radiation. A critique is made below, viz.

The killing of a cell (loss of its reproductive capacity or clonogenic killing) is the result of a multistep process.

The absorption of energy in some critical volume (or volumes) in the cell is the necessary first step.

The deposition of energy as ionisation or excitation in the critical volume will lead to the production of molecular lesions in the cell. Therefore more importance must be attached to the quality of the radiation that causes damage rather than to the radiation type. Hence it is important to review the current thoughts on radiation quantities with respect to protection, i.e., RBE, LET, LNT and Dose. Unfortunately, due to the practical needs in radiological protection legislation, it will be difficult to introduce changes in the system despite the scientific proposals.

The models assume that lesions are produced from the energy transferred at a site. This may not be the case and there is very little evidence that this is in fact true.

The models described have progressed over a period of time and have been adapted to include new developments and knowledge of the action of radiations.

The importance of irradiation time, LET, repair rates, (some of the models assume that the sensitivity of the irradiated material remains constant throughout the irradiation) and other subtle aspects of exposure have been brought to attention.

Unfortunately due to the strong support of dose and absorbed dose along with LET as the descriptors of damage, it has been difficult for other models to be established, mainly due to the general acceptance of these concepts and the apparent simplicity of use, irrespective of the fundamental flaws. However, no attempt has been made to incorporate the quality of radiation in terms of fundamental parameter(s) of the radiation. The molecular model of Chadwick and Leenhoute introduces the parameter Δ, a way of characterising the quality of radiation, but is not developed. The common parameter used throughout is absorbed dose. This is known to be a bad indicator of biological effect.

These models have tried to provide a generalised explanation of the interaction of radiation and the biophysical mechanisms. In generalising, compromises have been made with respect to critical lesions, the stage in the cell cycle, and radiosensitivity of cells. Also knowing that DNA double strand breaks are the critical lesions it is important to consider the spatial distribution and probability of interaction with the double strands when determining the accuracy and realistic nature of the model with respect to damage to mammalian cells.

Bond and Varma [8] in their hit-size effectiveness model have taken into account a critical volume without a specific target. They consider the passage of a particle track through the volume, which is assumed to contain the

radiosensitive target and each time a hit occurs the energy transferred in a stochastic manner may induce the biological endpoint if the threshold energy is exceeded. The model for practical reasons assigns a weighting factor for the low dose biological effects.

Again as with the other models the main basis of the Bond and Varma's model is that the quantity of energy transferred to the critical volume that determines the biological effect and has little to do with the quality of the radiation other than the energy. Several authors including Simmons [9] and Katz [7] have criticised this on the grounds that it does not correlate with data obtained from heavy charged particles and cell survival data respectively.

Use of the wide range of concepts defining quality parameters including; specific primary ionisation by Lea [2], dose restricted LET by Harder [3] and ionisation per unit track by Katz [7] and the microdosimetric parameters mentioned previously, along with the arbitrary constants used in the different models, have made the understanding of the mechanisms of radiation action on mammalian cells difficult to unify.

Recommendations of the ICRP [10] have developed from 1928 to the present day. Initially aiming to protect from deterministic effects, the concerns of genetic effects have over that period taken smaller role. The Linear No Threshold Theory (LNT) introduced in 1966 was a precautionary principle but appears to have gained prominence over the later years due mainly to public concern along with the media influence. However developments in radiation biology indicates that a fundamental theory of radiation damage does not exist

and alternative developments correlating dose-response vary widely from that proposed by LNT. This is particularly true for the case of low dose effects. It is clear that these recommendations have not changed significantly since 1928 despite the fact that our understanding in radiobiology has improved considerably over that period of time.

The models currently used are based on the concept that radiation induced cancer occur clonally from cells directly damaged by radiation, with genomic DNA being the critical target. The damage directly or indirectly caused to DNA by ionising events being the main cause in carcinogenic effects. It should be noted that much of this type of damage is indistinguishable from the spontaneous processes in DNA. Although the concept of double strand damage is required for both mutation and cell sterilisation their radiation quality has not been defined, i.e., what is it about the interacting radiation that is needed to cause that double strand break?

There is considerable debate about the role of bystander effects or the induction of radiation-induced genomic instability. Without quantification and determining the fundamental quality of the radiation that causes damage the question of mechanism for the mutation and death of cells is difficult and open to discussion.

The radiation quality definition along with the LNT theory in use today is based primarily on the cautionary side and because they have become the standard whether it be satisfactory or not. The quality of radiation defined today falls in the general category of 'dose', which is characterised by Relative Biological

Effectiveness (RBE), with the parameter most used being Linear Energy Transfer (LET).

The use of LET has several well known problems including: (a) It is assumed that charged particles expend their energy continuously and uniformly along tracks of negligible diameter and curvature. This assumption is consistent with the continual slowing down approximation (CSDA) but this is usually small in the case of low-LET radiation as the tracks of the secondary electrons can be markedly curved. This occurs at the end of their range when the curvature is so pronounced that the radius of curvature becomes similar to the interaction mean free path. (b) They do not take into account the fluctuations of range straggling and energy straggling that occurs within sensitive sites with dimensions in the order of microns or less e.g. 2nanometer. Fluctuations in the number of particles that penetrate a sensitive structure that are irradiated to a given dose are also unaccounted for. (c) The type of energy transfer process may be of importance but this is not expressed in the LET concept. Nuclear elastic collisions may have a differing damaging effectiveness compared with that for purely ionising collisions. (d) Restricted LET is an improvement but the value of cut-off is arbitrary, usually at 100 eV. There is much debate concerning validity.

The description of the quality of radiation in terms of LET provides an average of the rate of energy deposition at the micron level. However, energy deposition events occur in molecular systems at the nanometer level by processes not completely understood even in homogenous media. The molecular and atomic heterogeneity of biological systems adds an extra dimension of complexity.

Because of the limitations of LET, Rossi [11] suggested an alternative parameter - one that is directly related to energy deposited by individually charged particles and their secondaries in volumes of specified size. The assumption is that these volumes are spherical. Each deposition of energy within the sphere is termed an event and the event size, Y, is defined as Ey divided by d where d is the diameter of the sphere. Since LET is not constant in describing the quality, the diameter is specified i.e. P (Y0.5) represents that an event will have value Y in spheres of diameter 0.5μm. This is the subject of microdosimetry founded over 50 years ago [11].

The 1928 definition says 'quantity of radiation' but does not give any name for this quantity. However the 1937 definition reads 'quantity of dose of X or γ-radiation'. This implies that 'dose' is the name of the quantity for which 'roentgen' is the unit even though ICRU [12] did not intend this. Any attempt to compare radiations of different 'quality' requires the use of a micro/nano dosimetric description since specification of radiation in terms of 'quality' dose is a very poor predictor of biological effect. This is demonstrated in the Table 1.3.

Table 1.3 Representations of microscopic patterns of radiation tracks corresponding to 1cGy macroscopic absorbed dose of three different radiation's.

Source	Whole tissue	Individual cells	Chromatin fibre	DNA	Mean No of lethal lesions per cell.
External gamma-rays	-	20μm	25nm x 25nm segment	2nm x 2nm segment	~0.001
Dose Uniformity	Uniform dose = 1cGy	~ uniform Dose ~1cGy	Large fluctuations Dose = 0-10^3Gy	Very large fluctuations Dose = 0-10^6Gy	
Mean No of tracks	10^9/g	~50/cell no cell unirradiated	~10^6/segment ~20 segments hit per cell	~10^8/segment ~10 segments hit per cell	
Internal Radon-220	-	20μm	25nm x 25nm segment	2nm x 2nm segment	~0.01
Dose uniformity	Variable Doses = 0-2 cGy	Large fluctuations Dose = 0-30cGy	Very large fluctuations Dose = 0-10^4Gy	Very large fluctuations Dose = 0-$2x10^6$Gy	
Mean no of tracks	~10^7	~0.1/cell ~90% of cells unirradiated	~6 x 10^7/ segment ~1 segment hit per cell	~10^{-8} /segment ~10 segments hit per cell	
External 10MeV neutrons	-	20μm	25nm x 25nm segment	2nm x 2nm segment	~0.005
Dose uniformity	Uniform Dose = 1cGy	Large fluctuations Dose = 0-5cGy	Very large fluctuations Dose = 0-$5x10^3$Gy	Very large fluctuations Dose = 0-10^6Gy	
Mean no of tracks	~10^7/g	~1/cell ~37% of cell unirradiated	~$4x10^{-6}$ Gy/segment ~8segments hit per cell	~10^{-8}/segment ~10 segments hit per cell	

1.5 Dose is Unnecessary

Radiation protection quantities, such as effective dose and equivalent dose were developed after World War 2. They seemed reasonable at the time they were defined. However with wisdom of hindsight it is clear that their only use is for bureaucratic purposes to control radiation exposure, originally to radiation workers and later to both workers and the public. It is clear that neither quantity is of any use for making a clinical judgement in the case of an over-exposure. The attending physician would make clinical decisions based on patient's symptoms and laboratory studies.

Both quantities have undergone minor changes in their name and definition. Dose equivalent became Equivalent Dose and the name and symbol of the biologically related constant to calculate it changed from Quality Factor (Q) which is determined from the averaged LET at a point in tissue to the Radiation Weighting Factor (W_R) which is selected for the type and energy of particles incident on the body, the relevant absorbed dose being averaged over a tissue or organ. Table 1.4 shows the weighting factors for different radiations used currently. It should be noted that in the draft of the 1990 ICRP publication the weighting factors for Auger emitters were recommended as 5 but this was changed in the final version for no scientific reason.

Table 1.4 Weighting for different radiations

Radiation			W_R
Photons			1
Electrons			1
Neutrons			
	<10	keV	5
	10-100	keV	10
	>0.1-2	MeV	20
	>2-20	MeV	10
	>20	MeV	5
Protons			5
Alpha particles, heavy nuclei, fission fragments and **Auger-electron emitters**			20

This dose equivalent factor does not have a rigorous scientific basis. It is rather a rough estimate erring on the safe side for radiation protection purposes. It is our opinion that although in some situations an Auger emitter may behave similarly to an alpha emitter. This is not the general case. This weighting factor neglects to take into account the energy spectra and mean free path for interaction of the radiations emitted by the Auger emitter. In some cases the mean free path may be such that the behaviour is more comparable to a beta emitter for example, but care must be taken in interpretation.

In 1990 NCRP report 104 on Relative Biological Effectiveness of Radiation of Different Quality was intended to improve the value of Q (now W_R) by reviewing the RBE values in the scientific literature. The committee concluded that it was not possible to give a value for Q (now W_R) because of the wide range of experimental results. It recommended choosing an appropriate value. Three years later NCRP report 116 (1993) continued to use equivalent dose with

the old Q values relabelled W_R values, even though NCRP report 104 states that Q (now W_R) values could not be determined. The change in terminology from ICRP publication 26 to 60 is shown in the Table 1.5, interesting to note that even with the huge changes in our understanding in radiobiology no significant change has been made in the basic principles from publication 26 to 60 as summarised in Table 1.5.

Table 1.5 Changes in Dosimetric Terminology in ICRP publications

Publication 26	**Publication 60**
Absorbed dose	Absorbed dose
Dose Equivalent	Equivalent Dose
Committed dose equivalent	Committed equivalent dose
Effective dose equivalent	Effective dose
Committed effective dose equivalent	Committed effective dose
Quality factor (Q)	Radiation weighting factor (W_R)
Weighting factor (W_T)	Tissue weighting factor (W_T)

NCRP report 122 (1996) explains how to calculate both the effective dose equivalent (using its 1977 W_T values) and the effective dose using its 1991 W_T values. In the first case you divide badge readings in Sv by 5.6 and in the second case you divide it by 22. There is a decrease of 400% from 1977 to 1991. Since effective dose equivalent and effective dose are both estimates of radiation risk a difference of 400% suggests a significant error in one or both sets of W_T values.

1.6 Dosimetry problems with Auger-electron emitters.

1.6.1 Assigning Weighting Factors; Theoretical and Experimental Studies of Auger-electron Dosimetry.

The problem of assigning weighting factors using the current radiation models for Auger emitters is made even more difficult due to the lack of understanding of the processes and effect of these emitters. More detail is given in Chapter 3.

It has been realised for some time that conventional dosimetry significantly underestimates the energy deposited in radiosensitive targets when Auger emitters are located in deoxyribonucleic acid (DNA). Sastry et al in [13] have shown that a more accurate estimation is made by calculating the dose to the nucleus rather than averaging over all cells, cell components and the extracellular regions as in the ICRU (International Commission on Radiation Units and Measurements) and MIRD (Medical Internal Radiation Dose Committee of the Society of Nuclear Medicine, USA) methodologies. Charlton developed a Monte Carlo approach, to trace the history of each electron track so that a precise statistical estimate can be made of energy deposited per base in the DNA from which the resulting number of single strand breaks (SSB) and double strand breaks (DSB) created can be calculated. Humm [14] developed this method further to come up with the conclusion that the Auger electron shower would only provide a small increase of damage above the normal sensitisation. However no method of quantification related to any physical parameters was developed.

This clearly indicates that there is some confusion with regard to the dosimetry of Auger-electron emitters with respect to method of calculation and the assumptions involved in dose-averaging over the mammalian cell or its nucleus.

More fundamentally, the question may be asked: `What is the most important factor in terms of radiation quality that determines the irreparable damage to the DNA?' These methodologies assume that it is the dose delivered to the site of interest that determines the damage. However if that was the case why is there such a wide discrepancy in quantifying the effectiveness of Auger emitters, even when the averaging of dose over nucleus or cell is taken into account? This will be discussed at greater depth in Chapter 3.

Significant work on various aspects of dosimetry has been carried out. Younis and Watt [15] have calculated the bio-effect cross sections per decay for inactivation of ^{125}I, ^{77}Br, ^{3}H and ^{131}I from knowledge of the slowing down fluence of the charged particles and published survival data. They concluded that ^{125}I, ^{77}Br, and ^{3}H have qualities similar to those of heavy particles, indicating that the damage from ^{125}I and ^{77}Br is mostly due to direct action and ^{3}H from indirect action. This being consistent with the interpretation that electron damage is caused mainly at the end of the track. The use of a damage cross section as a radiation quality parameter has the advantage that it represents the actual probability of damage per unit fluence of charged particle tracks and thereby avoids the problems associated with averaging of doses delivered to the target site.

Goodhead [16], on the other hand, has suggested that at all subcellular levels even down to DNA, high LET radiations can produce unique initial damage different from that possible with low LET radiations. One can make physical arguments to suggest that this interpretation must be in error. The questions that arise are 'what degree of damage is required to be classified as damage to the

DNA? Is the unique damage caused by the high LET radiation due to the energy intensity of the track or to some other property related to the radiation? For example interaction with multiple sensitive target sites at risk, distributed along single tracks?'

Booz *et al* [17] have tried to distinguish between damage caused by ^{125}I incorporated into the DNA structure and the damage observed when the radionuclide is homogeneously deposited in tissue. They have also tried to assess the importance of the charge transfer phenomenon. Booz et al calculate that the energy potential due to multiple ionisation is about equal to that due to the deposition of Auger electrons. They conclude that it is useless to separate these two effects by radiobiological methods. They also estimate that for ^{125}I incorporated into specific biological targets of 20nm dimension, most of the energy deposited is above 40 keV/μm and therefore does not need to be subclassified. Halpern [18] disagrees with this. He concludes that the stacking of bases in DNA can be responsible for long range effects due to dissipation of charge. There is not enough evidence to prove this theory, particularly when considering the low effectiveness of electrons over a long distance and the presence of the large volume of water surrounding the DNA molecule. Water will be very effective in absorbing the electrons and in eliminating any possible long range effect which they may have.

At the cellular level, there seems little doubt that the intranuclear localisation of Auger-electron emitters is required to observe the biological effect of the Auger process. Kassis *et al.* [19] have reported that with V79 cells mitochondrial-bound (cytoplasmic) ^{125}I produces a cytocidal survival curve having a distinct

shoulder and a mean lethal dose (D37) of 462cGy, while 125I incorporated into DNA produces a logarithmic survival curve with a D_{37} of 80cGy. Link *et al.* [20] working with radiolabeled methylene blue, a dye that binds to the cytoplasmic melanin granules in melanoma cells, have shown that conspicuous cytocidal effects are obtained when the agent is labelled with the α-particle emitter ^{211}At but not with the Auger-electron emitter ^{125}I.

A number of investigators have obtained similar results with ^{111}In. Rao *et al.* [21, 22] have compared the ability of ^{111}In oxine, ^{111}In citrate, ^{114m}In citrate and X rays to reduce the spermhead population in mouse testes. The D_{37} of the four agents is 16cGy, 34cGy, 57cGy and 67cGy, respectively. The difference between ^{111}In oxine and ^{111}In citrate is ascribed to the higher nuclear fraction of the former (92% versus 30%). In the case of ^{114m}In, only 0.8% of the dose comes from Auger electrons, whereas in the case of ^{111}In, 20% comes from Auger electrons.

McLean and Wilkinson [23] have studied the survival of V79 cells *in vitro* after exposure to ^{111}In. They reckon that the dose to the cells from intranuclear decay is 3.5 mGy and from extracellular decay, 5.8pGy, a considerable difference. McLean *et al.* [24] have demonstrated that ^{111}In oxine, some of which is tightly bound to chromosomal DNA, is a potent producer of chromosomal aberrations, while extracellular ^{111}In chloride is a much weaker one.

A number of investigators have been concerned that traditional dosimetry schemes (such as MIRD) underestimate the doses to specific population groups within tissues when Auger-electron emitting radionuclides are concentrated by

cells and especially by the cell nucleus. Bialobrzeski *et al.* [25] have shown for ^{51}Cr-bleomycin that the doses calculated for cell nuclei and DNA in liver cells are higher that the cell-averaged values by factors of 2.5 and 5, respectively, and the corresponding dose equivalents (taking into account the quality factor for Auger-electron showers) by factors of 9 and 24 respectively. Similar thinking has been applied to ^{51}Cr labelled lymphocytes by Vezza *et al.* [26], who calculate the actual dose to be twice the conventionally calculated one.

Makrigiorgos *et al.* [27] have also written about the limitations of conventional internal dosimetry at the cellular level. They have prepared a model that takes into account the intracellular-to-extracellular radionuclide concentration and labelled cell density for radionuclides ^{99m}Tc, ^{201}T1, ^{111}In and ^{123}I, all commonly used in the practice of nuclear medicine. Who have shown that when selective intracellular uptake of a radiolabeled compound occurs in specific cells within a cell cluster, conventional dosimetry underestimates the radiation dose delivered to the labelled cells by two fold to more than 25-fold if the emitted electrons have ranges of a few micrometers or less. Under the same conditions, conventional dosimetry overestimates slightly the electron dose to the nonlabelled cells. This approach has been applied to the irradiation of liver and spleen macrophages by ^{99m}Tc labelled microaggregates [28] and of lung capillaries by ^{99m}Tc labelled macroaggregates [29]. In the case of the lung, ascribed doses to some individual cells were found to be as high as 30,000 times the calculated average dose.

1.7 DNA Damage

The models reviewed all generally assume that the DNA is the critical target and the damage to DNA from Auger processes continues to fascinate a number of investigators, as indeed it should. The typical forms of induced biological damage in the DNA are shown schematically in Fig 1.1.

Charlton and Humm [30] have refined the model presented at the Oxford meeting, which can be used to calculate initial DNA strand breakage following the decay of I^{125}. DNA is again modelled as a 2.3nm cylinder with a 1nm base-pair core and the Paretzke electron track code is employed to calculate the energy deposited in the sugar-phosphate and base volumes. Two spectral sources are used, the original of Charlton and Booz and a newer one of Pomplun (vide *supra*), in which the charge energy is handled differently. Two types of SSB and three of DSB are recognised. The distribution of SSB fits the experimental results of Martin and Haseltine [31], while values between 0.82 to 1.07 DSB per decay are obtained depending on the electron spectra postulated.

Fig 1.1 Model of DNA Damage [Ref 32]

Normal DNA

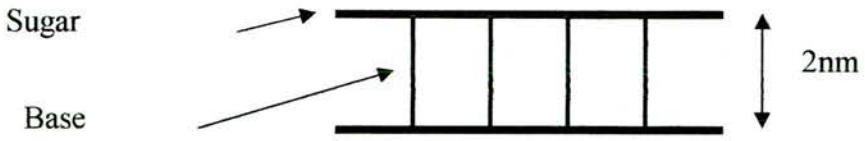

Base Damage

Cross Links

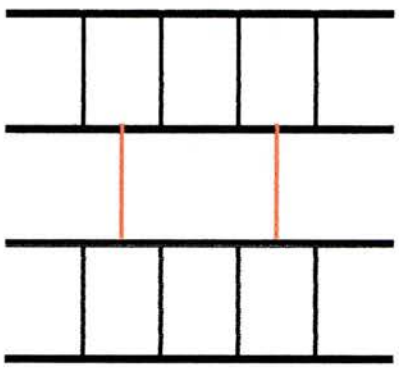

Single Strand Break (ssb)

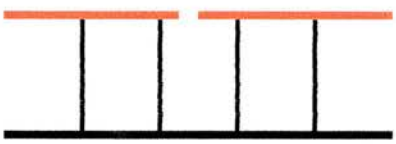

Single Strand Break (ssb+)

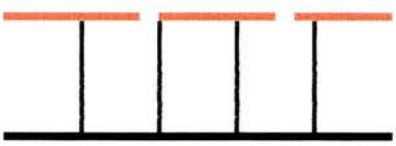

Single Strand Break (ssb)
Breaks >10 base pairs apart

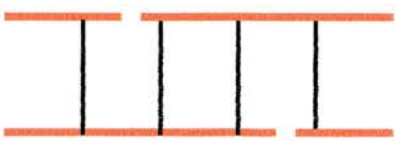

Double Strand Break (dsb)

Breaks <10 base pairs apart

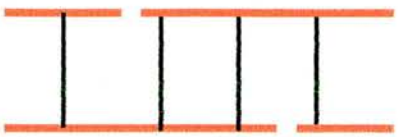

Double Strand Break (dsb+)
Breaks 10 base pairs apart

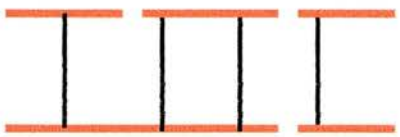

Double Strand Break (dsb++)
Breaks <10 base pairs apart

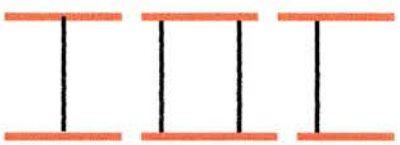

Each nucleotide consists of a phosphate, a sugar known as a deoxyribose and any one of four nitrogen containing bases. The four nitrogen bases are Adenine (A), Thymine (T), Guanine (G) and Cytosine (C), Watson and Crick showed that A always binds to T and G always binds to C, so forming the mirrored templates on replication.

Using their own method of calculating spatial energy distribution from low-energy electrons and the ^{125}I Auger-electron spectrum of Charlton and Humm [30], Unak and Unak [33] calculate that about one keV of energy is absorbed in regions of DNA 2nm from the decay site in both directions. When they assume that 5 eV deposited in DNA produces a SSB, they reckon that local absorption

of ^{125}I Auger electrons is able to produce at least one DSB without taking into account neutralisation effects from the highly charged residual tellurium ion.

Some investigations have begun into the relative role of direct and indirect damage in DNA from Auger cascades. Wright *et al.* [34] have made Monte Carlo calculations for the physical and chemical interactions of Auger electrons with liquid water. They have illustrated the distribution of watery radicals in the vicinity of a DNA duplex and calculated the yields of each aqueous species from the decay of a number of radionuclides. For ^{125}I decaying on the surface of a DNA cylinder, they calculate 44 indirect and 21 direct interactions per disintegration, or an indirect/direct ratio of about 2/1. They however do not conclude what the effectiveness is for this ratio, it is not clear whether the direct or indirect action is the more important.

Recently, Pomplun [35] has produced a new DNA target model for track structure calculations and applied it to the interaction of ^{125}I Auger electrons. He elaborates electron track interactions in a cylindrical model of DNA 14.3nm long and 2.4nm in diameter. (In contrast to the Wright model [34], he has the decay taking place within the cylinder.) In a series of histograms, he shows mean energy deposited by direct and indirect hits in phosphate-sugar strands and bases both on the ipsi-lateral and contralateral labelled filaments. As expected, the fraction of direct hits is greater on the contralateral strand. Assuming a minimum of 10 eV direct energy and 17 eV indirect energy to produce a strand break, Pomplun calculates 1.8 of a total of 3.8 SSB per decay are caused by direct interactions. Of the 0.94 DSB produced per decay, about 40% are due to direct action.

Makrigiorgos *et al.* [36] have compared DNA damage produced in V79 cells by incorporated ^{123}I with that of ^{125}I. Using neutral elution, they have measured DSB production in frozen cells. They have also compared their experimental results with theoretical ones derived from the Charlton and Humm model [30]. They have found ^{125}I to be 1.3 times as effective as ^{123}I in producing DSB, whereas theory has predicted it would be 1.6. If one assumes that each decay of ^{125}I produces one DSB, then each decay of ^{123}I produces, on average, 0.74 DSB. Martin *et al.* [37] have measured the induction of double strand breaks in plasmid DNA following neutron capture by ^{157}Gd. The (n,γ) reaction results in ^{157}Gd and is accompanied by internal conversion. The DSB are thought to be generated by the resulting Auger cascade, as they are produced only when the ^{157}Gd is bound to DNA and not when the atom is sequestered by EDTA.

1.8 Biological Consequence

At the biological level, a number of observations have been made, the first group involving photon activations. Nath *et al.* [38] have studied survival of Chinese hamster cells exposed to low-energy photons after IUdR incorporation. The enhancement of IudR sensitization is about 1.5 for 250 kVp X rays relative to 4 MV X rays and 1.4 and 2.7 for the 60 keV photons of ^{241}Am compared to 860 keV photons of ^{226}Ra when IUdR replacement of thymidine is 5% and 25%, respectively. The authors ascribe the enhanced sensitization to the Auger effect. In comparison, Miller *et al.* [39] have examined the radiosensitization of V79 cells in which 16% of the thymidine residues have been replaced with IUdR. Enhancement ratios at the 1% survival level are 1.8 for 15 MV and 1.95

for 100 kVp radiation. This modest 10% to 15% additional enhancement with 100 kVp X rays is much less than that predicted by the proponents of photon activation therapy.

Larson and colleagues [40] have examined the Auger electron contribution to bromodeoxyuridine radionsensitization in V79 cells. When cells with 32% of thymidine residues replaced by BrUdR are exposed to monoenergetic X rays just below (13.450 keV) or above (13.490 keV) the K edge (13.475 keV) of bromine, enhancement ratios of 3% to 12% are obtained depending on the means of calculation; most values are between 5% and 7%. The authors conclude that Auger electrons produced following photoelectric absorption of X rays by the K shell of bromine contribute minimally to observed BrUdR cellular radiosensitization. In a simpler system, the radiolysis of bromodeoxyuridine-monophosphate, Takakura [41] has compared the effects of 13.49 and 13.43 keV X rays. The ratio of G values for the formation of the major product, dUMP (debrominated Br-dUMP), is 2.2, and for the conversion of dUMP to uracil, 1.0. The author believes the results confirm that Auger electrons stripped from the K shell of bromine play the major role in the radiolysis of the nucleotide.

Another set of experiments is concerned with the relative biological effectiveness (RBE) of Auger emitters with themselves and other forms of radiation. Kassis *et al.* [42] have looked at the relative effectiveness of ^{125}I, ^{123}I and ^{77}Br on the survival of V79 cells. They find that the mean lethal dose (D_{37} survival) to the nucleus is about 80 cGy in all cases. However, the total number of decays needed to produce this D_{37} is about twice as much with ^{123}I as with ^{125}I, approximately equal to the ratio of the energy deposited in microscopic

volumes by ^{125}I and ^{123}I, respectively. When applied to 5 nm diameter spheres, all three radionuclides lie on the same line in an inverse plot of deposited energy versus decays required for 37% survival.

Pomplun *et al.* [43] have calculated the equivalence of ^{125}I decays to high-LET radiation. In sensitive biological volumes of 20 nm, they reckon a mean lineal energy equivalent of 270 keV/μm. They have tabulated published RBE values for a number of biological end points. For chromosomal aberrations, the values scatter between 6 and 77, for transformations between 32 and 38, and for mutations between 1 and 16. These values can be compared to the recommended ICRP quality factor of 20 for this level of LET, *i.e.*, 270 keV/μm. Rao *et al.* [44] have examined the effects of radiations of different quality on spermhead survival and the induction of spermhead abnormalities. They find an RBE of 6.7 for ^{210}Po α particles and 7.9 for DNA-bound ^{125}I when compared with 60 or 120 kVp X rays for spermhead survival. For abnormalities, the corresponding values are 245 and 59. Using ^{7}Be, a monoenergetic photon emitter (477 keV), a dose rate effect is demonstrated which should be taken into account when comparing acute and chronic exposures.

Whaley and Little [45] have addressed the issue of mutation induction by incorporated radioiodine. They have examined the mutational frequencies at the hprt locus for cells proficient (TK6) and deficient (SE30) in thymidine kinase, an enzyme necessary for the incorporation of IUdR into DNA. For cells proficient in thymidine kinase, the D_0 values for $^{125}IUdR$, $^{123}IUdR$ and X rays are 5.9, 24 and 75 cGy, respectively. No cell death can be produced in the deficient cells with $^{125}IUdR$; for $^{131}IUdR$ and X rays the corresponding D_0

values are 54 and 77 cGy. The induced mutant fraction for ^{125}IUdR in the proficient cells is 3.3 X 10^{-6} per cGy, for ^{131}IudR, 0.45 x 10^{-6}, and for X rays 0.05 x 10^{-6}. In deficient cells, no mutants are induced by ^{125}IUdR; for both ^{131}IUdR and X rays the induced fraction is 0.04 to 0.05 x 10^{-6}. The results demonstrate clearly the extraordinary ability of incorporated ^{125}I to produce mutations as well as cytocidal effects. The RBE of ^{125}I relative to ^{131}I for survival is 4.0; for mutations, 7.3; the RBE of ^{125}I relative to X rays is 12.7 for survival and 66 for mutations. Whaley *et al.* [46] have also shown that the DNA intercalating agent ^{125}I-iodoacetylproflavin (^{125}IAP) can induce mutations at both the hprt and tk loci. When these results are compared with those observed with ^{125}IUdR, ^{125}IAP shows a reduced effectiveness per decay; for survival the RBE is between 2 and 4, for mutations at the hprt locus between 3.5 and 6. ^{125}IAP treatment induces large-scale genetic events at the hprt locus at high frequency in comparison to X rays, 90% versus 50%.

1.9 Therapeutic Potential

A keen interest in the potential use of Auger-electron emitters for targeted radionuclide therapy continues. Humm and Charlton [14] have developed a method to assess the therapeutic potential of Auger-electron emission. Their projection depends on electron track structure methods and the prediction of double strand breaks presented earlier (*vide supra*). According to their calculations, the DSB produced per decay of ^{125}I, ^{123}I and ^{77}Br incorporated into DNA are 1.10, 0.73 and 0.38, respectively. An advantage of ^{125}I with its 60 d half-life is that relatively few atoms need be incorporated into the genome for effective tumor sterilization. Humm *et al.* [47] have also focused on ^{123}I and

^{77}Br as alternatives to ^{125}I therapy based on results with experimental tumors using ^{125}IUdR. Baranowska-Kortylewicz *et al.* [48] have demonstrated that ^{123}IUdR can be used effectively for the diagnosis and therapy of ovarian ascites tumors in mice. The diagnostic capability stems from the 140 keV photon emitted by ^{123}I, which is suitable for imaging.

Anderson and Holt [49] and DeSombre *et al.* [50] have examined the potential of estrogens labeled with ^{125}I, ^{123}I and ^{80m}Br for the therapy of malignancies bearing estrogen receptors. Nuclear binding has been demonstrated in endometrium, granulosa cells and breast cancer cells. DNA-incorporated ^{80m}Br has been shown to be radiotoxic, while unbound ^{80m}Br is not (Desombre *et al* [51, 52]).

Howell *et al.* [53] have compared dose rate profiles for potentially useful radionuclides to be used for radioimmunotherapy. As one might expect, high-energy beta emitters such as ^{90}Y would be most effective for treating large tumors (>1 cm), whereas for small tumors (~1 mm), medium energy beta emitters are more suitable, while micrometastases may be best handled with low-energy electron emitters.

Woo *et al.* [54] have examined the effects of ^{125}I labeled monoclonal antibodies on cultured cancer cells. they have found that one of the antibodies tested is internalized by the cells and produces cytotoxicity as well as chromosomal damage. They assume that the internalized ^{125}I interacts with the cell nucleus. This type of immunoglobulin might be suitable for radioimmunotherapy with Auger-electron emitters.

Hou and Maruyama [55] have developed a complex of ^{111}In-bleomycin which binds to DNA and have augmented its cytotoxicity to small-cell lung cancer cells with hyperthermia. Baranowska-Kortylewicz *et al.* [56] have conjugated IUdR to immunoglobulins. The pyrimidine nucleoside-protein bond is hydrolyzed by lysosomal enzymes. This complex could be used to deliver the radioiodinated compound to specific tumor cells. Lastly, Goodman *et al.* [57] have begun a treatment protocol for brain tumors that involves IUdR infusion and brachytherapy. They plan to treat below and above the K absorption edge of iodine to test the effectiveness of photon activation therapy.

1.10 Biological Implications of Auger Electrons

The biological implications of Auger electron cascades following inner shell ionisation of atoms have been of interest for over 25years. Due to the method of decay i.e. by Electron Capture and/or Internal Conversion, there is a cascade of numerous low-energy electrons spontaneously generated. The biological effects of such radionuclides incorporated into tissue cannot be predicted *a priori* because of the highly localised patterns of energy deposition by the electrons. Auger-electron cascades display a very complex energy spectrum, dominated by a large number of very low-energy electrons (~20-500eV) with ranges (~1-10nm) of macromolecular dimensions. In biological matter, as demonstrated by Sastry and Rao [58], Sastry *et al* [59] although the linear energy transfer (LET) of these electrons is about 10-25keV/μm, nevertheless their simultaneous actions may simulate high-LET-type biological damage which is comparable

with the effects of densely ionising alpha particles of high LET. This has been shown by Sastry and Rao [60] and Rao and Sastry [61].

1.11 Bio-Effectiveness of Radiopharmaceutical Nuclides: the 'Template' Model

In order for a radionuclide to be effective in a tumourcidal form it is necessary that two conditions be met. Firstly, the radiopharmaceutical must be selectively incorporated into the target tumour cells in a high enough concentration to be effective without causing lethal damage to the normal tissue and secondly, the radionuclide deposit its energy in the tumour cell and not in the healthy surrounding tissue. The second requirement is an ideal situation for Auger emitters, which could meet the conditions due to the nature of their decay and ranges of their emitted electrons.

With these difficulties in mind, a new approach, leading to the 'template' model of radiation action, has been made without any prior assumptions on quality specifications. The 'template' model for cell inactivation differs from other models as it uses the empirical radiobiological damage related to the chemical and physical properties of radiation track structure. The latter enables experimental investigation of damage at the nanometer level, achieved by treating the radiation tracks as probes to explore for key information on damage to critical radiosensitive regions. A criterion for the success of this model is that, for external irradiations, data for the damage cross-section can be unified onto a single curve independently of radiation type and energy. This is described in full detail elsewhere [62].

A present objective of this thesis is to apply the model to analysis of cellular damage caused by internal irradiations such as that initiated by incorporated radio-nuclides, especially Auger electron emitters and beta emitters. This gives a solution to the problems of internal dosimetry which can be explored in a meaningful way whilst providing more information for further testing the validity of the 'template' model. Details are given in the next chapter.

CHAPTER TWO

Semi-Empirical Modelling of Radiation Action: The 'Template' Model

2.1 Philosophy of approach.

The model presented here aims to provide a method of classifying the effectiveness of Beta rays; Electron Capture and Auger electron emitting radionuclides within the unified scheme developed for external radiations. The model is a unified one as it predicts the external irradiation damage for all radiation types e.g. heavy ions, neutrons, gamma, x-ray and electrons and is expected to include the internal Auger-electron emitters within the general scheme. A sensitive test of the derived model can be made by comparing the predicted effect cross-section with the experimental cross-sections. If successful, a practical measure of the bio-effectiveness of Auger emitters can be conveniently determined by generating a scaling/cytotoxicity factor of merit for the radionuclides. The latter factor may be expressed empirically in terms of the bio-effect cross section and the total equilibrium electron fluence per unit concentration of decays. Alternatively, from the model, the cytotoxicity factor can be expressed uniquely in terms of the physical cross-section of the intracellular DNA, the total electron yield per decay, and the physico-chemical quality parameters of mean free path for ionisation and the radical diffusion length which appear to be the most important parameters in determining the radiation quality. Use of these parameters also aid in the understanding of the radiation effects in cells since the radiation can act as a probe to explore damage induction and identify the critical targets, indicated to be predominantly the DNA. (Khan and Watt [63], Watt and Khan [64], [65]).

Lack of any definite success in relating energy deposition quantities to the induced radiobiological end-point e.g. inactivation of mammalian cell nuclei indicates the need for a more rigorous analysis of the selected quantities involved. Thus one can surmise that the intrinsic *quality* of the charged particle radiation tracks is given by the bio-effect cross-section, σ_B, i.e. the probability per unit fluence of charged particle tracks at equilibrium. This is an *absolute* measure of the *quality* of the radiation, independently of any model. Furthermore, the net bio-effectiveness, B, is given by the product: $B = \sigma_B.\Phi_{eq}$, where Φ_{eq} is the equilibrium fluence of secondary charged particles. By this means, the charged particle tracks released in the irradiation can be used as a 'probe' to explore for the existence of radio-sensitive structures within the irradiated site e.g. virus, phage, or mammalian cell nucleus etc. The big advantage in this approach is that the bio-effect cross-section can be analysed in a graph plotted against physical track quantities of different types e.g. LET, track and dose restricted LET, and the microdosimetry quantities: lineal energy, y, and specific energy, z , etc., to determine which physical track parameter(s) best correlate all the data into a unified curve. (Watt et al [66]).

The analyses start with the published experimental radiobiological survival data followed by extraction of the relevant bio-effect cross-sections as described in the next section, 2.2, below. Subsequently, comparison of these results can be made with various accurately known physical parameters, which are descriptive of the radiation tracks.

The outcome is surprising as the radiation quality, σ_B, for mammalian cell nuclei is found to be dependent on the linear spacing between ionisations and is optimum when that spacing correlates with a 2 nanometer spacing in the radiosensitive target size. As the 2 nm structure is observed only when double-stranded DNA is present, it seems that the radio-sensitivity is strongly identified with double-strand breaks in the DNA

2.2 Development of the Template Model.

There are several important points to note in the development of the Template model. These include: (a) On the basis of empirical analyses of the observed effect cross-section for cellular end-points of interest, the radiosensitive target (segments of double-stranded DNA) is identified as the dominant critical target in mammalian cells. (b) In order for a double strand break (dsb) to occur, both strands must be damaged within the 10 base pair separation as commonly agreed, to stop the process of replication during the mitotic period of the cell. In the absence of repair the dsb will inactivate the cell, leading to permanent damage. (c) The radiation is delivered to the critical target by direct or indirect action within the mitotic cycle taking into account the repair, mitosis times, and duration of the irradiation at the relevant equilibrium fluence that can be quantified for the purpose of calculation. (d) It emerges that it is the spacing or linear primary ionisation mean free path (λ) of the radiation that is the important parameter in causing damage at the site of interest. That is, for inactivation, it is necessary that the radiation interact with the DNA double strand meeting the requirements stated in (b) and (c) above. (e) The condition in (d) must correspond with the geometrical cross section of the DNA along with the cross

section for induction of dsb's. That is, for effective damage the radiation mean free path for primary ionisation must be related to the location of the DNA double strand both in time and space i.e. in a 'template' action between individual paired interactions within the charged particle track and the DNA double strand. (f) Indirect effects due to radicals diffusing from the track may also contribute to the damage. These are accommodated by the chemical diffusion length, (Λ), for radical action.

2.3 Extraction of the Observed Charged Particle Fluence and Bio-Effect Cross-Sections.

Empirical quantities required for analysis are the equilibrium slowing down fluence of charged particles at the point of interest and the cross-section for production of the biological end-point. Data for heavy charged particles are often quoted directly as effect cross-sections and therefore can be readily used. However, mostly the data is given in terms of surviving fraction as a function of absorbed dose for the appropriate biological end-point. These must be converted from absorbed dose to fluence of relevant charged particles at equilibrium as indicated in equation 2.1 and subsequently to bio-effect cross-section as indicated in equation 2.2. This is a much more complex procedure for electrons (from X-rays; Bremsstrahlung; Characteristic X-rays; beta particles; Auger electrons, etc.) than for heavy charged particles and neutrons. The experimentally derived cross-section gives an absolute measure of the effect cross-section, [67-70].

The Charged Particle Fluence, deduced from the dose delivered at point, P, is given by :

$$\Phi_P(cm^{-2}) = 6.25\times10^8 \times \frac{D_P(Gy).\rho(g/cm^3)}{\overline{L}_T(keV/\mu m)} \qquad 2.1$$

where L_T keV/μm is the track averaged LET for the equilibrium charged particle spectrum. The effect cross-section, $\sigma_{BP}(\varphi, t)$ at P is given by the slope of the survival curve at that point, viz:

$$\sigma_{B,P}(\varphi,t) = -\left[\frac{\partial \ln(F)}{\partial \Phi}\right]_P \qquad 2.2$$

Assuming that the mean number of lesions can be expressed as a function of fluence (or dose) and that Poisson probabilities may be applied, then the cross-section at the point, P, for a delivered dose, D_P, is:

$$\sigma_{B,P}(cm^2) = 1.6\times10^{-9} \times \frac{\overline{L_T}(keV/\mu m)}{\rho(g/cm^3)} \times \left(\frac{-\partial \ln F}{\partial D}\right)_P \qquad 2.3$$

In the equations given above, F is the surviving fraction at point ,P, and φ is the charged particle fluence at equilibrium. D is the absorbed dose in gray and track average LET is in keV/μm.

In practice, the surviving fraction is obtained at the initial slope whenever possible to minimise the complications with the repair term.

Conventionally, the Relative Biological Effectiveness (RBE) is given by the dose ratio for a stated % effect, usually 37% survival for the same biological end-point as illustrated in 2.4 i.e,

$$RBE = \frac{D_{37,REF}}{D_{37,\alpha}} \qquad 2.4$$

for alpha particles with respect to the selected reference radiation.

D can be obtained from either the initial slope or the D37 value from the dose-response survival curve, Alkharam and Watt [70]. For the analysis of the model the useful experimental data available has been limited for various reasons including; the wide number of parameters used in calculating the delivered dose, the timing and method of radiation delivery. Also the number of Auger electron emitting radionuclides are limited due to the preference in the use of ^{125,131}I in nuclear medicine. Most research tends to be connected using these radionuclides.

Once the cross sections are determined or evaluated for the biological endpoint, the next step is to study the trend as a function of the spacing of the interactions or linear primary ionisations within the cell in order to determine the likelihood of interaction with the critical radiosensitive site, in this case DNA double strands.

Some difficulty arises when determining the cross sections as not all experimental data in the literature provide the relevant cross sections, mainly because of the use of dose and LET. These latter imply that an averaging over the cell volume is used. The damage is not localised further than the cell and DNA, ignoring the fact that it is the DNA and the scission of the double strand that is likely to be the critical factor in cell survival. The cell may be receiving only a quantity of energy that is not contributing to the final damage but only as dose to the cell. However it should be noted that D and LET are used to

determine the fluence at equilibrium for charged particles, it is the Lambda that controls the quality.

Where actual cross sections are not obtainable they are determined from dose-response curves. The problem here is obtaining data that are consistent in terms of location of the radionuclide, timing of dose delivery i.e. which part of the cell cycle rate at which the dose is given to the cell or DNA, incubation period, method of radiation delivery. Also the data does not exist for the wide number of Auger electron emitting radionuclides used in medicine. These large numbers of variables make the possible data that can be used to test the model limited. The calculated radionuclide data used in the programs listed below are shown in Appendix 1.

2.4 Calculations of Physical Track Structure Parameters: Computer Programs.

To determine the role of physical track parameters in the structure of the observed bio-effect cross-sections, it is necessary to have the capability to investigate all physical track parameters commonly used for specification of quality. First, it was decided to calculate the data for a liquid water medium, chosen because water provides a good simulation for soft tissue. Furthermore, data for all existing types and energies of ionising radiation are required to permit comparisons to be made of typical quality parameters and to investigate the extent to which the cross-section data can be correlated into a single curve when expressed as a function of the selected radiation quality parameter(s?). To be fully meaningful, the track calculations must be extendable down to threshold energy of about 20 eV which just excludes the chemical bonding

energies. Averaged parameters are typically obtained by a suitable numerical integration usually fluence-weighted, as described in [71]

Before further development of the model is carried out the basic principles behind the calculations of the slowing down fluence spectra are detailed below. The calculations consider a source of electrons distributed uniformly throughout an infinite homogenous material and emit electrons of kinetic energy E_0 at a constant rate N_0 per unit volume and per unit time.

The differential spectrum of electron fluence is given by:

$$\phi(E) = N(E)/TR^2 \qquad 2.5$$

(TR^2 being the cross-sectional area of the detector)

The energy spectrum is given by:

$$y(E_0, E) = \phi(E)/N_0 \qquad 2.6$$

The mean distance travelled by an electron before it comes to rest i.e. its range, is given by:

$$R(E_0) = \int_0^{e_0} y(E_0, E)dE \qquad 2.7$$

$$R(E_0) = \int_0^{E_0} (-dE/dx)^{-1} dE \qquad 2.8$$

The collision stopping power i.e. the distance an electron travels for a small increment in E is

$$y(E) = \frac{\int_0^{\infty} N(E_0)y(E_0, E)dE_0}{\int_0^{\infty} N(E_0)dE_0} \qquad 2.9$$

The above equation is applied to secondary electrons of non uniform energy produced by x or γ rays.

These equations are utilised to generate the spectra for both beta and Auger electron emitters using the programs discussed later in this chapter.

The spectrum (it is this electron spectrum that is exposed to the biological system) is generated in several steps. Decay schemes from MIRD were collated mainly from the MIRD publication [72], and used to take into account all of the electrons together with gamma and Auger K, L shell emissions.

The cross sections were derived in several stages for the calculation of bio-effect. It is assumed and generally accepted that it is the electrons direct or indirect that are the major cause of damage in a biological system. For this reason the gamma photons and the $K_{\alpha\beta}$ x-rays were converted to electrons i.e. taking into account their interactions via photoelectric and the Compton effect. This process is carried out using the relevant Computer Programs for compilation of the various quantities listed below (section 2.4.5). The programs, on CD, can be found in the envelope on the inside back page of this thesis.

The beta spectra are generated in the same manner and can be compared with photon generated and Auger electron emitters generated by electron capture nuclides.

All data were extended down to 20eV using various analytical methods including extrapolation and use of the collision stopping power as explained above.

For internal Auger emitters the spectrum is used to evaluate the fluence and in turn the bioeffect cross-section. This was done by determining the concentration per unit volume which gives rise to fluence under equilibrium conditions

through the relationship; (Range = fluence / concentration). In considering the mean free path of the radiation the other aspect to be considered is the spectra of the electrons in particular the slowing down part of that process.

It is known that electrons are most effective in causing biological damage at the end of their tracks. This reflects decreased velocity as the electron/particle slows, the energy deposition increases because nearby atoms are influenced for a longer period. The region of increased deposition is known as the 'Bragg Peak'. The rapid decrease beyond is due to the capture by slowly moving particles. An electron traversing a material dissipates its energy in a very large number of inelastic collisions with atoms of the material. In the great majority of these collisions, the energy lost by the electron is of the order of 10eV/collision. The aggregate effect of a large number of such collisions yields a nearly continuous process of slowing down.

For the reasons stated above, the model incorporates the effect of slowing down charged particle spectra. The model uses the methodology developed initially by McGinnies [73]. The steps in the analysis of the data with respect to the slowing down of the electron is outlined in the following sections. In the template model the minimum electron energy is extended empirically from the 400 keV cut-off in water obtained by McGinnies [73] and Sugiyamas [74], down to 20eV in the present work. ICRU Report 17 contains information on the methodology for electrons and protons.

2.4.1 Quality Parameters Calculated: Monoenergetic Electrons (30eV to 30MeV); Characteristic K_α X-Rays (Carbon to Uranium); Medical X-rays (50 kV to 300 kV; 8 MV and 26 MV bremsstrahlung); Some β emitters and electron-capture nuclides (Auger electrons, etc. extended in this thesis); γ–ray spectra (Am-241, Cs-137 and Co-60).

Calculations have been made, in the continuous slowing down approximation, of track and dose-average LET, restricted LET (Δ), relative variances, the mean linear primary ionisation and the corresponding mean free path, CSDA ranges, the mean energies required to produce a primary ion pair and kerma factors. The minimum cut-off energy is 30 eV. Each set of data tables is divided into 4 parts viz. data for the instantaneous electron energies; averages over the whole primary electron tracks; averages for the secondary charged particle equilibrium spectrum; spatial concentration of primary and secondary source electrons, fluence of primary and secondary electrons and a quality modified fluence. For photon irradiations there is additional information on the weighted mean free paths for electron production, the weighted mass energy transfer coefficients, the mean photoelectron and Compton electron energies and their net mean range.

For the purposes of the present thesis, new extended calculations have been performed for 19 β–emitters and 16 electron capture nuclides. This is a formidable task, aimed at completing the validity tests for the 'template' model of radiation action (section 2.7) and resolving complications concerning the meaning of 'unified action' for the bio-effect cross-section.

Use the computer program XSCEL.FOR for photon input data to be converted to electron equilibrium spectra, etc. Use PELSLD.FOR for electron input data.

2.4.2 Heavy Charged Particles: 100 eV/amu to 1 GeV/amu.

Data have been computed for 74 heavy particle types ranging from protons, deuterons, tritons to Uranium ions. Quantities calculated are:

(1) Delta-ray data for ions of specific energy, E/A_i. Quantities are β_t^2 ; Average Energy of delta-ray, T_{Av} eV; Average Range, μm; Maximum delta-ray energy and maximum Range.

(2) Instantaneous Ion Data: E/A_i; E keV; β_t^2; z^2/β_t^2; I nm^{-1}; LET; R, Range; W eV.

(3) Averaged values for Equilibrium Spectra: E keV; I_{aV} /nm; mean free path, nm; $L_{T,Av}$; $L_{D,Av}$; $L_{T,100}$; Variance $L_{T,100}$; $L_{D,100}$; Variance $L_{D,100}$; Ranges.

Use computer program: HCPLET.FOR

2.4.3 Neutrons: 100 eV to 100 MeV (monoenergetic). 2 keV; 24 keV; 144 keV; Cf-252 spontaneous fission and Am/Be neutrons.

Mono-energetic neutrons cause biological damage via the source density of H and O atoms generated in the soft tissue – taken to be liquid water in this instance. Data are tabulated for neutron energies ranging from 100 eV to 100 MeV. Quantities of interest are source densities of hydrogen and oxygen viz: $N_H.\sigma_H$ cm-3; $N_O.\sigma_O$ cm-3; partial KERMA factors and Equilibrium Fluence of charged particle recoils generated in liquid water. Track data for elastically scattered H recoils are: mono-neutron energy, En; maximum H recoil energy, $E_{H,max}$; Range of maximum energy recoil; Average recoil energy, $E_{H,av}$; Average fluence-weighted range of recoils; Delta energy maximum; Delta range

maximum; average delta-ray energy; Average delta-ray maximum and fluence weighted W values. Analogous data are obtained for elastically scattered O recoils. Other parameters of interest are:

Averaged values for the H and O equilibrium spectra are: $E_{max,}$ keV; I_{aV} /nm; mean free path, nm; $L_{T,Av}$; $L_{D,Av}$; $L_{T,100}$; Variance $L_{T,100}$; $L_{D,100;}$ Variance $L_{D,100.}$ Also, Frequency and Dose-average lineal energies, specific energy densities and Kerma Factors are listed for microdosimetry.

Use the Computer Programs: NYSP.FOR, NTLET.FOR and NYNALP.FOR

2.4.4 Beta ray spectra.

'betacon.for' converts Cross's ICRU tables of normalised beta spectra into a distribution of energy (keV) for use with 'pelsld.for'.

'betaspec.for' calculates beta energy spectra shape for beta rays emitted by any radionuclide.

'bemic.for' calculates microdose spectra in lineal energy or specific energy density from input primary electron data of photoelectrons etc, (see xscel.for), or primary beta spectra from radionuclides.

Computer Program BETACON.FOR, BETASPEC.FOR, BEMIC.FOR

Details of the computer programs used for the various calculations are listed in the CD ReWrite / ROM located in the envelope on the back cover of this thesis.

The computer programs are in a version of Fortran. Input files, some of which are NAG routines, must be called. The main reason for including the Programs here is to give access to the text for clarification of the relevant equations.

The PROGRAMS are:

1) xscel.for, for photons.

2) pelsld.for, for electrons.

3 hcplet.for, for heavy particles.

4) nysp.for; ntlet.for and nynalp.for, for neutrons.

5) bemic.for; betacon.for and betaspec.for; for β radiation.

6) fominc.for

7) Auglsq.for

Programs GACO.DAT (coeffts. for gamma-ray interactions) and WATER.DAT (absorption coefficients for a water medium) must be included as input files in XSCEL.FOR and PELSLD.FOR full details of the programs can be found in the CD ROM (Appendix 2)

Calculations of slowing- down (equilibrium) spectra in liquid water can be performed within the foregoing computer programs. Detailed discussion for application to electrons (specifically electron capture nuclides and beta decays) are given in Chapter 4.

2.5 The Radiobiological Database.

An extensive radiobiological database, reported in over 200 published papers up to 1997, has been compiled for calculation of the effective cross-section for various end-points especially inactivation. Detailed data is provided for:

(i) inactivation of non-mammalian cells. Charged particles and sparsely ionising radiations on enzymes, phages, viruses, bacteria E-Coli, Bacillus Subtilis and yeast cells.

(ii) inactivation of mammalian cells. Charged particles, neutrons and sparsely ionising radiations on hamster cells, mouse cells, and human cells.

(iii) Chromosome dicentrics produced by charged particles on human cells, mouse and hamster cells. Neutrons and sparsely ionising radiations on human and hamster cells.

(iv) HPRT mutations caused by charged particles, neutrons and sparsely ionising radiations on human and hamster cells.

(v) Oncogenic transformations caused by charged particles, neutrons and sparsely ionising radiations on mouse cells.

(vi) Single-strand breaks produced in DNA by densely and sparsely ionising radiations.

(vii) Double-strand breaks in DNA, induced by charged particles, neutrons and sparsely ionizing radiations in cells.

Results from the programs are listed in reference 70.

Using the methodology above and the well established data on heavy particles the significance of the 2nm correlation and the predictability of the Template model can be shown. This is done in the following sections.

Figure 2.1, is a plot of mean spacing of ionisation (nm) i.e. Lambda and the cumulative probability of damage for cell nuclei, T1 Phage and enzymes. The plot shows clearly that at 2nm there is a significant inflection in the curve for cells and T1 Phage which is not observed for enzymes and bacteria which have only single -stranded DNA or zero DNA. This suggests that the observed lower

radiosensitivity of the cells is due to the proposed mechanism that the key lesions are the induction of double-strand breaks in the DNA , by single charged particle tracks. This has been argued in more detail elsewhere by Watt et al, [1, 70].

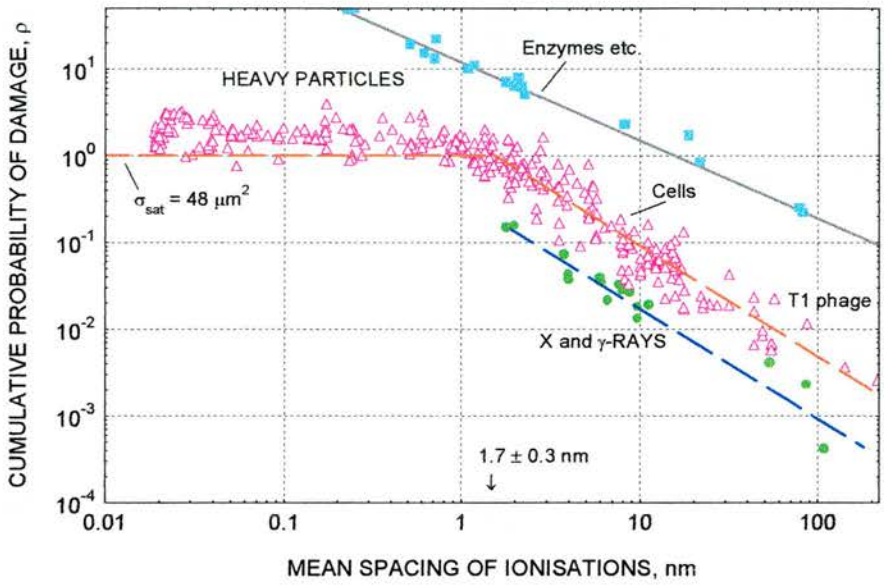

Figure 2.1 **Plot of mean spacing of ionisations (nm) and the cumulative probability (ρ), illustrating the 2nm importance.**

Figure 2.2, is a plot of cross section for V79 cells versus lambda for various external radiations. The graph shows the point of inflection around the 1-2nm range. From the graph, one can interpret the existence of several cellular sub-targets and the negligible role of delta rays in unsaturated conditions. It is concluded that the correlation of 2nm with the DNA spacing is the main damage mechanism and that the sub-targets are segments of the DNA with double-strand breaks being the key lesion.

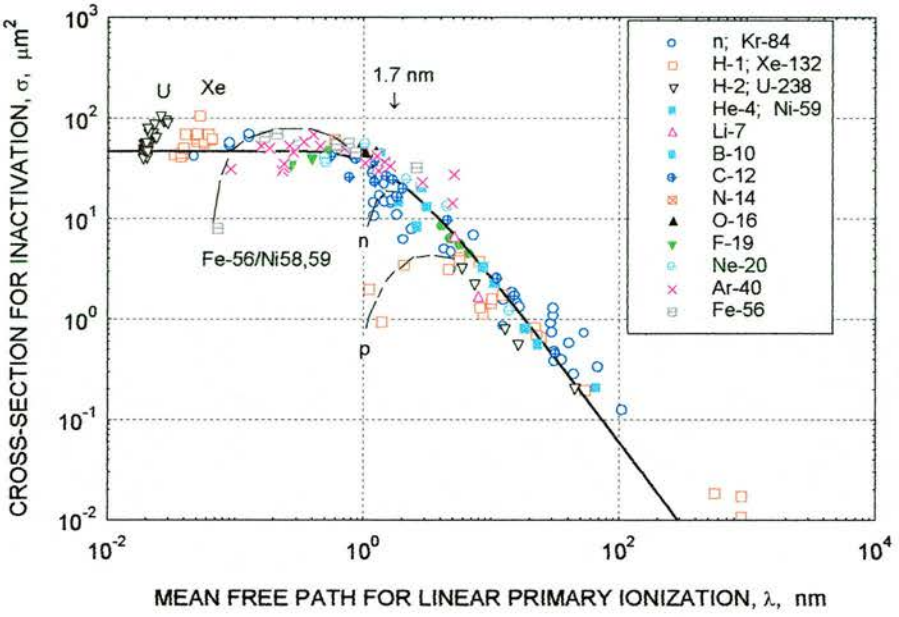

Figure 2.2 **Plot of Lambda (λ) and the cross section for inactivation, illustrating the importance of 2nm spacing.**

Figure 2.3, is a plot of lambda versus cross section for HF19, human kidney and V79 cells for heavy and x and gamma rays, the inflection around the 2nm region is again present. However it should be noted that Co-60 shows up as an anomaly. This may be due to the correlated effects of simultaneous electron cascades as may be the case for Auger electron emitters. The apparent anomaly disappears when the averaging of the effect cross-section is taken into account. The proposed 'Template Model' for V79 Chinese hamster cells are shown as solid lines.

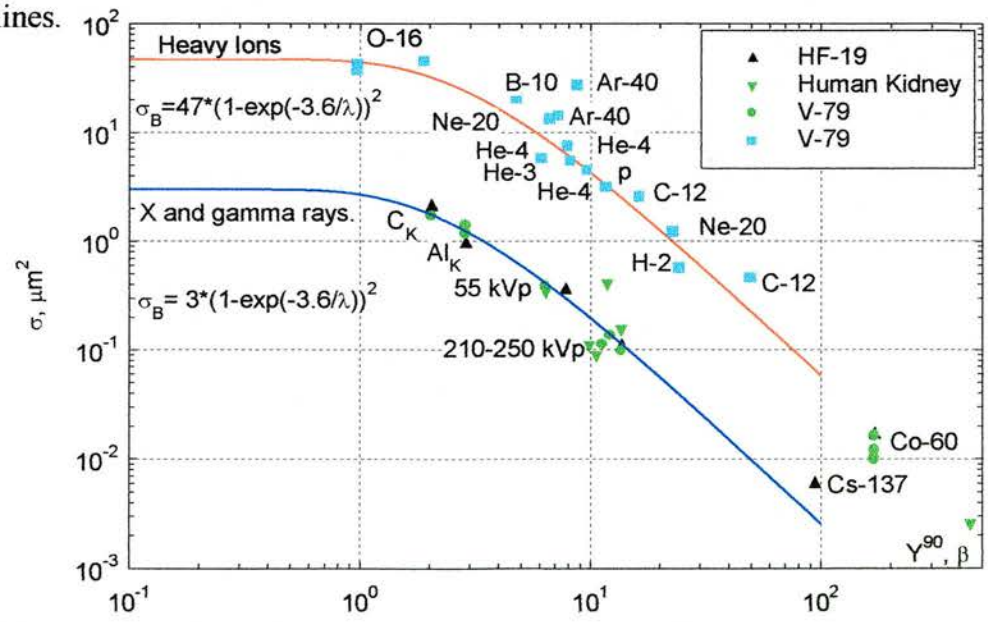

Figure 2.3 **Plot of Lambda (λ) and the cross sections from template model shown in solid lines.**

There are several points that are brought out by looking at damage or RBE from heavy fast particles. The graphs show that the mean free path for linear primary ionisation 'λ' is equal to 2nm or as shown in the graphs above as 1.7±0.3nm. For $\lambda < 2$nm saturation damage occurs. The excess damage caused by the δ-ray contribution is small. The increasing dose does not affect the position of the maximum RBE as a function of λ.

Having now demonstrated that the basic premise of the model is quantifiable and having identified the significance of the 2nm correlation for damage, the next step is the comparison of the model with beta spectra, which are well established, and gives a good comparison with the Auger emitters. This is carried out next.

2.6 Cumulative Probability of Damage.

To compare, on the same graph, the data for inactivation of various biological targets which may differ greatly in size e.g. enzymes, bacteriophage, viruses, and cells, the experimental data are converted to the ratio of the observed effect cross-section to the saturation cross-section. This ratio is called the cumulative probability of damage and can be greater than unity because of the secondary effects in the saturation region, to be discussed later. The resulting graph of the cumulative probability expressed as a function of different track parameters represents the result of the 'probe' investigation.

When plotted against the mean spacing of ionizations, represented by the ionization mean free path, the curves shown in figure 2.2 are obtained. This is interpreted as follows. (a) there is no sign of structure for enzymes, viruses and ΦX 174 phage. (b) there is a distinct change of slope in the curve for mammalian cells and T1-phage i.e. for the targets containing double-stranded DNA. The most important difference between ΦX 174 phage and T1-phage is that the former contains ss-DNA whereas the latter contains ds-DNA. The fact that they lie on different curves suggests that the ds-DNA is a key lesion. In addition T1-phage has no significant membrane, yet the data obtained lies on the curve for mammalian cells all of which have membranes, indicating that possible damage to the membrane cannot be the most significant lesion. Additionally, for heavy particle irradiation of mammalian cells, there is a clear point of inflection at a mean free path of ~ 1.7 nm. Bearing in mind that the mean chord through the DNA helix is of this magnitude, this dimension is entirely consistent with the likelihood that double-strand breaks in the DNA are the critical lesions.

Finally it is interesting to note that electrons, X and gamma-rays lie on a line which is nearly parallel to that of the heavy particles but about an order of magnitude less in effectiveness. The explanation offered for this is that electrons are most damaging at energies of about 150eV to 200eV, in the last few nanometres of their range (5nm to 7nm). It is therefore physically impossible for electrons to reach a saturation level of damage of the type produced by heavy particles. Heavy particles can sustain a mean free path of ~ 2nm throughout the whole cell nucleus (~6000 nm diameter) whereas electrons cannot. The low efficiency of the electrons (and X and gamma rays) is attributed to the presence of

multiple radiosensitive sites in the cell nucleus. Electrons can inactivate at most only one site. The difference in magnitude between the cumulative probability of electrons and heavy particles is about a factor of ten to twenty times, dependent on cell type and shape, at the same mean free path for primary ionization. One can intepret this as the approximate number of radiosensitive sites at risk upon a mean chord traversal by the track. It therefore accounts for, and explains, in fundamental terms the need for a quality, or radiation weighting factor, in a dose-based system. Evidence for the existence of multiple radiosensitive sites within the cell nucleus can be deduced from the results in figures 2.2 and 2.3.

The fact that the best correlation of damage data is achieved when plotted against the mean free path for linear primary ionization rather than the LET or restricted LET implies that the delta electrons must have minimal or negligible effect. Since the LET, the linear collision stopping power, is determined by the first moment of energy transfer whereas the linear primary ionization is determined by the zeroth moment of energy transfer, the better correlation of the biological data with the latter means that the energy transfer in the collision plays no significant role! Consequently absorbed dose (and therefore LET) cannot be relevant to the specification of radiation damage! This challenges the very basis of the theories and practice used in our system for assessing radiation damage in protection and therapy. Further justification for this claim is given below.

2.7 Delta-ray effects and target multiplicity

Referring to figure 2.2, which shows the plot against the mean free path for linear primary ionization of the measured bio-effect cross-sections for inactivation of V79 Chinese hamster cells by heavy accelerated ions ranging from protons and neutrons to uranium ions, reveals interesting diagnostic information on damage mechanisms. First, the tail of the uranium ion data plotted for lambda near $3x10^{-2}$ nm, has a maximum cross-section extending to twice the saturation cross-section shown by the line at 48 μm^2. The excess is attributed to the yield of delta-rays in the saturation region. By comparison of the delta ray yield in the cell nucleus ~ $3x10^5$ and the resulting proportion of the bio-effect attributed to delta rays, one can estimate that the mean efficiency of a single delta ray is only ~ $5x10^{-6}$ [69]. Other methods of estimating the lack of importance of electrons is to select a band of lambda values in the unsaturated region, say near lambda values of about 14nm. Then, since particles of different effective charge but having the same lambda will differ only in the spatial distribution of delta rays which in turn is determined by the velocity squared of the ion, it follows that a plot of effectiveness against the maximum delta ray energy (proportional to ion velocity squared) should be constant independently of the spatial distribution of delta rays. Figures 2.1 and 2.2 show that, within the spread of errors, the data are consistent with this premise for neutrons and particles heavier than protons.

Referring to the line curves drawn in fig 2.2 for Fe56/Ni58,59, the maximum in the curve occurs at delta ray energies > 10 keV i.e. the delta electrons have sufficient energy to traverse the cytoplasm and interact with the neighbouring cell nuclei to enhance the cross-section above the saturation value. The dashed curve

crosses the saturation line at smaller lambda values when the delta ray is reduced in energy to < 10 keV and, importantly, the range of the accelerated ion becomes smaller than the mean chord through the cell nucleus. As lambda becomes still shorter with decreasing velocity of the iron ions, the cross-section continues to decrease below the saturation value. This is consistent with the presence of site multiplicity - as the range decreases below the nuclear diameter, fewer sites are penetrated and the effect cross-section decreases below the saturation value. Similar effects are seen in the proton data. But in the case of protons there is an additional complication because the proton range decreases below the cell nuclear diameter before saturation damage can be achieved at the requisite lambda of ~ 2nm. There is plenty of information supportive of this interpretation for other target sizes.

2.8 The 'template' model of radiation bio-effectiveness.

Taking into account the foregoing interpretation of the damage mechanism and what is known about radiation action due to direct ionization and indirect action by radical diffusion as well as a modifying factor to allow for the repair of damage, it becomes a relatively simple matter to write down a model of radiation action. It is a model for the absolute bio-effectiveness of ionizing radiations and, at this stage, is believed to be a model also for the number of double-strand breaks induced in the DNA. Definitions of the parameters used are given after the equations.

$$B = \sigma_{g,DNA} \cdot \Phi_{eq}$$

$$i.e.\ B = \sigma_{g,DNA} \cdot \frac{n_0}{\bar{d}} \cdot \left[\int_E R(E).\varphi(E)_{eq} \cdot \varepsilon_{dsb}(\lambda(E)).dE \right] . U(Z,t_i) \text{------} \quad (2.9)$$

$$\sigma_B = \sigma_S \cdot \varepsilon_{dsb}(\bar{\lambda}) . U(Z,t_i)$$

$$\varepsilon_{dsb}(\lambda) = [1 - \exp(-2\Lambda + s)/\lambda)]^2 \quad \text{-----(2.10)}$$

$$\sigma_S = [\sigma_{g,DNA} \cdot n_0 \cdot \frac{\bar{R}}{\bar{d}}]; \ \frac{\bar{R}}{\bar{d}} \leq 1$$

Dual track action may occur at very high dose-rates, in which case the effect cross-section can be written as the cumulative probability, defined as the ratio to the cross-section for saturation damage:

$$\frac{\sigma_B}{\sigma_S} = \left[\varepsilon_{dsb}(\bar{\lambda}) + 2 . \frac{(\varepsilon_{ssb}(\bar{\lambda}))^2}{n_0^2} \cdot \sigma_S \cdot \phi_{eq} \right] . U(Z,t_i)$$

$$= \varepsilon_{dsb}(\bar{\lambda}) . \left[1 + \frac{2}{n_0^2} \cdot \sigma_S \cdot \phi_{eq} \right] . U(Z,t_i) \quad \text{-----(2.11)}$$

Equation 2.11 indicates that dose-rate effects cannot be greater than 1% at 37% survival i.e. when the mean number of events/cell, $\sigma_B.\Phi_{eq} = 1$.

2.9 Definition of quantities used in the 'template' model.

$B = \sigma_B.\Phi_{eq}$, is the bio-effectiveness or the mean number of lesions produced in the cell nucleus.

σ_B is the cross-section for the stated biological end-point, in this case inactivation of mammalian cells. It is also the total cross-section for induction of double-strand breaks (dsb) in the DNA of the cell nucleus.

σ_S is the saturation effect cross-section, shown by the horizontal line drawn to smaller values of λ through the point at λ = 1.8 nm (e.g. see figure 2.3). σ_S is

spectrum-dependent for tracks having R/d ≤ 1. For heavy ions in V79 cells, σ_S~ 45 μm^2 and for equilibrium electron tracks $\sigma_S \sim 3\mu m^2$, as shown in figure 2.3. The ratio σ_B / σ_S represents the cumulative probability for inactivation. It can have a value greater than unity in the saturation region for heavy ions where delta-ray effects may contribute to the damage, as shown in figures 2.2 and 2.3.

d = the mean chord length through the cell nucleus (~ 6μm).

$\mathbf{R_p}$ = the mean projected range of the relevant tracks. If Rp > d, Rp/d =1 which partially allows for the reduced multiplicity of targets (number of DNA segments) at risk for the short range 'stopper and insider' tracks in the cell nucleus.

$\mathbf{n_0}$ = the number of dsb segments at risk per track traversal (~ 15 for fast ions). n_0 will depend on the dimension of the mean chord distance through the cell i.e. whether it is flattened by plating or free in suspension.

$\sigma_{g, DNA}$ = the projected geometrical cross-sectional area of the intranuclear DNA. It is dependent on cell type and on the stage in the cell cycle. For V-79 hamster cells, the projected area of the DNA averaged over the cell cycle is about 3.0μm^2.

σ_S, the saturation cross-section defined above, can be expressed as $\sigma_{g, DNA}.n_0.R_p/d$. If $R_p > d$, $R_p/d = 1$. The cell radiosensitivity function, $Z(F,t_i)$, is presumed to correct for changes in the DNA configuration during the cell cycle.

Φ_{eq} = the equilibrium fluence of the relevant charged particles in the cell nucleus. Values for most radiations are given in reference [69]. $\varphi_{eq}(E)$ is the differential fluence in the energy spectrum.

$\varepsilon_{dsb}(\lambda)$ = the efficiency for production of dsbs in the DNA by direct plus indirect action is given by: $\varepsilon_{dsb}(\lambda) = (1-e^{-(2\lambda+s)/\lambda})^2$.

$\boldsymbol{\lambda}$ = the mean free path for linear primary ionisation of the equilibrium particle tracks [Watt 69, 71]. (More strictly, the mean *spacing* between ionizations rather than the mean free path is the relevant quantity, especially for electron tracks, but numerical data on spacings are not yet available).

Λ (~ 1.5 nm) is the mean diffusion length in the immediate vicinity of the DNA molecule for active radicals (indirect action) originating from a line source and 's' ~ 1 nm is the thickness of a single strand of DNA.

$\varepsilon_{ssb}(\lambda) = 1 - e^{-(2\Lambda+s)/\lambda}$, is the efficiency for ssb production in the DNA by direct plus indirect action in a single DNA strand of width s nm.

$\mathbf{U(Z, t_m, t_r, t_i)}$ = the probability that dsb's in the DNA remain unrepaired. t_m, t_r, and t_i are respectively the time to mitosis, the mean repair time and the duration of the irradiation.

Radiosensitization due, for example, to the presence of oxygen will occur only if the lambda value for the radiation is greater than λ= 2nm i.e. in the region of unsaturated damage. Allowance for radiosensitization or radioprotection due to chemical additives is affected by the consequent change in the diffusion length, Λ, in the efficiency term,

$$\varepsilon_{dsb}(\lambda) = (1 - e^{-(2\Lambda+s)/\lambda})^2$$

Looking at this in terms of the cell cycle there is a need to consider the effect of timings and the affect this will have on the effectiveness of the nuclide, Watt (185,186,187) has discussed the relationship between the timings stated above, for heavy particles. These relationships are shown in summary below.

2.10 For Synchronised Cells:

$$U(Z,t_{m,r,c,i}) = \frac{1}{t_i}\int_{t_c}^{t_c+t_i} Z(F,t)\cdot e^{-(t_m-t)/t_r}\cdot dt \qquad 2.11$$

This represents the probability that radiation induced dsb's in the DNA will remain unrepaired at the end of the cell cycle for synchronised cells. t_c represents the time into the cell cycle at which the irradiation begins.

2.11 For Asynchronised cells:

$$U(Z,t_{m,r,i}) = \frac{1}{t_i}\cdot\frac{1}{t_m}\int_0^{t_m}\int_{t_c}^{t_c+t_i} Z(F,t_j)\cdot e^{-(t_m-t_j)/t_r}\cdot dt_j\cdot dt_c \qquad 2.12$$

This represents the probability that radiation induced dsb's in the DNA will remain unrepaired at the end of the cell cycle for asynchronised cells.

Z (F,t) is an approximation for the change in radiosensitivity during the cell cycle. The radiosensitivity of the cell is a difficult parameter to model since the cell and its contents are not static and change over time. However these times can be generalised into different degree of activity i.e. S phase being less active than the G1 and G2 of the mitosis phase.

What is important here is the interaction of the radiation with the critical target (DNA double strand) and although the effect of the cell cycle will play a role in the cell inactivation, it is the ability of the radiation to create dsb's that will be the most important factor. It is necessary however, to take into account the fact that at G1/2 phase the probability of interaction with the DNA double strand will increase compared to the S phase.

Before the model is adapted for Auger electron emitting radionuclides a review of Auger electron emitters and their dosimetry is carried out in the next chapter.

CHAPTER THREE

Auger Electron Emitting Radionuclides and Dosimetry of Internal Emitters

3.1 Auger electron emitting radionuclides: A background to the Auger effect.

In the early 1920's Pierre Auger [75] was investigating electron tracks produced by photoelectric interaction of low energy X-rays, in a cloud chamber. He observed that in many instances multiple electron tracks emanated from the same point in the chamber. He concluded that the multiple electron emissions arose from the inner shell atomic electron transitions in which the energy gained (δE) would, instead of being released as a characteristic photon, be transferred to an orbital electron ejected with an energy (δE)-E_b,. Where, E_b is the binding energy of the ejected electron. This non-radiative transition process which, competes with the radiative transitions (characteristic x-ray emissions) has been called the Auger Effect in honour of its discoverer. The probability of emission of a characteristic x-ray is given by the fluorescence yield (ω). The probability of an Auger transition is given by 1-ω.

The Auger effect is a process in which an excited positive ion loses energy by the emission of an electron with a characteristic kinetic energy rather than by the emission of a photon.

Apart from hydrogen and helium, all the elements in the periodic table can emit 'Auger electrons' and can be identified by their Auger spectra. However, even hydrogen and helium can be detected by their influence on the Auger spectra of other elements in compounds.

The efficiency of the Auger emission varies across the periodic table by an order of magnitude. This variation depends upon the electronic structure of an atom rather than upon it's atomic number.

The energy of the Auger electron is small, typically 10-1000eV. It's mean free path in condensed material is short (~ 0.4-4nm).

3.2 The Auger Process.

When an atom is struck by an energetic particle or photon, a vacancy may be formed in one of its inner electron shells. This vacancy can be filled by another electron making either a radiative or non-radiative transition, i.e. either the excited atom, relaxes by the emission of a photon, which typically is an x-ray, with probability ω, or it may eject an Auger electron, with a probability σ, where $\omega + \sigma = 1$. It is however sometimes difficult in practice to demonstrate this identity because of cross transfers of energy between different electron subshells. This has been discussed by Fink *et al* [76].

Auger electron emission is the preferred relaxation process for exciting electron energies below 10keV, and for atoms with atomic numbers below 33, as described by Wentzel's [77] simple relation for the probability of x-ray emission, by the formula.

$$\omega = (1 + b\,Z^{-4})^{-1} \qquad 3.1$$

Where Z is the atomic number, and b equals $1.12x10^6$ for the initial creation of a K hole and equals $6.4x10^7$ for the initial creation of an L_3 hole.

The complex cascade that follows in the resulting filling up of the vacancy is dominated by non-radiative (NR), Auger (A), Coster-Kronig (CK) and super Coster-Kronig (sCK) [78] processes. Briefly these can be illustrated diagrammatically as figure 3.1.

Fig 3.1 Diagrammatic representation of the types of transitions.

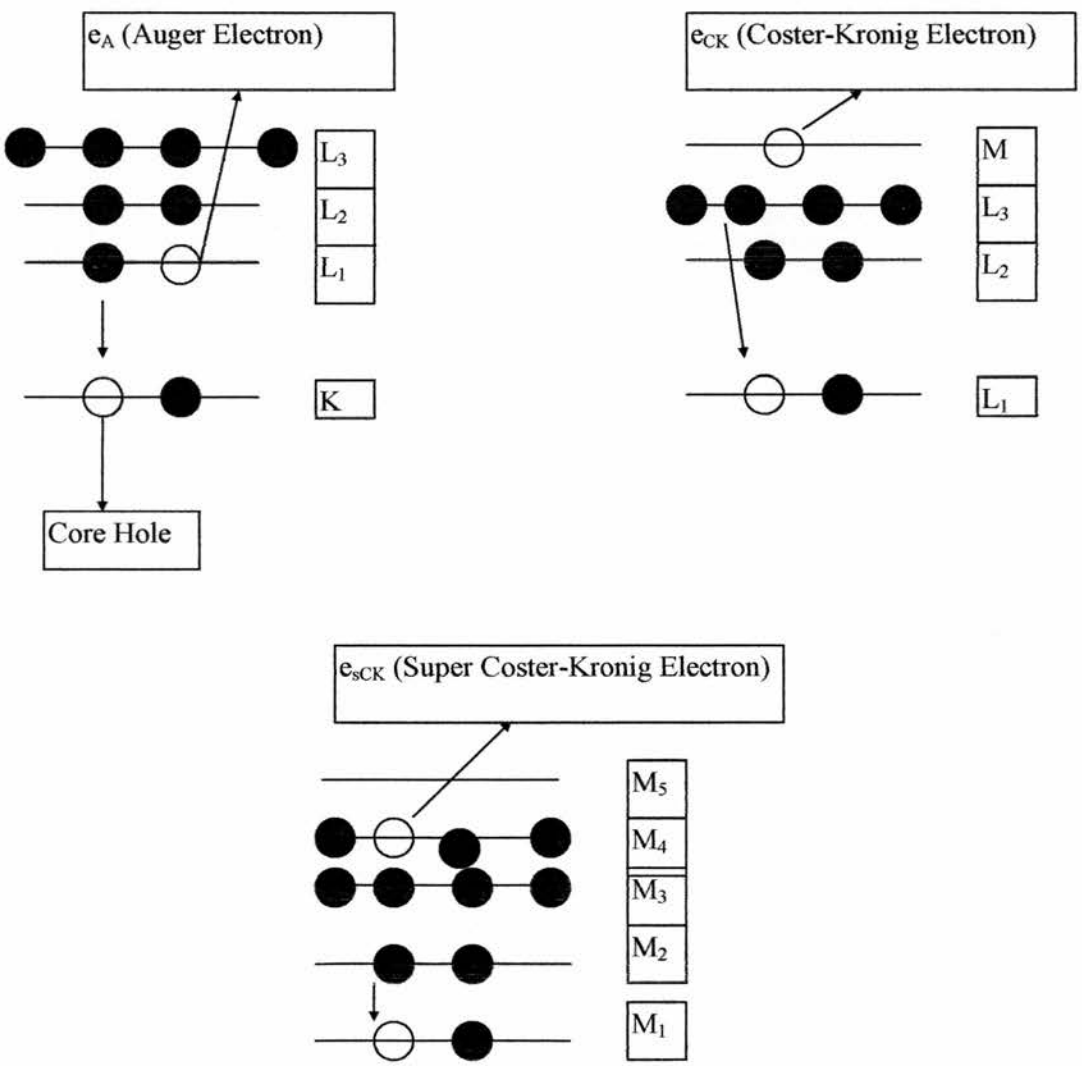

K, L, and M being the inner electron shells. This is demonstrated clearly for the Auger process in SnO_2 as shown in Fig 3.2.

Fig 3.2 Diagrammatic representation of the transitions in Tin oxide.

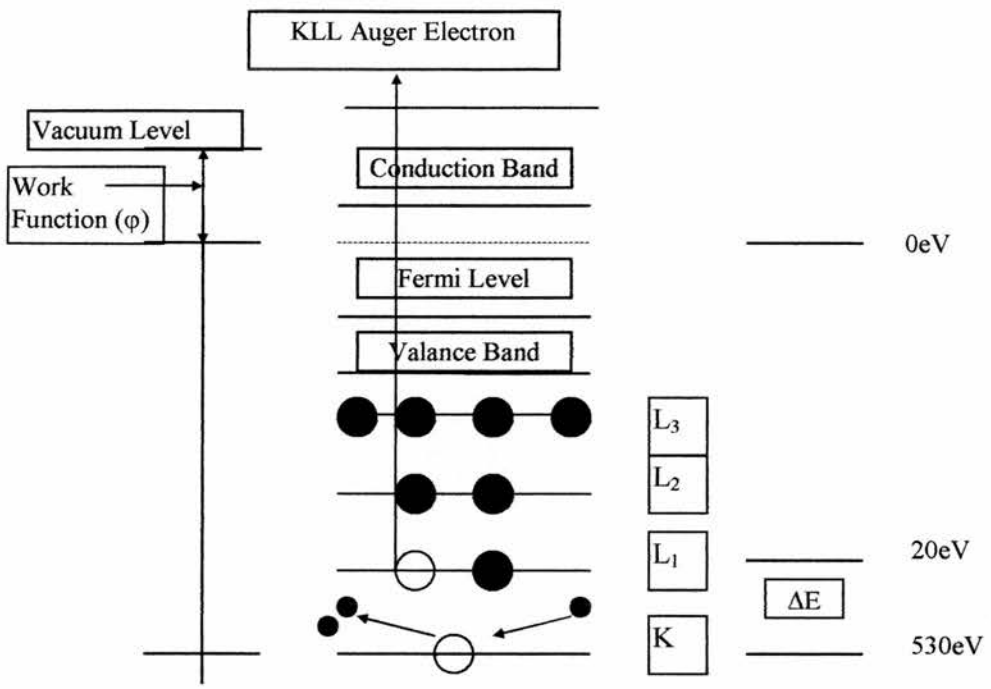

The experimentally determined relationships between x-ray, Auger and Coster-Kronig yields for the K and L shells were shown by Krause [79]. The main results are shown below diagrammatically, Fig 3.3.

Fig 3.3 Relationship between yield and atomic number (Z) of Auger electron for different shells.

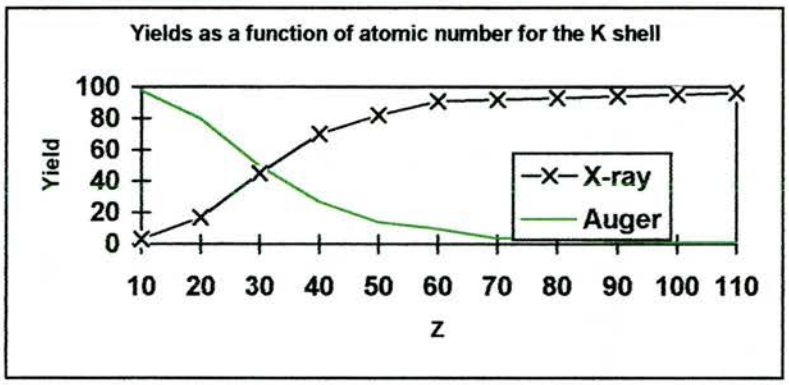

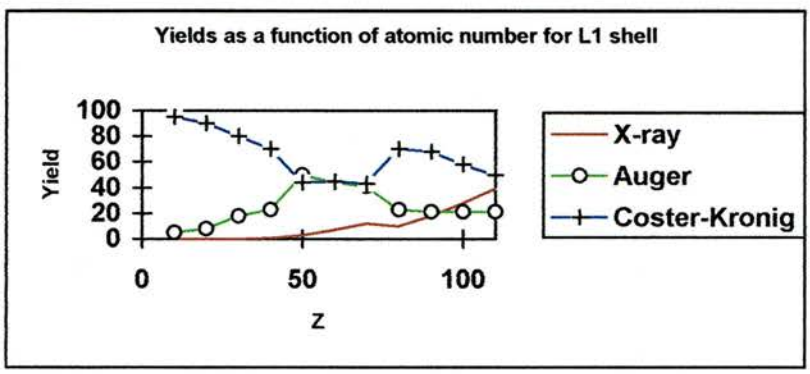

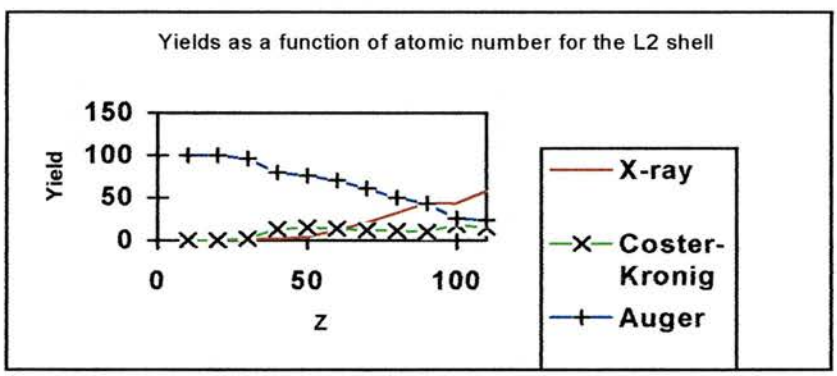

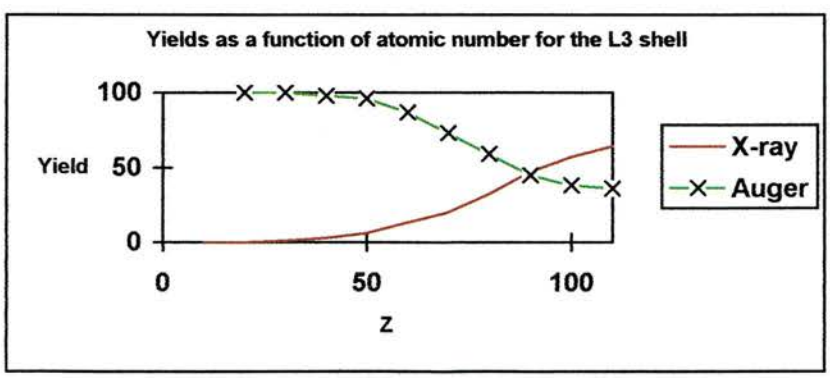

The results indicate that the Auger method is particularly sensitive to the lightest elements only, but this is not true since the different Auger transitions combine to give an analytical method, the sensitivity varying only by an order of magnitude for all elements in the periodic table.

These processes can be expressed as follows. Let the inner-electron shell be K, the outer-electron shell be L, the energy of the photon be M, the respective electron binding energies be E_K, E_L and E_M, and the kinetic energy of the Auger electron be E_A, then,

$$K = E_K - E_L \qquad \text{Photon Emission} \qquad 3.2$$

$$E_A + E_M = E_K - E_L \qquad \text{Auger Electron Emission} \qquad 3.3$$

or

$$E_A = E_K - E_L - E_M \qquad 3.4$$

Such an Auger transition is described as a KLM Auger transition.

From this it can be summarised that the ejection of Auger electrons involve a concealed radiative process as discussed by Butt [80] However, this cannot be true because KLL transitions, which involve a change in both the principle quantum number n and the azimuthal quantum number l, imply that Auger electron emission does not involve a radiative process and should be regarded as a simple two-electron coulombic readjustment of the initial 'hole'. In the KLL Auger transitions, only two electron shells are involved, and either one may label the process as K-L_1L_2, KL_1L_2, or if there is an ambiguity as to exactly which electron levels are involved, one may write $KL_1L_{2,3}$ or simply KLL, with the convention that the subshells are written in order of increasing index.

Alternatively if the final electronic state of the atom is known, it may also be added i.e. $KL_1L_2(3p)$.

A KL_1L_2, Auger transition of a free atom with atomic number Z can be described as;

$$E_A(Z) = E_K(Z) - E_{L1}(Z) - E_{L2}(Z) \qquad 3.5$$

Or, for a solid;

$$E_A(Z) = E_K(Z) - E_{L1}(Z) - E_{L2}(Z) - \varphi \qquad 3.6$$

Where φ is the work function of the material.

In these equations the statement $E_K(Z) - E_{L1}(Z)$ is true but because of the interaction between the two holes which occur in the final Auger state, $E_{L1}(Z)$ is not even approximately equal to $E_{L2}(Z + \Delta)$, where Δ generally lies between 0.5 and 1.5. Δ an empirical constant, summarising the extra kinetic energy that an electron acquires as it escapes from a multiply charged anion. The value of this kinetic energy was calculated by Hedin and Johannson [81]. Packer and Wilson [82], published tables of Auger energies for values of E_A between 0 and 1500eV based upon a relation in which Δ is equal to either 0 or unity. In addition to knowing how the energy of an Auger transition can be calculated, one must also know what Auger transitions can occur. Considering all transitions based upon the K and L electron levels which are shown diagrammatically Fig 3.4

Fig 3.4 Diagrammatic representation of electron levels.

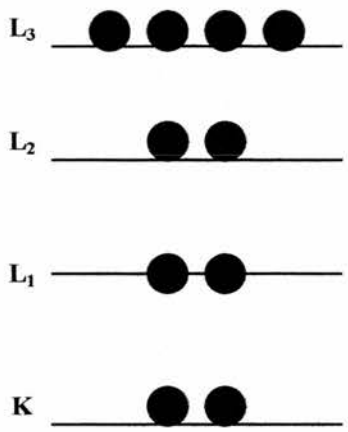

six transitions are possible: KL_1L_1, KL_1L_2, KL_1L_3, KL_2L_2, KL_2L_3 and KL_3L_3. This is true for the high-atomic number elements ($Z \geq 80$) where spin-orbit coupling predominates over coulomb interactions and the two holes involved in the Auger process can be regarded as being in a definite state of l and j: 0, 1/2 for L_1; 1, 1/2 for L_2; 1, 3/2 for L_3. j-j coupling occurs in these cases to give six possible Auger transitions. For the lowest -atomic-number elements ($Z < 20$) and for binding energies less then several kiloelectronvolts, pure L-S coupling occurs and only five Auger transitions occur because for such elements, couplings intermediate between the two extremes of L-S and j-j are possible. This was observed by Hornfeldt *et al* [83] who have evaluated the relative energies of all these KLL Auger transitions.

In addition to having characteristic energies, Auger transitions have different probabilities, which depend almost entirely upon, and can be calculated from the transition rate matrix elements.

For primary- electron energies of 3keV, the initial hole is created in 10^{-16}s. This hole lives for at least 10^{-15}s (time which is independent of atomic number), which means that the excited atom 'forgets' the original excitation and, as a result, the primary energy is dependent only on the energy levels of the atoms involved.

Another consequence of the time over which transitions occur appears in Coster-Kronig [78] transitions. In such transitions, the initial hole occurs in an electron shell and is filled by an electron from a subshell with the same principle quantum number. This is the case with L_1L_2M Auger transitions, which is energetically possible when the atomic number is less then 40. In 'super Coster-Kronig' transitions (where electrons involved in the Auger transitions come from the same principle quantum number, $M_1M_2M_3$), there is a particularly large overlap of the wavefunctions involved, and the transitions occur very rapidly in about 10^{-16}s (about the time required for an electron to make a single orbit).

Burhop and Assad [84] have shown that Coster-Kronig transitions are about 10 times broader than simple Auger transitions. They are typically between 2 and 10eV wide. The occurrence of Coster-Kronig transitions lead to changes in the intensities of the Auger signals , e.g. if the L_1 shell is ionised, fast Coster-Kronig L_1L_2Y transitions occur, and the simple Auger process L_1XY is less likely because of competition from the L_1L_2X Auger process which has in turn been introduced via the L_1L_2 transitions.

3.3 Auger and Coster-Kronig (CK) electron energies

From a zeroth order approximation the basis for estimation of the energies is as follows:

Considering an Auger or CK transition abc, in an atom of atomic number Z, in which an initial vacancy in the subshell 'a' is filled, leaving a vacancy each in the higher subshells b and c. The transition energy is given by,

$$E^{Z}_{abc} = B^{Z}_{a} - B^{Z}_{ba} \qquad 3.7$$

which is the energy of the electron ejected into the continuum, B^{Z}_{a} is the binding energy of the electron in the subshell 'a' of the neutral atom Z, and B^{Z} is the energy required to remove one electron from b and one from c. The latter quantity depends on the multiplet structure of the interacting pair of holes in the final atom.

Quantum mechanical calculations of Larkins [85] takes this into account and the transition energy is obtained as the difference between the total energies of the initial and final electronic configurations. B^{Z}_{a} is experimentally known. The quantity B^{Z}_{bc} is estimated using the experimental binding energy (B^{Z}_{b}) for an electron in the state b in the atom Z. For the electron in state c, it's binding energy in the atom (Z+1) is used. This takes approximately into account the altered binding energy of electron c because of the presence of the hole in state b. This is the basis of the Z/(Z+1) rule, and details of multiple structure are ignored. In it's simplest form, this rule gives the energy as

$$E^{Z}_{abc} = B^{Z}_{a} - B^{Z}_{b} - B^{Z+1}_{c} \qquad 3.14$$

and in a symmetrical form, taking account of the identical nature of the electrons,

$$E^{Z}_{abc} = B^{Z}_{a} - (1/2)[B^{Z}_{b} + B^{Z+1}_{b} + B^{Z}_{c} + B^{Z+1}_{c}] \qquad 3.15$$

These equations show that E^{Z}_{abc} must be positive for the CK transition abc to be possible and the CK electron energies are small. The use of these equations need to be considered carefully.

The common feature of all three electron generation processes i.e, photoelectric, electronic capture and internal conversion is that they produce an electron vacancy in the deep inner atomic shells e.g. K, L, M, N and O shells of the residual atom. The resulting emissions are (a) characteristic atomic x-rays due to radiative (R) transitions and (b) characteristic electrons due to non-radiative (NR) transitions of the Auger, Coster-Kronig and super Coster-Kronig type. Both types of transitions, radiative and non-radiative, are initiated by a primary vacancy and compete with each other in filling the initial vacancy. This leads to upward mobility of the vacancy to higher atomic shells or subshells. The newly produced secondary vacancies repeat the process and this goes on until all vacancies are moved to the outermost shells and the atom reaches a stable electronic configuration.

Auger electron energies are calculated using the Z/Z+1 rule of Chung et al [86].

$$\mathrm{E}^{z}_{abc} = B^{z}_{a} - \frac{1}{2}(B^{z}_{b} + B^{z+1}_{b} + B^{z}_{c} + B^{z+1}_{c}) \qquad 3.10$$

abc = transition.

3.4 Auger emitters used in medicine.

Some radionuclides which are potentially useful for tumour therapy by emission of Auger electrons are:

^{51}Cr, ^{64}Cu, ^{67}Ga, ^{73}Se, ^{75}Se, ^{77}Br, ^{80m}Br, ^{94}Tc, ^{99m}Tc, ^{114m}In, ^{115m}In, ^{123}I, ^{124}I, ^{125}I, ^{167}Tm, ^{193m}Pt, ^{195m}Pt.

Some radionuclides which are useful for therapy by alpha particles with additional emission of Auger electrons are:

^{211}At, ^{212}Bi, ^{255}Fm.

Some radionuclides which are potentially useful for electron Auger-therapy with simultaneous PET (Positron Emission Tomography) diagnosis are:

^{73}Se, ^{94}Tc, ^{124}I.

Decay modes and half-lives of the above radionuclides are listed in Table 3.1

Table 3.1 Decay modes and Half lives of some Auger electron emitting radionuclides.

Radionuclide	Decay Mode	$T_{1/2}$
^{51}Cr	IC+EC	2.77days
^{64}Cu	$EC+\beta^-+\beta^+$	12.7hours
^{67}Ga	IC+EC	3.36days
^{73}Se	$EC+\beta^+$	39.8hours
^{75}Se	IC+EC	1.20days
^{77}Br	IC	2.38days
^{80m}Br	$IC+EC+\beta^-+\beta^+$	4.42hours
^{94}Tc	$IC+EC+\beta^+$	4.42hours
^{99m}Tc	$IC+\beta^-$	6.01hours
^{114m}In	IC+EC	4.95hours
^{115m}In	$IC+\beta^-$	4.49hours
^{123}I	EC	13.2hours
^{124}I	$EC+\beta^+$	4.18days
^{125}I	IC+EC	60.1days
^{167}Tm	IC+EC	9.25days
^{193m}Pt	IC	4.33days
^{195m}Pt	IC	4.02days
^{211}At	$IC+EC+\alpha$	1.01hours
^{212}Bi	$IC+\beta^-+\alpha$	7.21hours
^{255}Fm	$IC+\alpha$	5.30hours

Energetic photons and beta rays can have csda ranges of cm dimension in the microscopic domain of conventional dosimetry. However, this is not so for Auger electrons many of which have short ranges of the micron / nanometer order.

Complete experimental Auger and Coster-Kronig electron spectra are available in very few cases. These have been calculated with a certain degree of confidence by several authors including; Chung and Jenkins [86], Mc Gurie [87], Charlton and Booz [88], ICRP [89] and Howell *et al.* [90, 91]. While the average spectrum per decay is useful for interpretation of radiobiological results, the spectra of individual decay events are needed for dosimetry at the micro and nanometer level.

The average spectrum methodology has been accepted as standard. A brief summary is given in the next chapter including comments on reasons for inappropriate use of this method for Auger electron emitters.

3.5 Current theory in internal dosimetry

3.5.1 Basis for dosimetry

In higher organisms DNA is organised in discrete pairs of chromosomes and the induced re-organisation of these chromosomes can lead to cellular lethality and possibly mutations. Chromosomal re-arrangements frequently lead to a wide variety of cancers depending on the type of re-arrangement of the chromosomes. The chromosome aberrations have been shown to depend on a wide set of parameters including dose, rate, temperature, cell cycle (G2 being the most sensitive stage as is shown clearly by Geard [92].

Lea [2] concluded that chromosome breaks were caused by several ionisations produced by a single charged particle and that for low-LET radiations the yield

of two-break aberrations, those that are of particular interest, follows the well known form:

$$Y = \alpha D + \beta D^2 \qquad 3.11$$

Where Y = the yield of lesions and D= the absorbed dose. α and β are coefficients to be determined. This equation implies that the aberration is due to two chromosome parts being damaged by the same particle track, the linear term in dose, or two chromosome parts being individually damaged by two separate particle tracks, the quadratic term in dose.

When a moiety of the DNA is damaged in isolation i.e. without damage to neighbouring groups, this is known as a 'singly damaged site'. Such a site would be expected to be produced by e.g. the reaction of a single radical or reactive molecule or a single ionisation. It is clear that repair of singly damaged sites has the potential to be carried out efficiently and accurately using the complementary undamaged strand as a template.

Even though a variety of damaged sites are produced, it is possible to propose mechanisms for their successful repair using known enzymatic functions, Friedberg *et al* [93]. However, it should be noted that it has been shown [93] that 2.6 million SSB's are necessary on average to kill a cell from H_20_2 SSB's present in cellular DNA at a lethal dose of 10gray of ionizing radiation.

The ability of a lesion to kill a cell can be measured as the number of lesions necessary to kill 63% of the cells at risk. (At this fraction of cells killed, it can be shown that, on average, each cell has sustained one lethal event.)

The efficiency of ionising radiation in killing cells while producing relatively low levels of DNA damage lies in its ability to produce damage in which more than one moiety in a localised region of the DNA is damaged. These lesions are known as 'locally multiply damaged sites' (LMDS).

3.5.2 Structural Organisation of DNA

At the lowest order of organisation, DNA is coiled around histones into nucleosomes. These structures are disk-like with a thickness of 5.7μm and a radius of 5.5μm, two coils of DNA wrapped around each circumference 2.7μm apart. The nucleosome core is made up of histone proteins, but is not tightly packed. The DNA and proteins contain hydration (bound) water (0.3g/g). (This corresponds to five water molecules per nucleotide). 60% of the particle volume is water, hence the core particle structure is a relatively loose complex of compartments, and the solvent spaces are accessible to smaller molecules such as sucrose and glycerol (0.3μm in diameter) but not to larger molecules such as cyclodextrin (1.6μm in diameter). Pores exist into which smaller molecules can enter and these pores have a diameter between 0.3 and 1.6μm. Small molecules, even though they enter the structure do not exchange with the water of hydration and apparently cause no change in the structure of the nucleosome up to a concentration of $10\mu m^3$ (sucrose).

It is important to note that when Auger emitters are attached to DNA in the cell nucleus, the energy is not deposited throughout the cell nucleus and the dose to the DNA is not equal to the cell nuclear dose.

The values of the mean energy deposited per decay to DNA from Auger emitters attached to DNA have been published for a few radionuclides, J.L Humm [94]. There is some evidence that double strand breaks lead to cell death, G.M Markrigiogos et al [95]. Some have concluded that DNA may not be the appropriate biological target KG Hofer, et al [96]. It has also been shown that cell death by Auger emitters attached to the DNA requires hundreds of decays per cell nucleus, AI Kassis, et al [97], KG Hofer et al [98].

These conclusions regarding the suitability and effectiveness of Auger emitters in causing DNA strand breaks and cell death hint at the idea that it may not be the dose delivered that is important but some other properties of the radiation that is the defining factor in causing damage.

Beta particles e.g. from H-3 and K-40 have ranges, micron to millimetres. These can produce damage of similar magnitude to that produced by an electron generated by gamma rays. If these emitters are incorporated into the DNA there is a possibility of biological affects caused by the actual transmutations of the nuclides. This cannot be properly accounted for by any specification of absorbed dose.

Alpha particles in condensed organic media have ranges in the order of micrometers. The tracks from these radionuclides are non-uniformly distributed in tissue and therefore the effects can not be adequately quantified in terms of absorbed dose.

Auger emitters can cause very high doses in localised regions. However this dose may be insignificant if spread over the tissue. The application of absorbed dose in not expected to be valid for the same reasons given for alpha particles.
It is clear that the free radicals that react within a cell will do so at short distances (nanometres) from their site of origin. Therefore, in attempting to describe the nature of damage produced by ionising radiations in the DNA in mammalian cells, the spatial distribution of the species produced within the spur, blobs and short tracks must be considered in conjunction with the structures in which the DNA is packaged.

Kassis *et al* [99] have shown that radiobiological effects following the decay of such radionuclides are not readily predictable because of their dependence on the localisation of the radionuclide relative to the radiosensitive target within the nuclear DNA, the energy, number, interval of release etc. of the Auger electrons and the pattern of energy deposition of these electrons at the microscopic level. They have also shown that the extreme radiotoxicity of ^{125}I incorporated into the DNA as the halogenated pyrimidine nucleotide is independent of specific activity, when decaying in close proximity to DNA, the radiotoxic effects of ^{125}I and ^{195m}Pt produce high-LET-type curves. ^{125}I incorporated into the DNA in Mid-S-Phase is more radiotoxic than when in early S-Phase. Auger-electron-emitting radionuclides that are concentrated by cell and are not bound to or incorporated into DNA produce low LET-type survival curves, whether localised in the cytoplasm or more diffusely distributed within the cell.

3.5.3 MIRD Internal Dose Methodology

The Medical Internal Radiation Dose (MIRD) [100] Committee was established by the society of Nuclear Medicine in the 1960's to assist the nuclear medicine community in estimating absorbed radiation dose to organs and tissues from radioactive material located inside the human body.

The MIRD scheme [100] is primarily intended for calculating radiation absorbed doses received by patients who are undergoing nuclear medicine tests and not for the purpose of directly linking the dose to the radiation effects. In the MIRD scheme [100], the body is considered to consist of source organs which, accumulate a significant amount of radioactivity and target organs, which are irradiated by the source organs. The *absorbed dose* to a target organ from its exposure to a source organ is given by:-

$$D_{t\leftarrow s} = A_s S_{t\leftarrow s} \qquad 3.24$$

A_s = accumulated activity in the source organ.

$S_{t\leftarrow s}$ = mean dose in the target organ per unit accumulated activity in the source organ and is usually referred to as the S-factor.

The methodology assumes the following:

1 Localisation of energy is homogeneous.

Within the "source" organ, an arbitrary mass of tissue contains the same amount of radioactivity as any other mass of tissue. The concentration of radioactivity is uniform.

2 The radioisotope label is an alpha-emitter.

The range of an alpha particle is of the order of 40-80 microns in tissue. "Local Energy deposition", i.e. all energy deposited where it is created.

Radiation does not extend beyond the anatomic boundaries of where the pharmaceutical localises, i.e. Source organ = Target organ.

3 One alpha emitted per nuclear decay. Each Bq of radioactivity contained within the "source" organ results in a like number of alpha particles being emitted per sec. Integrating the activity (1 Bq = disint/sec) over time gives the total number of nuclear disintegrations.

The model has modifications which allow it to account for multiple radiations with fractional abundance, radiation other than alpha and radiation from multiple sources but the three assumptions are not eliminated, they are valid throughout. The method uses Monte Carlo techniques, which has the disadvantage in cumulative dose statistics (i.e. organ dose, organ dose-volume) as an outline is required. MIRD scheme allows the total absorbed dose to every target organ to be derived including the situation of a target organ and source organ being the same.

Energy is deposited in a very erratic and stochastic fashion, so dose is only meaningful when the mass Δm is great enough to average out the statistical variation in the number of energy events that occur in the volume.

Dose represents energy deposited in the medium by any process, including the production of ion pairs, electronic excitation, and deposition of normal energy. Since this is the definition of dose, and since each of the three final expressions of energy absorption are certain to have different biological effects, dose is not in itself an adequate prediction of biological effect.

A further complication of the concept of dose is that energy may be transferred in one location in the medium and absorbed at another location away from the initial transfer point. Only the energy absorbed in the local medium is of any importance in establishing the final level of damage in the medium.

The primary interactions of photons, neutrons and charged particles are quite different and the direct consequences of the primary collisions can also be quite different. Thus, the energy absorbed to produce a track is not a very good quantity for clarification in radiation research in spite of its wide usage.

3.5.4 ICRP Internal Dosimetry.

It is the absorbed dose averaged [101] over a tissue or organ and weighted for the radiation quality that is assumed to be correlated with biological effects. The primary radiation protection quantity, equivalent dose, was defined to place all ionising radiations on a common scale of biological harm, without regard to the particular tissues irradiated or biological endpoint involved. The total biological harm is given by the joint distribution of the equivalent dose in the irradiated tissues and the sensitivity to the radiation dose.

3.5.5 Conventional Dosimetry.

MIRD and ICRU methods for estimation of doses to organs containing radionuclides are essentially the same. They assume that the radionuclide and the radiation energy are uniformly distributed in the organ. Using these assumptions, the average dose rates and cumulative average doses to any organ from radioactivity localised in the same organ or from another organ acting as the source of radiations are calculated. These two methods provide good first

steps towards dosimetry of radionuclides in the body. These methods commonly termed 'conventional dosimetry' are given by:

$$R_{con} = (A/m) \Sigma \Delta_i \phi_I \qquad 3.13$$

where:

R_{con} = average conventional dose rate (rad/hour)

m = mass of organ (g)

A = radioactivity at any instant (μCi)

ϕ_i = absorbed fraction of the ith radiation

Δ_i = equilibrium absorbed dose constant = 2.13 $n_i.E_i$

n_i = average yield of the ith radiation/decay

E_i = average energy of the ith radiation in MeV

The average absorbed dose to the organ is obtained by replacing the instantaneous activity A by the cumulative activity

$$\tilde{A} = \int A(t).dt \qquad 3.14$$

These methods assume that the average dose rates and doses to the organ as a whole are also the same to the cells of interest in the organ. For radiations with macroscopic mean free paths theses methods are acceptable and adequate, however, it is inadequate for radiations of microscopic mean free paths, such as low energy electrons. This has been clearly demonstrated through *in vitro* experiments by Fienendegen, [102], Chen et al [103], Hofer [104], Commerford et al [105], and by Kassis et al [106], and through *in-vivo* studies with thallium-201 in the testes of mice, a good comparison with man, by Rao et al [107].

For a realistic calculation it is necessary to have information of the radionuclide decay schemes and the radiation track structure along with information on the

physiological distribution of the radionuclide in the biological system of interest.

3.6 Dosimetry of Auger Emitters.

The dosimetry of internal emitters was neglected for a long time because the energy deposited in tissue by Auger electrons is usually negligible compared to the total energy released in the decay of the radionuclide.

Conventional internal dosimetry i.e. the MIRD [100] Schema, ICRP [10] and the ICRU [101] procedures, are used with the assumption that the radionuclide and the radiation energy are uniformly distributed in the organ. Low-energy electrons from Auger emitters contribute negligibly to the macroscopic dose and their potential for localised damage is ignored. This approach does not consider either the chemical form and the subcellular distribution of the Auger emitter, or the possibility that the radionuclide may be concentrated by the cells. The cellular geometry and the packing of cells in the organ are ignored. The inadequacy in conventional dosimetry has been shown by Adelstein *et al* [108] and Rao *et al* [109]. These results indicate the need for subcellular dosimetry of internal Auger emitters.

The limitation of conventional internal dosimetry has also been demonstrated by the study of Makigiorgos *et al* [110], Feinendgen [111], Chan *et al* [112], Lomerford *et al* [113], Martin and Haseltine [31], and by Kassis *et al* [114]. The importance of these electrons was first noted by Carlson and White [115]. In nuclear chemistry, they demonstrated that a large number of non-radiative

transitions follow the creation of a vacancy in the inner atomic shell and since each positive charge on the residual atom is the consequence of an electron emission, anywhere from 1-20 Auger electrons can be emitted per K to L shell vacancy with an average of about 7-10. The energies of these electrons depend on the atomic binding energies of the atom, most with <500eV and <25nm in unit density matter.

The higher than expected influence of localised Auger electron emitters has been demonstrated by Hofer [116, 117] using the radionuclide I-125 which produces high energy concentrations within nanometer distances of the point of decay. The decay of I-125 via EC and IC is followed by stochastic cascade of low-energy Auger and Coster-Kronig electrons from the excited tellurium daughter atom. The number of electrons emitted in a single decay ranges from 1-50 with energies <1keV and ranges <50nm as shown by Charlton and Booz [118] Hofer has shown that decay of I-125 attached to the cell membrane has relatively little biological effect. It should be noted that Hofer's calculations were based on LET, which as mentioned is not a good predictor of biological damage at the microscopic level.

The large variations between individual cells, particularly for inhomogeneous distribution of radionuclide is generally neglected, cell hit probabilities overlook the nature or magnitude of the energy deposition in the cell even full distributions of specific energy in the cells do not include information on the internal distribution and quality of the energy within the cell volume.

3.6.1 Principles of Current Auger Dosimetry.

From the conservation of Energy

$$\mathbf{T} = h\nu - E_b - T_a \qquad 3.15$$

$$= h\nu - E_b$$

T_a - kinetic energy given to the recoiling atom is nearly 0 and is neglected.

$$T_a/T = M_o/M_o \qquad 3.16$$

M_o = rest mass of electron

M_o = rest mass of recoiling atom

For the photo electric effect, the fraction of hν that is transferred to the photoelectron is:

$$T/h\nu = (h\nu - E_b)/h\nu \qquad 3.17$$

This is a first approximation of the total fraction of hν that is transferred to all electrons.

The binding energy E_b must be taken into account and part or all of it is converted into electron kinetic energy through the Auger effect.

The role of the Auger effect is to provide an alternative mechanism by which the atom can dispose of whatever part of the binding energy E_b is not removed by a fluorescent X-ray. If no X-ray is emitted, then all of E_b is disposed of by the Auger process. In the Auger effect the atom ejects one or more of its electrons with sufficient kinetic energy to account collectively for the excess energy - thus any energy invested in such Auger electrons contributes to the kerma.

An atom may emit a number of Auger electrons, more or less simultaneously, in a kind of chain reaction cascade. The atom thus exchanges one energetically 'deep' inner shell vacancy for a number of relatively shallow outer shell vacancies. (These vacancies are finally neutralised by conduction-band electrons.)

3.6.2 The Energy Budget in the Auger Effect.

Suppose a K shell vacancy is produced , with binding energy $(E_b)_k$. Assume that the vacancy is filled from by an electron from the 'L' shell, as is most often the case. Let the binding energy in that shell be $(E_b)_l$, then, either the atom will emit an X-ray of energy $h\nu_k = (E_b)_k - (E_b)_l$, or it must dispose of that energy (as well as the remaining energy $(E_b)_k - h\nu_k$) through the Auger effect. Assuming that the attempts are entirely for the Auger effect, it may eject an electron from any shell outside of that in which the original vacancy occurred, in this the K-shell. If an M-shell electron is ejected, it will have a kinetic energy T_m equal to {Check the foregoing paragraphs to clarify the above"}

$$T_m = (E_b)_k - (E_b)_l - (E_b)_m \qquad 3.18$$

$(E_b)_m$ = binding energy in the M-shell

Now the atom has two electron vacancies, one in the L and one in the M-shell. Assume that two N-shell electrons move in to fill those vacancies, and that the atom emits two more Auger electrons. If they both happened to be ejected from the N-shell, the atom would then have four N-shell vacancies - one of these Auger electrons would have the kinetic energy

$$T_{Nl} = (E_b)_l - Z(E_b)_N \qquad 3.19$$

and the other would have

$$T_{N2} = (E_b)_m - Z\,(E_b)_N \qquad 3.20$$

Then the total kinetic energy of the three Auger electrons generated so far would be:

$$T_a = T_m + T_{N1} + T_{N2} = (E_b)_k - 4(E_b)_N \qquad 3.21$$

This process is repeated, increasing the number of electron vacancies by one for each Auger event that occurs, until all the vacancies are located in the outermost shell(s). The total amount of kinetic energy carried by all the Auger electrons together is equal to the original shell binding energy $(E_b)_k$ minus the sum of the binding energies of all the final electron vacancies.

Since an Auger chain reaction or 'shower' suddenly produces a multiply charged ion which may have a net positive charge even in excess of 10 elementary charges, the resulting local coulomb-force field can be quite disruptive to its molecular or crystalline surroundings.

3.6.3 Spatial distribution of energy density.

Generally the average absorbed energy densities are calculated for concentric spheres of tissue equivalent matter with the decaying radionuclide located in the centre. In these calculations it is assumed that the electrons are emitted isotropically, radiating outwards losing energy according to their stopping power. Moor and Sastry [119], Sastry and Rao [120] and Kassis et al [121], have produced plots of energy density versus the distance from the decay for K-40, I-125 and Br-77 respectively, taking into account the changes in dE/dR as

the electron slows down. The curves show a decay as the distance is increased as one would expect due to the short range of the Auger electrons.

3.6.4 Tissue Localisation of radionuclides.

The distribution of radionuclides in the tissue is a major cause of inhomogeneiety of fluctuation in energy deposition. Large inhomogeneities are inevitable over distances greater than the range of decay particles, unless the radionuclide is homogeneously distributed at a sufficient high concentration so that the mean distance between radionuclide decays is small compared with the particle ranges.

Generally studies involving spatial and temporal distribution of radionuclides have involved LET description of tracks and fluctuations described as hit probabilities. Fluctuation in subcellular targets is not carried out.

Considering that the dosimetry at the level of the cell or cell nucleus is of direct importance in comparing the effectiveness of similar radiations under different biological and physical conditions Fisher et al [122], in their in vitro simulations have shown that the spatial distribution of alpha particle sources can greatly influence the biological consequences to populations of cells that receive identical absorbed doses.

The microdosimetry of radionuclides depends largely on the chemical properties of the radionuclide mainly because the distribution in tissue and within cells at any given time is dependent on the solubility and chemical properties of the

radioactive atom or molecule. Radionuclides may be concentrated in different tissue or tissue components and deposit different amounts of energy in intercellular material, cell cytoplasm and cell nuclei. In these cases dosimetry and the measurement of biological effect based on the MIRD and ICRU methods become very inaccurate.

Kassis et al [99], have shown that concentrations of monovalent cations of potassium, rubidium and thallium are 50-130 times greater within cells in vitro than in the surrounding medium.

Rao et al [123], have shown that enhanced localisation of thallium occurs in or near the spermatogonia of mouse testes, which produces an increased biological effectiveness when compared with other radionuclides in causing sperm damage and weight loss in mouse testes and in killing cultured mammalian cells. They showed that a significantly larger average dose was delivered to the cells than would have been calculated by conventional methods of macroscopic dosimetry. These conclusions are further demonstrated by Kassis et al [124], Rao et al [125, 126]. It is clear that intracellular localisation of Auger electron emitting radionuclides produce an enhanced dose to cells and subcellular targets greater than those radionuclides that do not decay by Auger electrons.

When considering localisation within cells and dosimetry it is important to note that there will be large fluctuations in energy deposition in individual cells particularly at low concentrations of radionuclide. This is of particular importance in diagnostic medicine. The fluctuation at low concentrations

implies that a simple average energy deposition among cells will not adequately describe the probability of biological damage.

The pattern of energy deposition within a cell nucleus is known to influence its biological effectiveness. The energy deposition from low-energy electrons and alpha particles within cells, having a greater effectiveness than the same energy deposited by high-energy electrons, has been demonstrated by Goodhead et al [127]. This implies that information related to absorbed dose received by cells is not sufficient in predicting the probability of biological effect. It is clear that the microscopic pattern of energy deposition over nanometer distances is important in determining the quantity and quality of biological damage. LET - based calculations cannot describe accurately the mean energy in subcellular targets of dimensions such as DNA (2nm) and it cannot describe the fluctuations of energy deposition in the targets.

The radiation spectra provided by ICRP [10] and MIRD Committee [100, 128] are generally inadequate for radionuclides that decay by EC and IC i.e. Auger emitters. For the Auger emitters the very low-energy N and O shell electrons, which comprise the bulk of the electron emission for high Z elements, have been ignored in the ICRP and MIRD spectra. One of the main reason for this is due to the fact that these electrons are not important when calculating the dose to large volumes as is the practice of the two bodies. These low-energy electrons become important when calculating dose delivered to small volumes i.e. $<1\mu m$ as shown clearly by Howell [129].

The Auger electron spectra of radionuclides are discrete, reflecting the energies of orbital transitions within the atom. This implies that only a finite number of electron energies are possible. The number can vary from a few for low Z elements to hundreds for high Z elements.

Charlton and Booz [130] have shown that the permutations of individual electron spectra from Auger cascades in high Z atoms can be many thousands. This is mainly due to the fact that the creation of an inner atomic shell vacancy is a highly stochastic process. The permutation is much larger for atoms that undergo more than one Auger cascade per disintegration e.g. I-125 and Pt-193m.

There are several assumptions in the calculations of Auger electron spectra, which include: the frozen orbital approximation, where the electron transition probability data are for atoms containing only a single inner shell vacancy. The Auger electron energies are usually calculated using the Z/Z+1 approximation of Chung and Jenkins [86], Pomplun et al [131] who have a code to calculate binding energies for atoms with multiple inner-shell vacancy configurations but using the same frozen orbital approximation for the transition rates. This method does not account for the Coster-Kronig transitions therefore it is not a significant improvement on Chung and Jenkin's model.

A variety of methods have been used to determine the energy deposited in target regions by low-energy Auger electrons. One of the most commonly used is Cole's [132] empirical expression for the range energy relationship given below.

$$E(R) = 5.9\,(R + 0.007)^{0.565} + 0.00413\,R^{1..33} - 0.367\ (\text{KeV}) \qquad 3.22$$

and

$$R = 0.00431\,(E + 0.367)^{1.77} - 0.007\ (\mu\text{m}) \qquad 3.23$$

Where E is the energy in keV and R the range of the electron in μm. The differential energy dE/dR giving the stopping power in keV/μm for the electron.

For condensed media Howell et al [129] have improved the fit for energies less than 20eV for the range 3.8-20eV, producing the equation:

$$dE/dR = 29.5 - 666.67\,R \qquad 3.24$$

These equations are used to obtain absorbed doses in various target volumes containing the radionuclide.

Other methods have been used to calculate electron energy loss for incorporated radionuclides. Makrigiorgos [110] applied the restricted dose mean-LET with a cut-off energy of 100eV. Booz et al [133] produced a 3rd order polynomial fit. These methods provide average energy deposition in small targets.

The other main method of calculating energy deposition information from Auger electrons is through the use of Monte Carlo track structure calculations. The track structure codes simulate 1-100,000 electron tracks through the target

volume generally in a gaseous state, although recent models have simulations for water taking into account the hydration shell around the DNA molecule. There are numerous codes available including those of Paretzke [134], Terrisol et al [135] and Wright et al [136].

It should be noted that the more practical method of Cole [132] has been shown to provide an accurate estimate of average energy deposition in Auger emitters down to nanometer volumes.

3.6.5 ICRP Quality Factor and Radiation Weighting Factor for Auger Electrons.

The ICRP recommendations [138] implied that all electrons and radionuclide emissions such as beta rays and Auger electrons were considered to be equally radiotoxic and were assigned a quality factor (Q) of 1. It has become clear that this cytotoxicity of Auger electron emitters is much greater than expected especially when localised in the DNA. The ICRP introduced the concept of weighting factors W_R dropping the use of H and Q where,

$$H_T = W_R D_{T,R} \qquad 3.25$$

H_T = equivalent dose.

$D_{T,R}$ = absorbed dose from radiation R.

For a mixed radiation field H_T being,

$$H_T = \sum_R W_R D_{T,R} \qquad 3.26$$

The ICRP have assigned $W_R = 1$ for all electrons with the exception of Auger electron emitters bound to DNA but no specific value has been assigned for these radionuclides.

The recommendations of the ICRP above are clearly not satisfactory. It would be ideal if individual Auger electron emitting radionuclides / radiochemicals could be assigned a specific weighting factor, which is dependent on the decay spectra, localisation i.e. DNA, cytoplasm etc on the basis of its effectiveness in causing biological damage. This is an unrealistic aim as there is such a large number of radiochemicals used in nuclear medicine and medical research. These radiochemicals vary hugely in the manner of localisation, uptake, retention and decay spectra being a few of the factors that need to be taken into account when considering the dosimetry of Auger electron emitters.

Howell et al [139] have made attempts to improve the ICRP methodology, by considering results from experimental work using I-125. They have produced the equivalent dose as:

$$H_T = H_{T(Auger)} + H_{T(other)}$$
$$= W_{Auger} \sum_{R(Auger)} D_{T,\,R(Auger)} + \sum_{R(other)} W_{R(other)}\, D_{T,\,R(other)} \qquad 3.27$$

From the experimental work they have concluded that equivalent dose for subcellular distributions can be written as:

$$H_{T,\,R(Auger)} = (1 + f_0\,(W_{R(Auger)} - 1)) \sum_{R(Auger)} D_{T,\,R(Auger)} \qquad 3.42$$

Where

$W_{R(Auger)}$ = weighting factor for Auger electrons only.

f_0 = fraction of the organ activity bound to DNA.

The above formalism implies that it needs modification to account for positional effects i.e. where the Auger emitter is located in the target organ. There are

some results which indicate that it may be a factor of 2 greater when bonded to DNA compared to when it is not.

The equivalent dose ($H_{T,\,R(Auger)}$) needs also to be modified to take into account the fact that f_0 will vary during the period in which the dose is delivered.

Paschoa et al [140]. Have proposed an alternative method of Auger dosimetry considering the nuclide K-40. The dose D_N to the cell nucleus assuming a point source of Auger electrons at the centre of the nucleus is determined as;

$$D_N = \sum (f_i E_i / V_i) \sum (f_j E_j / V_j) (r_N / R_j) \qquad \text{for } R_i < r_N < R_j \qquad 3.29$$

Where f_i or f_j is the frequency per decay of emission of an Auger electron i or j, E_i or E_j corresponding to the energies of i and j electron; V_i or V_j the spherical volume of radius R_I or R_j these being the range of the Auger electron i or j; r_N is the radius of the nucleus. The range R, is determined using the Cole methodology described earlier. This model takes into account the volume and hence the spatial localisation but retains the application of absorbed dose with all its problems as a predictor of biological effectiveness.

Others have made verifications on the spherical model, for e.g. Nettleton et al [141] who considered an elliptical cell shape, with no significant difference found when compared to the spherical geometry used by others. They have used the S (absorbed dose per unit cumulated activity) factors in their calculations with it's limitations. S factors assume that the absorbed dose in individual cells is the same as the average dose in the organ.

Paschoa et al [140] have shown that K-40 is 140 times more effective than Cs-137 (a gamma emitter) in producing the same level of energy deposition. They have also shown that the M-XY and outer shell Auger electrons contribute about 90% of the total Auger electron energy deposition. They estimate the average uniformly distributed energy distributed energy deposited for males is around $3x10^8$ keVμm^{-3} and $2x10^8$ keVμm^{-3} for females. This is a reasonably high level of energy deposited, considering that ~100eV or greater in the DNA has been shown by Goodhead et al [16] to cause DNA double strand breaks (dsb's). How is it then that 'man' does not express the possible genetic changes. The answer has to be the fact that damage is repairable over a give time period and not all forms of damage are lethal and the specific localisation of the radionuclide i.e. in the DNA of the susceptible cell is a prerequisite for effective damage.

McLaughlin et al [142] have shown that the D-37 was 80 decays/cell for I-125. De Sombre et al [143] have shown that D-37 is in the range 300-600 decays/cell for I-123. This difference is unlikely to be due to the difference in decay of the radionuclides as I-125 has 2-Auger cascades per decay with on average 14 electrons. I-123 has 1-Auger cascade with 8 electrons, less than a factor of 2 difference.

Again this indicates that the effectiveness of the radiation is due to something other than the quantity of radiation. It is more likely to do with some fundamental parameter that is necessary to produce the end point of interest, i.e. for effective/irreversible damage at the end point and with which some

parameter of the radiation must correlate. It is the belief here that the spatial correlation of the radiation in question with the spatial separation of the DNA double strand is the important relationship in causing effective/irreversible damage.

Having examined the characteristics of Auger electron emitters and the current methods of dosimetry for these radionuclides, the next chapter explores the application of the template model to determine the cytotoxicity of these emitters.

CHAPTER FOUR

Application of The Template Model for Auger Electron Emitters

4.0 Dosimetry of Auger Electron Emitters: Need for Change?

4.1 Introduction

Unsolved difficulties persist in the conventional dosimetry of Auger electron emitters, particularly those used internally as radio-pharmaceuticals in nuclear medicine as shown in chapter 3. As a consequence, the effects of these nuclides are usually estimated by taking a worse case scenario. This may differ considerably from the true situation. Also, there are profound difficulties in designing and executing appropriate test experiments for modelling purposes.

In this chapter, the 'template' model, described for external radiations in chapter 3, is easily modified for use with incorporated radionuclides. A major factor of importance is the slowing down (sometimes called 'equilibrium') electron spectrum. It is expected that a better understanding of the damage mechanisms involved will emerge and that a method of classifying these nuclides in terms of their bio-effectiveness per decay (or cyto-toxicity) will enable a more effective use of these radionuclides. The development and testing of the model for Auger emitters is discussed in the sections below.

4.2 Probability of Damage by Internal Radio-nuclides.

The partial equilibrium fluence of electrons, group 'j', generated by a homogeneous source concentration of electron-emitting radionuclide is given by:

$$\varphi_{eq,j} = \frac{A.t_i.n_{el}}{V}.f_j.R_j \qquad ---(4.2.1)$$

where, $A.t_i$ = number of nuclear decays / cell nuclear volume, V.

n_{el} = the total (average) number of electrons per decay.

f_j = the fraction of electrons in group 'j' per decay.

Under conditions of charged particle equilibrium the fluence is equal to the CSDA range, R, of tracks per source concentration of electrons.

Fuller definitions of the symbols are listed previously, in section 2.9.

The partial bio-effect cross-section, in the absence of repair is :

$$\sigma_{B,j} = \sigma_{S,j} \cdot \left[1 - \exp\left(-(2\Lambda + s)/\lambda\right)\right]^2$$

$$\sigma_{S,j} = \sigma_{g,DNA} \cdot n_0 \cdot \frac{\overline{R_j}}{\overline{d}} \qquad ---(4.2.2)$$

and the total bio-effectiveness per decay per cell (B) is obtained by summation over electron groups 'j' to get:

$$\sigma_B.\Phi_{eq} = \sum_j \sigma_{B,j}.\phi_{eq,j} \qquad -----(4.2.3)$$

$$= n_{el} \cdot \sum_j \left[f_j.R_j\,\sigma_{S,j}.\varepsilon_{2,j}(\lambda)\right] \text{-----} \quad 4.2.4$$

Note that values of the ranges, R/d, are constrained to unity for R > d, the mean chord length through the cell nucleus. This is handled automatically in the computer program, 'FOMINC.FOR' listed on the CD ROM.

4.3 Cytotoxicity Factors

The 'cytotoxicity, factor, C_F, is the bio-effectiveness for one decay per cell nucleus. It is given by:

$$C_F = \sigma_B . \Phi_{eq} . C_A = \frac{1}{V_{cell}} . n_{el} . \sum_j \left[f_j . R_j . \sigma_{S,j} . \varepsilon_{2,j}(\lambda) \right] \quad --- \quad (4.3.1)$$

To get the bio-effectiveness of the radiation, multiply C_F by the number of decays per cell.

{Note: the survival fraction, F, in the absence of repair, can be obtained directly from the relation: F=exp(-B) or: - ln(F) = B = $\sigma_B . \Phi_{eq} = \sum_j \sigma_{B,j} . \phi_{eq,j}$, obtained in equation 4.2.3 }.

4.4 Determination of Cyto-toxicity Factors for Auger Electron Emitting Radionuclides Incorporated Into Soft Tissues in Equilibrium Concentrations

Taking the above conclusions into account, the model is developed for Auger electron emitting radionuclides. These cyto-toxicity factors or 'factors of merit' will aid in the selection of these radionuclides for the induction of biological end-points in mammalian cells e.g. cell death.

These factors should help in selecting the Auger electron emitter that will provide the appropriate toxicity for the application in therapeutic treatment in nuclear medicine, where the radionuclides may be incorporated into tumours. They can also be useful in selecting the appropriate radionuclide for diagnostic purposes keeping the patient dose to a minimum while providing effective imaging.

Auger electron emitting radionuclides have complex decay schemes with the production of a cascade of electrons that follow the initial decay as indicated previously. The decay patterns of these radionuclides must be included in the cyto-toxicity factor. The cyto-toxicity factor represents the bio-effectiveness per unit source concentration of decays. This takes into account the contribution of the emission or fluence produced by the radionuclide in causing effective damage to the double strand of the DNA.

4.5 Assumptions

The model is developed on the experimental observation that it is the fluence and the mean free path for interactions of the charged particle tracks in the equilibrium spectrum that are the dominant factors in the production of damage. This is logical common sense assumption since it implies that the interaction at the site of interest is more effective in causing damage then the average energy delivered to the volume of interest. When using dose/energy delivered, the damage may not be related to the quality of the radiation but just to the quantity and unnecessary dose/energy may be delivered which does not contribute significantly to the critical lesion or observed damage.

Within the equilibrium electron spectrum, the secondary radiation (e.g. delta rays) do not contribute significantly to the damage. It can be argued that highly localised electron deposition from Auger electron emitters will contribute significantly to the damage. But in order for electrons to be damaging it is at the end of the electron track that the energy deposition is significant and the

probability of this happening near the DNA strands is very small. This is due not only to the obstruction of the electron path from the matter surrounding the DNA molecule including water but also the physical distance. In the case where the radionuclide is localised in the DNA, the electron and delta ray will contribute to the damage. However, here it will be the primary ionisations that are the main contributors to the damage. If it were possible to deliver only delta rays to the critical target excluding primary ionisation, one could determine the significance of these secondary radiations. In order to do so one would need to devise a method to make the end of the electron track occur at the critical target near the possible lesion of interest. This is highly unlikely. Looking at it from the point of view of desired spacing i.e. Lambda (λ) equal to 2nm combined with a range of 6nm at 200eV electrons the damage in this case would be very localised. The effect of binding the isotope to the DNA will be most effective for electrons with an energy equal to 200eV. For energy greater than 200eV the spacing is not correct and therefore the damage probability will be low. One other piece of evidence against the fact that the electron damage may be significant in this scenario, is the lack of damage present from the large number of naturally occurring, beta and gamma emissions within the body from K^{40} and C^{14}. Were these emissions significant the number of dsb's and hence mutations would be considerable. The correlation of the ionisation interaction spacing with the DNA strand separation is such that when these are the same or close the damage is likely to be maximum. It is clear from the experimental work that damage to the DNA is the important factor in creating irreversible damage and the most significant forms of damage are the different dsb's as indicated in the DNA damage model (see page 30).

It is also assumed that the contents of the DNA segments within the cell are uniformly distributed although there is a factor which allows for change in DNA concentration, and therefore of radiosensitivity, through the cell cycle. The geometry used for the cross section calculation is taken to be spherical.

To pursue the objectives of a unified model for all radiation types and for all mammalian cells, but for the same biological end-point, the bio-effective cross sections (the probability of inducing the effect per unit fluence) may be expressed as ratios to that of the projected saturation cross-section of the targets of interest. This allows for the 'bio-effectiveness probability' to be determined in a quantitative way. This not only makes the model a generalised one that covers different radiation types but also different critical targets. In this case it is assumed that the DNA is the fundamental critical target, as has been demonstrated to be the case by several authors both analytically and experimentally. It may be that multiple or specific types of lesions are required for some end-points, such as chromosome aberration or transformation but still the underlying critical target seems to be the dsb in DNA. The ratios give the cumulative probability, or intrinsic efficiency, for the induction of the biological endpoint by an individual track in the radiation spectrum. The experimentally determined cross sections for a variety of radiations, expressed as a function of LET, by Cox and Masson [144] Thacker et al, [145] and Wulf et al, [146] led to several conclusions:

1 Energy concentration increases the biological effectiveness of a radiation track around 50-100keV/μm, the increase in effectiveness is much greater than the proportional increase in average energy deposition but the effect is dependent on the radiation type.

2 Low-LET effect cross section is an underestimation of the true target size and concentrating energy in a reduced number of targets is more effective than spreading the same energy over many targets.

3 There is a saturation of cross section for slow ions of LET>=200keV/μm and concentration of energy above this is wasted. This is also dependent on the radiation type and therefore cannot be unified to a satisfactory extent (see Simmons and Watt, [147]

Saturation cross sections for slow ions are smaller than the mean projected area of the mammalian cell nuclei, illustrating the ability of a mammalian cell to survive the passage of one or more slow heavy ions through its nucleus. Wright et al, [135] have shown that the probability of inactivation of a cell by an alpha particle is ~0.3-0.5 and <=0.1 for thin cell nuclei. This is most likely due to the non-uniform distribution of the target material, allowing ionising tracks to pass through without striking the necessary target. For this reason we use $\sigma_{g,DNA}$ and not $\sigma_{g,\,cell}$.

Taking the above assumptions into account the model is applied to electron capture nuclides, mainly Auger electron emitters, in the following sections.

4.6 Test of validity of the 'template' model

4.6.1 Testing of the Model

The experimental data (which was collected mainly through an intensive literature search both using the normal journals and use of the Internet to search medical and clinical websites), reported in the literature and summarized in Table 4.1 are in the form of dose-survival curves. The survival fractions may be measured either in decays per cell of the radionuclide or in the more traditional way in terms of absorbed dose. [Note that accurate measurement of absorbed dose, the specific energy deposition averaged over a mass of cellular material, is not a trivial problem because of the inhomogeneous distribution of energy deposition by short range straggled electrons.]

Experiments are wide ranging. They explore phenomena such as:

1 The effect of radiosensitisers and radio-protectors;

2 The influence of incorporation into the cell nucleus and sometimes specifically into parts of the DNA molecule;

3 The trend of induced damage above and below the K-edge of e.g. iodine or bromine-labeled molecules, stimulated by monoenergetic synchrotron radiation;

4 The ploidy of the cell nucleus and whether the cells are synchronized in the cell or left in the more natural asynchronised form.

Despite this range of available data, the experimental information, which can be best used as a sensitive test of the model is really very restricted and rests on evaluation of the bioeffect cross-section of mammalian cell nuclei.

Typically the experimental effect cross-section can be extracted from the survival curves and expressed in two forms either:

1 As the D37 absorbed dose (in gray) for which there will be on average a single inactivation per event. By the time the D_{37} dose is reached there is expected to be signs of the effect of repair.

2 As the D_0, in nuclide decays per cell. The D_0 represents the final slope of the survival curve at low doses (decays) and is considered to be repair independent.

For pure exponential survival, the D_0 and D_{37} should be equal if expressed in the same units. The data were collected initially from selected papers of known experts in the field. However, due to the limited findings the search was broadened to include the general area of radionuclides both in literature and Internet searches. The data shown was filtered to include relevancy and those with clear experimental methodologies. Comments on the data are made in the sections following; where necessary the required results were extrapolated from the available graphs or tables and in some cases from analytical methods. The selected data is shown in Table 4.1.

Table 4.1 Collected Data on Cell Survival

k	Isotope	Cell line	Irradiation	Localisation	Compound	Temp (C)	D_{37} or D_0
1	In-110 [148]	Rat Testes	Non-uniform distribution	-	-	-	1.9Gy
2	In-111 [148]	Rat Testes	Non-uniform distribution	-	-	-	2.2Gy
3	I-125 [149]	Ch Ham V-79	14hr	Mono irradiation 16% incorporation	IUdR above K edge	37	1.2Gy
4	I-125 [149]	Ch Ham V-79	14hr	Mono irradiation 16% incorporation	IUdR below K edge	37	1.8Gy
5	Br-77 [149]	Ch Ham V-79	14hr	Mono irradiation 60% incorporation	BrUdR above K edge	37	1.5Gy
6	Br-77 [149]	Ch Ham V-79	14hr	Mono irradiation 60% incorporation	BrUdR below K edge	37	1.6Gy
7	I-125 [150]	Ch Ham V-79	14hr	Syncronised in G1/early S-phase	Tetraploid	-	Do= 121 decays
8	I-125 [150]	Ch Ham V-79	14hr	Syncronised in G1/early S-phase	Diploid	-	Do= 60 decays
9	I-125 [150]	Ch Ham V-79	14hr	Syncronised in G1/early S-phase	Hexaploid	-	Do= 137 decays
10	I-125 [150]	Ch Ham V-79	14hr	Synchronised at G1/S, DNA	-	-79	0.9Gy
11	I-125 [150]	Ch Ham V-79	14hr	Synchronised at G1/S, DNA	-	20	Do= 0.65Gy
12	I-125 [151]	Monolayer Ch Ham embryo cells	24hr	-	-	-	0.66Gy

Table 4.1 continued.

k	Isotope	Cell line	Irradiation	Localisation	Compound	Temp (C)	D_{37} or D_0
13	I-125 [152]	-	-	96% Cytoplasmic	Iododihydroxhodamine, mitochondria,	-	109 mBq/cell
14	I-125 [152]	-	-	DNA	Iodoprflavin	-	3.5mBq/cell
15	I-125 [153]	Ch Ham V-79 lung fibroblasts	18hr	DNA	Iododeoxy-uridine IdU	-	1.5mBq/cell
16	Se-75 [153]	Ch Ham V-79 lung fibroblasts	18hr	Cytoplasmic proteins	Seleno-methionine	-	145 mBq/cell
17	Br-77 [153]	Ch Ham V-79 lung fibroblasts	18hr	DNA	Bromodeoxy-uridine	-	4.8mBq/cell
18	Tl-201 [153]	Ch Ham V-79 lung fibroblasts	18hr	cell	-	-	45mBq/cell
19	Cr-51 [153]	Ch Ham V-79 lung fibroblasts	18hr	2% DNA bound	-	-	230mBq/cell
20	In-111 [154]	Spermhead	-	92% nucleus	oxine	-	0.17Gy
21	In-111 [154]	Spermhead	-	30% nucleus	Citrate	-	0.35Gy

Table 4.1 continued.

K	Isotope	Cell line	Irradiation	Localisation	Compound	Temp (C)	D_{37} or D_0
22	In-114m [154]	Spermhead	-	30% nucleus	citrate	-	0.59Gy
23	Tc-99m [154]	Spermhead	-	69% nucleus	HDP	-	0.54Gy
24	Ga-67 [154]	Spermhead	-	30% nucleus	citrate	-	0.44Gy
25	Tl-201 [154]	spermhead	-	-	-	-	0.55Gy
26	Tl-201 [154]	Primary oocyte	-	-	-	-	0.035Gy
27	In-111 [154]	Primary oocyte	-	-	oxine	-	0.061Gy
28	In-111 [154]	Primary oocyte	-	-	citrate	-	0.010Gy
29	I-125 [155]	Mammalian cells	-	-	IdU	-	0.44Gy
30	I-125 [155]	Mammalian cells	-	-	IdC	-	0.44Gy
31	Tc-99m [156]	Testes	-	48%Cell. 20%Nuc. 13%DNA	Tc-HDP	-	0.59Gy
32	Tc-99m [156]	Testes	-	40% cell. 13% nuc. 6%DNA	Tc-pyro-phosphate	-	0.84Gy
33	Tc-99m [156]	Testes	-	22%cell. 7%nuc. 4%DNA	Tc-pertech-netate	-	0.70Gy

Table 4.1 continued

k	Isotope	Cell line	Irradiation	Localisation	Compound	Temp (C)	D_{37} or D_0
34	I-125 [157]	Ch Ham V-79-513 cells. In vitro.	18hr	Monolayers, 100% Nucl.	IuDR(IdC)	37	0.44Gy
35	Po-210 [157]	Ch Ham V-79-513 cells. In vitro.	18hr	Monolayers, 100% Nucl.	Po-citrate	37	0.70Gy
36	I-125 [157]	Swiss Webster mice. In vivo	36 irradiations	100% cytoplasmic	HIPDM	37	0.68Gy
37	I-123 [157]	Swiss Webster mice. In vivo	36 irradiations	100% cytoplasmic	IMP	37	0.62Gy
38	I-125 [157]	Swiss Webster mice. In vivo	36 irradiations	DNA 100% Nucl.	IUdR	37	0.085Gy
39	I-125 [157]	Swiss Webster mice. In vivo	36 irradiations	-	IdC	37	0.077Gy
40	Po-210 [157]	Swiss Webster mice. In vivo	36 irradiations	80% cytoplasm, 20% DNA	-	-	0.10Gy
41	I-125 [158]	Male Swiss Webster mice	Intertesti-cular 29 day incubation	100% nucl. 100%DNA	IUdR + MEA	37	0.31Gy
42	I-125 [158]	Male Swiss Webster mice	Intertesti-cular 29 day incubation	-	IUdR-MEA	37	0.085Gy
43	I-125 [159]	Ch Ham ovary cells	15min	Synchronised G1/S,	-	-90	153.1Gy
44	I-125 [159]	Ch Ham ovary cells	30min	Synchronised G1/S,	-	-90	51.7Gy

Table 4.1 continued.

K	Isotope	Cell line	Irradiation	Localisation	Compound	Temp (C)	D_{37} or D_0
45	I-125 [159]	Ch Ham ovary cells	1hr	Synchronised G1/S,	-	-90	42.8Gy
46	I-125 [159]	Ch Ham ovary cells	2hr	Synchronised G1/S,	-	-90	30.8Gy
47	I-125 [159]	Ch Ham ovary cells	3hr	Synchronised G1/S,	-	-90	24.7Gy
48	I-125 [159]	Ch Ham ovary cells	4hr	Synchronised G1/S,	-	-90	16.4Gy
49	I-125 [159]	Ch Ham ovary cells	5hr	Synchronised G1/S,	-	-90	12.1Gy
50	Trans Pt-195m [160]	CHO cells	-	DNA	-	-	1.2mBq/cell
51	I-125 [160]	CHO cells	5hr early S	Synchronised DNA	IUdR	4	Do=0.006-0.02Gy
52	I-125 [160]	CHO cells	8hr mid S	Synchronised DNA	-	-	Do=0.056Gy
53	I-125 [160]	CHO cells	12hr late S	Synchronised DNA	-	-	Do=0.358Gy
54	Cr-51 [161]	Mouse testes	-	85%cytoplasm 15%cell nucleus	-	-	1.95Gy
55	I-125 [161]	Mouse testes	-	cytoplasmic	-	-	0.68Gy

Table 4.1 continued.

K	Isotope	Cell line	Irradiation	Localisation	Compound	Temp (C)	D_{37} or D_0
56	P-32 [162]	Bacterio-phage T1	9hr	-	-	-196	Do=16.8 decay/phage
57	P-32 [162]	Bacterio-phage T1	9hr	-	-	4	Do=7.11 decay/phage
58	P-32 [162]	Bacterio-phage T4	9hr	-	-	-196	Do=10.7 decay/phage
59	P-32 [162]	Bacterio-phage T4	9hr	-	-	4	Do=7.0 decay/phage
60	P-33 [162]	Bacterio-phage T1	9hr	-	-	-196	Do=30.1 decay/phage
61	P-32 [162]	Bacterio-phage T1	9hr	-	-	4	Do=8.2 decay/phage
62	P-32 [162]	Bacterio-phage T4	9hr	-	-	-196	Do=24.5 decay/phage
63	P-32 [162]	Bacterio-phage T4	9hr	-	-	4	Do=10.2 decay/phage
64	I-125 [163]	V79	14hr	DNA	5-I-125-iodo -2-deoxy-uridine	-49	Do=40 decay/cell
65	I-125 [164]	Human lymphoblast diploid TK6	22hr	random	I-125 dUrd	37	Do=28 decay/cell
66	I-125 [164]	"	22hr	random	I-125 dUrd	-70	Do=28 decay/cell
67	Br-77 [165]	Mammalian cells V-79	18hr	Bifilar DNA label	-	37	311 decay/cell

4.7 Comments on the Available Data

The data above indicates the wide variety of experimental procedures used in the study of Auger electron emitters and their effects.

The number of isotopes investigated cover the broad spectrum of Auger electron emitters used in medicine. However, the favoured isotopes for experimental work appear to be the halogens, in particular Iodine and its derivatives. This is probably due to its extensive use in medicine for therapy and diagnostic purposes and also most likely due to the fact that the action and decay scheme of I-125 have been studied and modelled by a large number of authors.

The data presented here indicate that the choice of cell line or target under investigation is limited which, for the purposes of testing this model, is very restrictive thereby making the interpretation of the analysis unsatisfactory from a statistical point of view. For the testing of the model the data of main interests are from experiments where the Auger electron emitter has been located in the DNA of the cell nucleus.

The table shows that a large number of compounds are used in the delivery of the radiation to the target of interest. Some of these compounds as in Ref. [158] behave as radioprotectors influencing the action of the radionuclide. The effect of these radio and chemical protectors are not fully understood, in particular the change in response of the cell to the protector. This further complicates the use of the data in testing of this model.

Some of these compounds are assumed to have specific targeting properties for example the DNA or the cytoplasm as in Ref. [153]. It is difficult if not impossible to find a compound that will deliver different isotopes to a specific location of interest within the cell, which makes comparison of information under controlled situations very difficult. Ideally one would be able to find a compound that could be directed to deliver the dose from different radionuclides to the same location i.e. the DNA of the cell. Because one Auger emitter cannot be located in a particular location with a specific compound it makes the study of the effects of different Auger electron emitters complex. Generally it is done through a correlation, where the decay schemes of the different isotopes and total dose delivered are compared to determine the effectiveness. Use of the template model should eliminate this approach as the parameters under consideration are universal to all the radiation types and have unique characteristics dependent on the radionuclide.

Table 4.1 contains information on the temperature, location and irradiation time for the target. However; these are very difficult to obtain accurately for all cases with the exception of Ref. [159].

The doses recorded in terms of D_{37} and D_0 values are either determined directly from survival curves or extrapolated from the data within the references. Unfortunately the method of determining the dose delivered to the target by the individual authors varies considerably making estimation of the true dose and its distribution very difficult. This is particularly so in the cases where the dose is estimated as an average per cell as in Ref. [152] and when it is expressed as a

number of decays as in Ref. [150] and others. Dose expressed in terms of number of decays is intrinsically more useful for the purposes of this model.

4.8 Several Conclusions Can be Drawn From the Data Obtained:

Looking at results from ref. [149]. For both Iodine and Bromine nuclides, photon stimulation above the K-edge is more effective in causing cell death i.e. lower D_{37} values. This is to be expected, as the cascade of the emitted radiations will be greater above the relevant K-edge and therefore it is more likely to interact with the double strand of the DNA. Iodine is more effective in causing damage compared to Bromine even though it has a much lower incorporation. This is most likely due to the larger number of electrons emitted per decay by the Iodine atom than Bromine. However, it is noticeable that at below the K-edge the Bromine is more effective compared to iodine. It is not clear whether this is due to level of incorporation, size of the atom, the quality of the radiation emitted, or simply the basic dosimetry. A possible explanation is that the mean free path for primary ionisation is closer to 2nm (the DNA double strand spacing) for Bromine than it is for Iodine as shown by Watt [71]. The effect observed here maybe due to external mono-chromatic photon stimulation above and below the incorporated stable Br and I edges, and nothing to do with I-125 or Br-77 nuclides. If this is so, the effect the author's observe may simply be because they used the same mass energy absorption coefficient above and below the K edges i.e. they used the un-doped soft tissue kerma factor which would give an anomolously high result.

Looking at Ref. [152], it is clear that the localisation in the DNA improves the effectiveness significantly here by approximately 97%. This is further demonstrated in Ref. [154] where, for the various Auger electron emitters tested

the greater the localisation in the nucleus the greater the effect. However it is true that this does not prove that DNA damage is the main contributor to cell death as argued by Hofer et al Ref. [159], but the work in Ref. [63] gives very good support that this is most likely the case.

Ref. [159] and [161] indicate the importance of irradiation time in the G1/S phase of the cell cycle. There is no evidence unfortunately to indicate the effectiveness for different radionuclides at different parts of the cell cycle, although some information is available for external irradiations. Both of the cases in ref.[159] and [161] are for Iodine. It would be interesting to see the effects when related to lambda and cell cycle. It is assumed here a lambda that corresponds to the spacing of the DNA double strand would be more effective than for other spacings as explained earlier.

The experimental data does not in general contain any information about how the quality of the radiation may determine the effectiveness of the Auger electron emitter. These results are based on cell survival due to the dose delivered. The questions of multiplicity of targets and probability of interaction i.e. the cross section for interaction with the critical target is not explored. In effect it is the quantity of radiation rather than quality that is used as a classifier of damage. It is not clear how the quantity of radiation affects the responses of the cell. No conclusion can be drawn with regards to whether it is the specific damage i.e. to the DNA or the overall quantity that is important. For the reasons mentioned previously it is difficult to imagine that quantity is more important than the quality.

4.9 Limitations of Data

Unfortunately due to the incompleteness of the available data i.e. in terms of methods of dose evaluations, temperature of the experiment, the period in the cell cycle during which the irradiation was given, not all the data can be used in the model. The most accurate and comprehensive data are those produced by Hofer et al. For this reason the critical evaluation of the model is concentrated around this set of data.

4.9.1 Analysis of Data

The abstracted data shown in table 4.1 has to be selected and the appropriate data expressed in such a way that they will be useful in the testing of the model. As stated in sections 4.6, the data has intrinsic limitations for testing the validity of this model, particularly those due to the large number of biological end-points, the varied cell types, methods of radiation delivery, methodology of dose estimation etc. The problem of the limited types of Auger electron emitting nuclides used in research and medicine complicates the issue further. However an attempt is made to re-express the data using the programs described in chapter 2. Once these cross sections are calculated comparison is made with the experimental values. These results are presented in the figures below and in chapter 5. The decay data on the 16 radionuclides concentrated on in the thesis which was used in the programs described in chapter 2 to calculate the cross-sections, are shown in Appendix 1.

4.10 Parameters of Interest for the Model

In order to calculate the cyto-toxicity factors for the Auger electron emitting radionuclides, the magnitude of the parameters established in the equations are obtained from independent sources in the available literature and from the basic physical data shown in Table 4.1. Then the equations for the model have to be processed for the data which are plotted and analysed. Below is a list of the important parameters used in the model. The program details are given in chapter 2. Not all the variables are listed here. Fuller details are given in the program listing. Note that the cyto-toxicity factors are only meaningful if we can first show that the model is valid e.g. to Hofer's data. Upon the satisfactory test of the model, within the limitations discussed, cyto-toxicity factors can be proposed. Also, the capability to calculate such cyto-toxicity factors comes directly from the 'template model' and not the experimental data.

4.11 Collected/Required Parameters.

rho (g/cm^3): this is the density of target (taken as water).

cell vol (μm^3): the volume of the target/cell nucleus under consideration.

temp(^0K): temperature of cell or the experimental temperature.

dia (μm): diameter of cell nucleus.

d37 (Gy): dose at 37% survival, obtained from the curves or extrapolated data.

d0 (Bq): 1/e dose in nuclear decays per second at the final slope, obtained from the curves or extrapolated data.

t_r (h): irradiation time.

t_m (h): time to mitosis.

4.12 Derived Parameters

crsd37,(μm^2): cross section for 37% survival in Gy.

tnel(k): averaged total number of electrons released per decay.

dflam,(nm): Λ, the radical diffusion length.

crdna,(μm^2): geometric cross section of DNA

dlam (nm): λ, the mean spacing between interactions.

rlambr,(nm): Average λ weighted by the Auger electron yields per decay.

rltbr,(keV/μm): Average LET weighted for the Auger electron yields.

crsd0,(μm^2): cross section per electron.

crdec (μm^2): cross section per decay.

conc (μm^{-3}): decays per cell volume.

tbcr (μm^2): calculated bio-effective cross section for electrons for single track action.

tsat(k): total saturation cross section per electron.

fl37%,(μm^{-2}): fluence at 37% survival.

str (nm): mean chord through a single strand of DNA (1.0 nm).

cst (nm): 2Λ+str, the mean track distance over which reaction is probable with a single DNA strand.

dbr (μm): mean chord length through the cell nucleus.

fltot (μm^2): total fluence of electrons generated by the experimental D_0 decays.

epsd (i): efficiency of dsb production by group 'i' electrons.

avlam (nm): average lambda for the decay electrons.

avlet (keV/μm): average linear energy transfer for the decay electrons.

fld0 (μm): fluence per unit source concentration of decays.

crsbi (μm^2): bio-effect cross section for group 'I' electrons with the dual track term included.

rtbcr (μm^2): total effect cross section for electrons with the dual track term included.

It is clear that Hofer's data provides the best information with respect to verification of the model, mainly due to the detailed nature of the experiments and a rather novel method of controlled irradiation of the cells. For this reason this data is analysed in detail below along with other supporting evidence for the model.

4.13 Evidence in support of the model.

The support for the model is provided in three stages. Firstly the results are compared with the probe experiments with heavy particles. Secondly the model is tested for the Auger emitters with the experimental findings of Hofer *et al* on their synchronised CHO cells labelled with ^{125}Iodine.

4.14 Determination of slowing down (SLD) spectra for beta emitters and characteristic x-rays as a preliminary step in calculating the cross-section and fluence for Auger electron emitters.

In the process of investigating the validity of the model for beta ray and Auger electron emitters, the bio cross-section and fluence data must be calculated. This is achieved by calculating the slowing down (SDL) spectra for the relative electrons as a preliminary step. One of the main reason for this is that the data on beta emitters and the Auger electron emitters is well established and gives a good indication of the model's predictability. The equilibrium SLD spectra is the spectra of charge that ultimately determines the bio-effect of Auger emitters and Beta emitters.

The SLD spectra of beta ray, compared with the Auger emitters, which have complex decay schemes along with the characteristic x-rays and Auger electrons, should give an accurate indication of the success of the model defined here. The derivation of the SLD spectra is described in chapter 2. The results in graphical form are shown in the figure 4.1.

Before the SLD can be calculated the primary electron distributions for these beta emitters in water is looked at, Fig 4.1 shows the results. All the nuclides show a general trend. Fig 4.2 shows the plot of fluence (cm/keV/decay) verses the electron energy (keV) which is the slowing down spectra (SLD) of the electrons emitted by the nuclides. . It should be noted that these results also show very good correlation with the heavy particle shown in chapter 2.

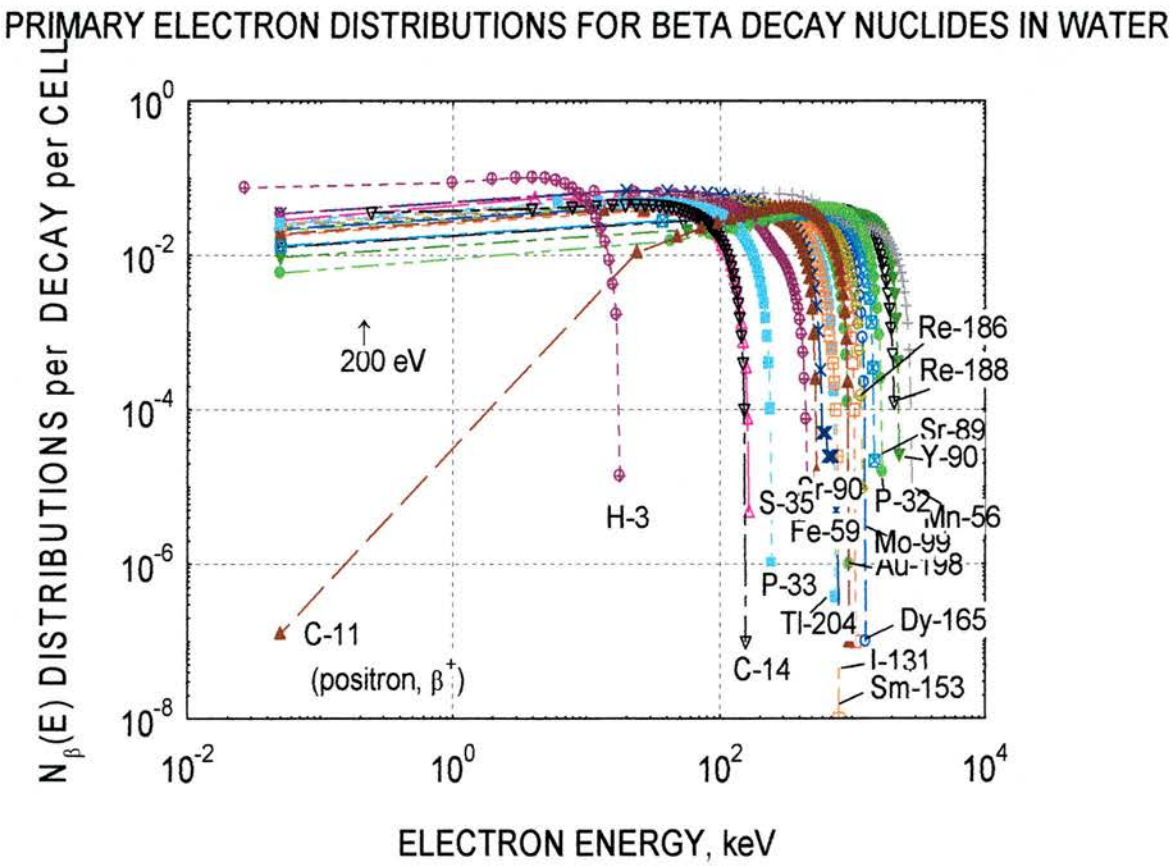

Fig 4.1 Graph showing the primary electron distributions from beta emitters in water, the results having been extended down to 30eV.

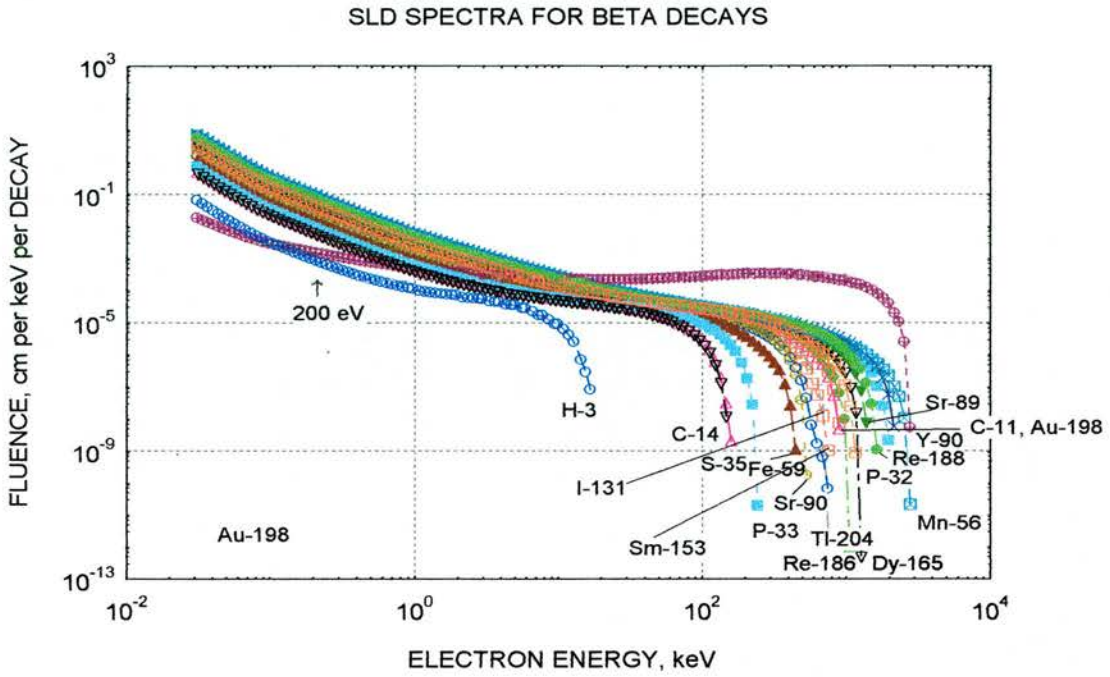

Fig 4.2 Graph showing the SLD spectra for 19 beta emitters the results having been extended down to 30eV.

The next step is to carry out the analysis for the radionuclides of special interest in this thesis i.e, the Auger electron emitters. As a first step in this process the slowing down spectra for the electron capture nuclides for photon decay, and for the Auger electron cascade, generated and analysed to determine the correlation with the beta data. Collected data for the SLD spectra for photon decay are shown in figures 4.3 and 4.4. collected data for SLD electron spectra for examples of the Auger electron cascade are shown in Fig 4.5, 4.6 and 4.7 as indicated.

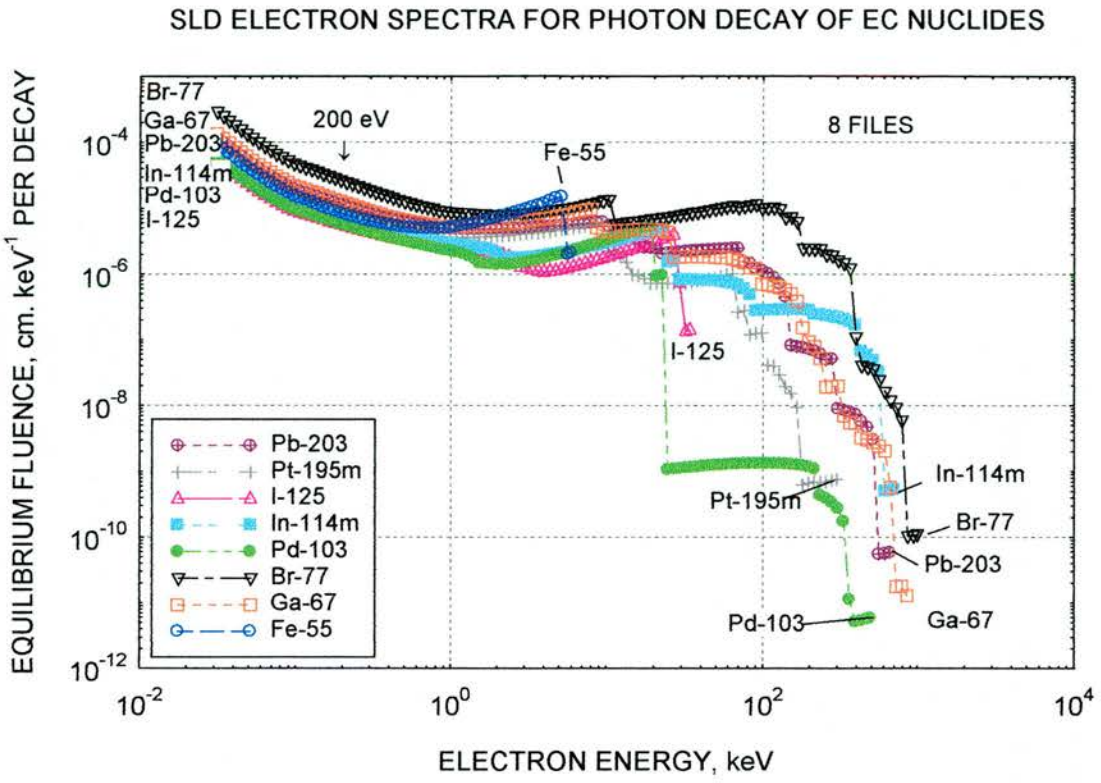

Fig 4.3 Graph showing the SLD spectra from photon decay of EC nuclides the results having been extended down to 30eV.

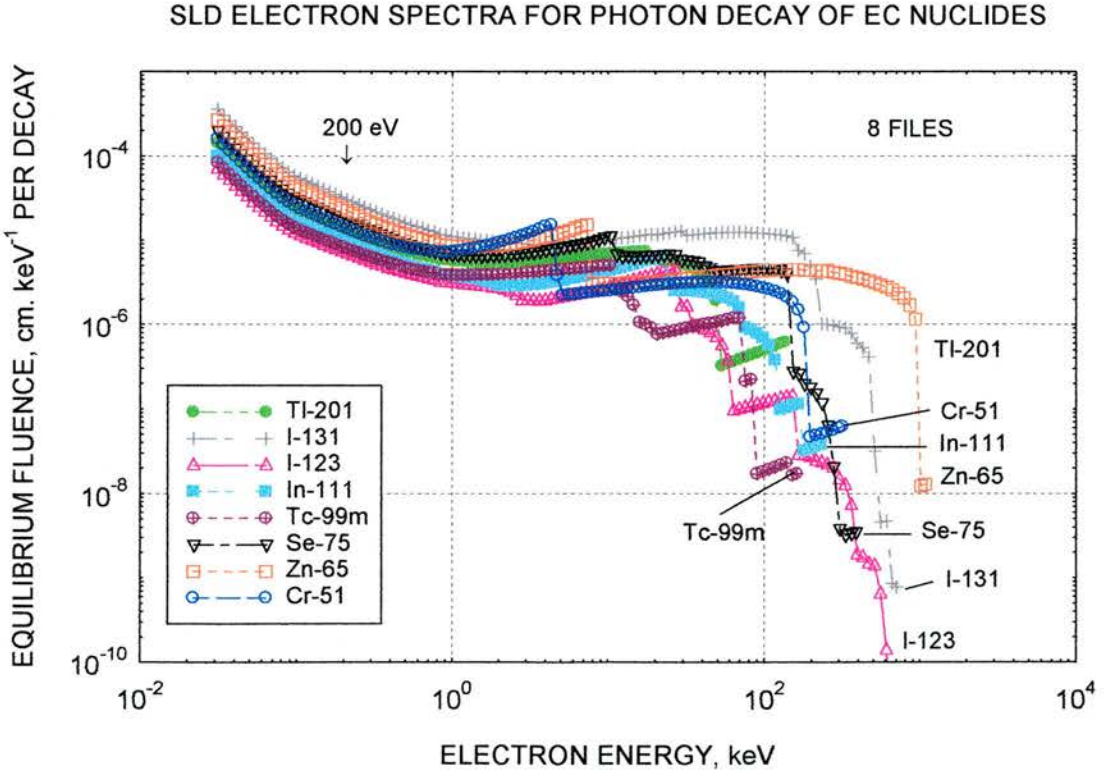

Fig 4.4 Graph showing the SLD spectra from photon decay of EC nuclides the results having been extended down to 30eV.

Examples of the slowing down electron spectra (fluence per decay verses electron energy) of the 16 Auger electron emitters are shown in figure 4.5, 4.6 and 4.7. Figure 4.8 to 4.10 gives examples of the comparative primary electron spectrum generated by primary photon and Compton electrons generated by the 16 electron capture nuclides.

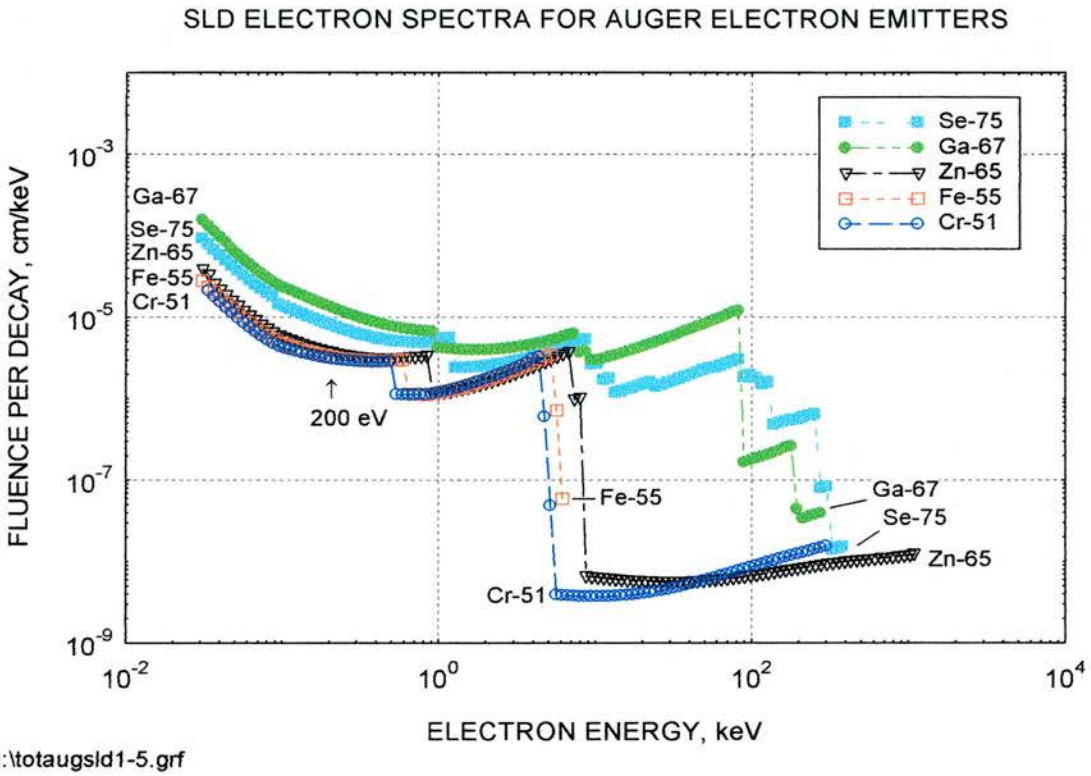

Fig 4.5 Graph showing the composite SLD electron spectra for some Auger/conversion electrons. The results are extended down to 30eV.

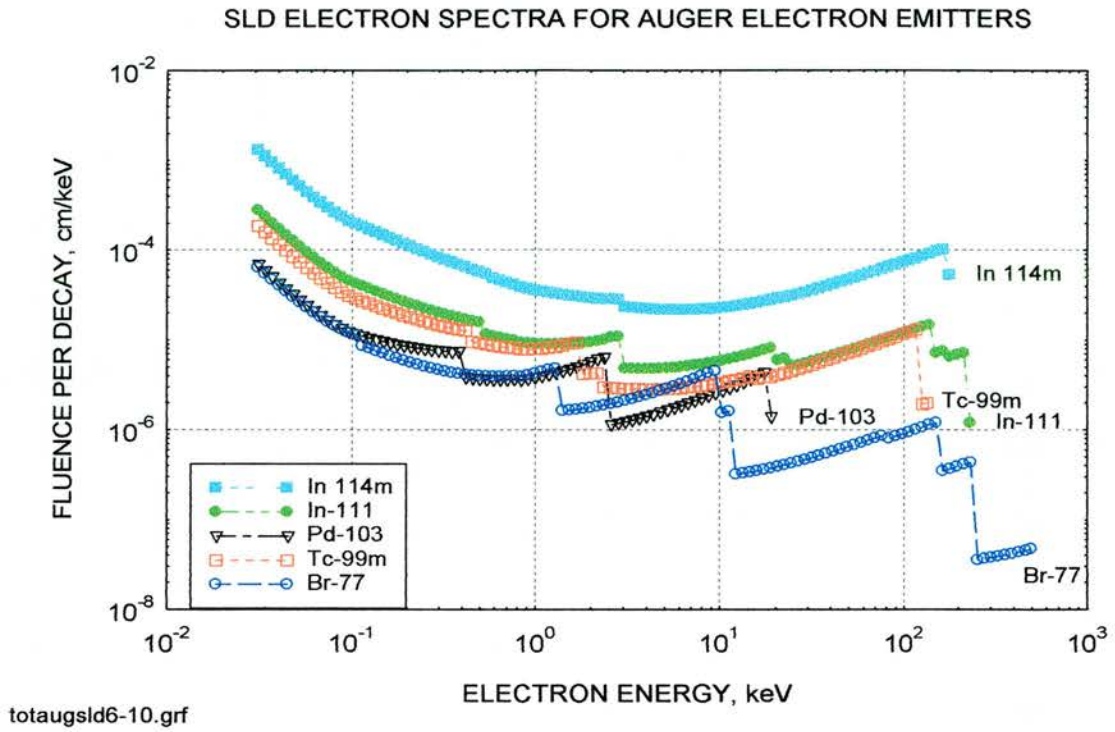

Fig 4.6 Graph showing the electron spectra for some Auger/conversion electrons. The results are extended down to 30eV.

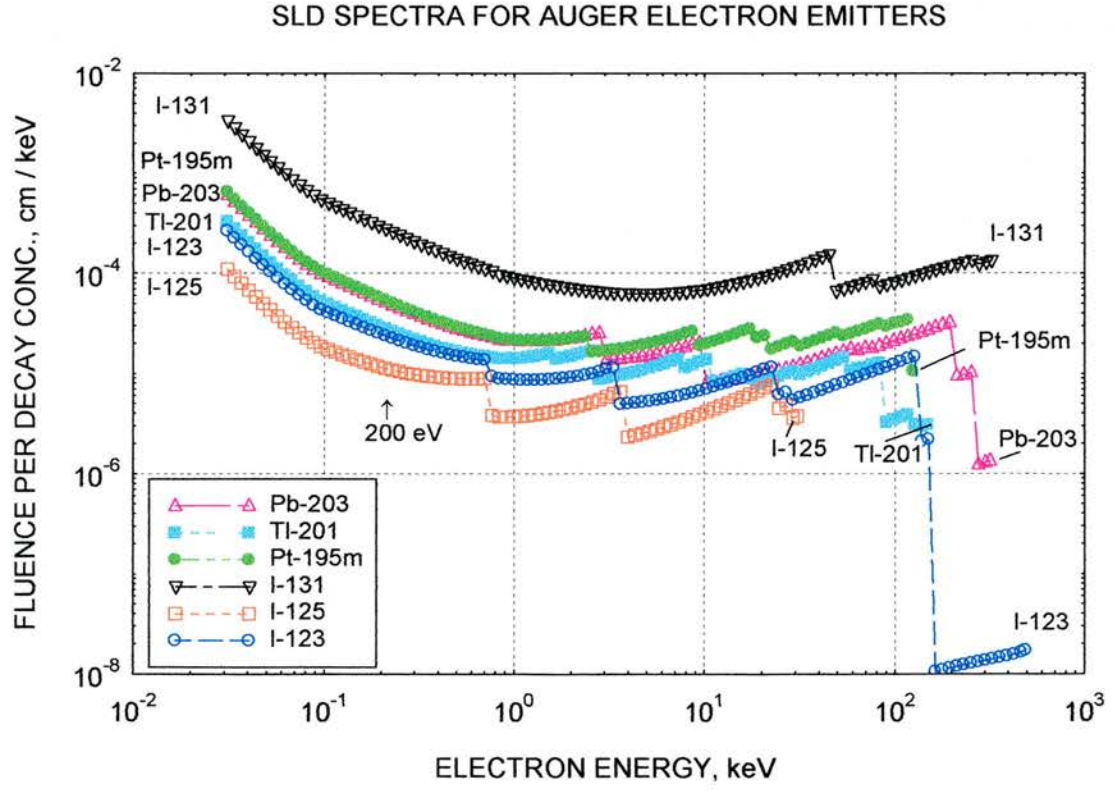

Fig 4.7 Graph showing the electron spectra for some Auger/conversion electrons. The results are extended down to 30eV.

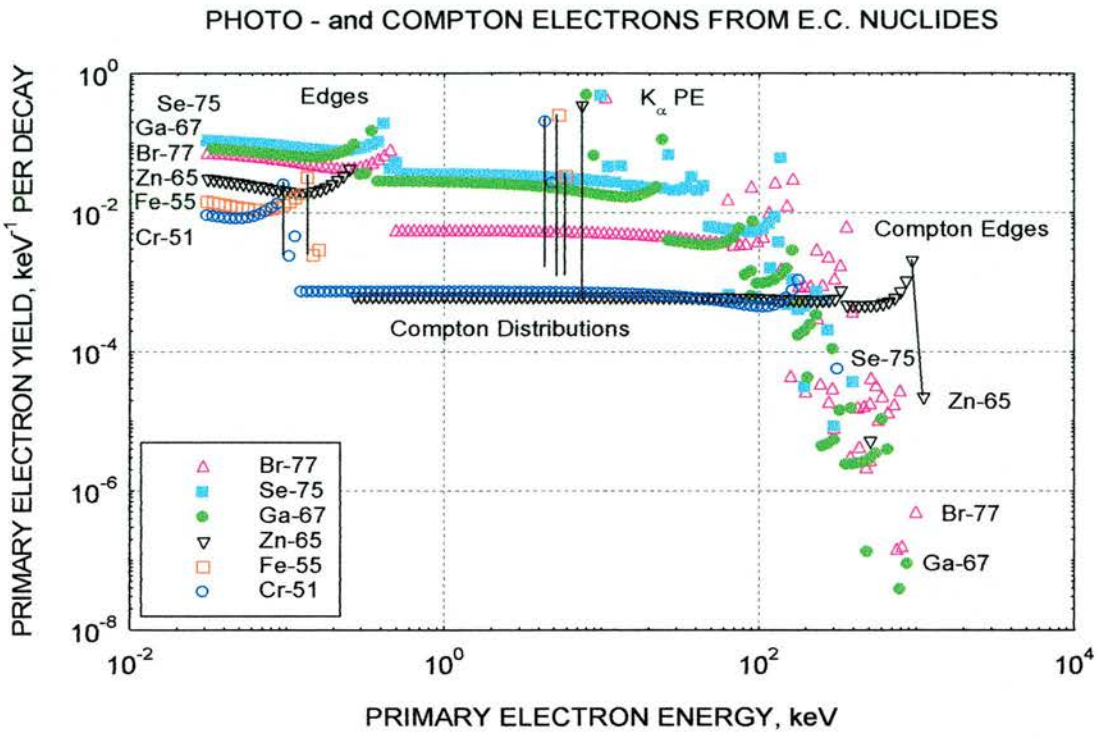

Fig 4.8 Graphs showing the composite primary electron yield from photo and Compton electrons produced by electron capture nuclides.

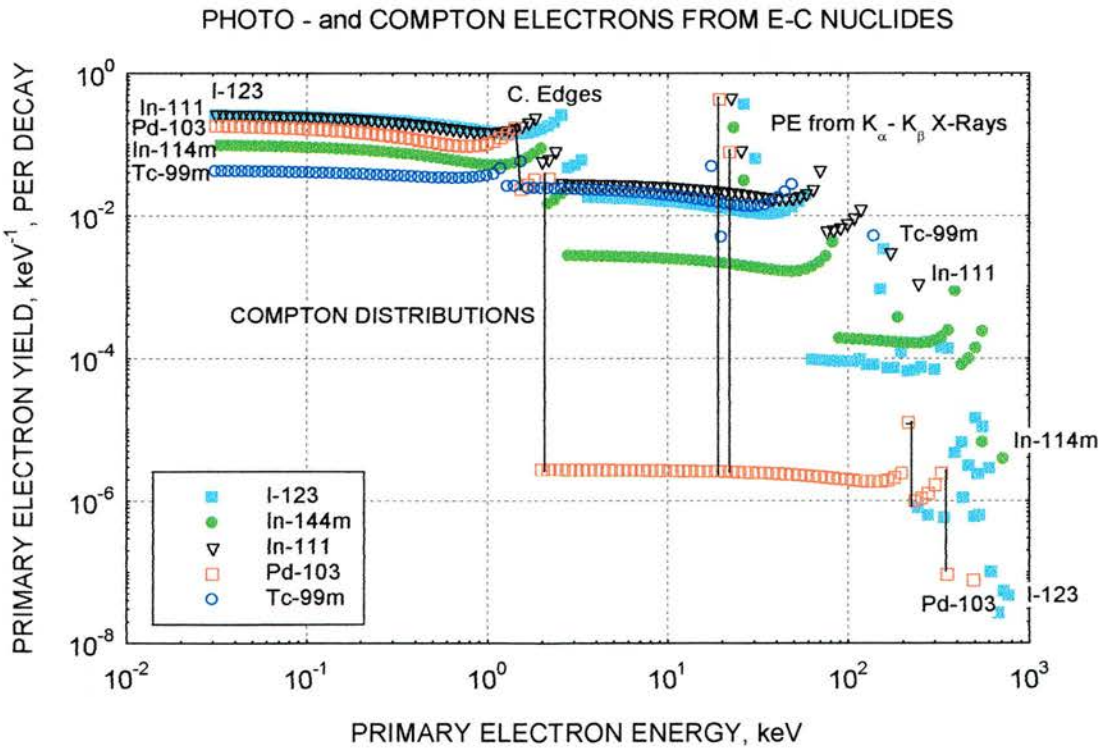

Fig 4.9 Graphs showing the primary electron yield from photo and compton electrons the results having been extended down to 30eV.

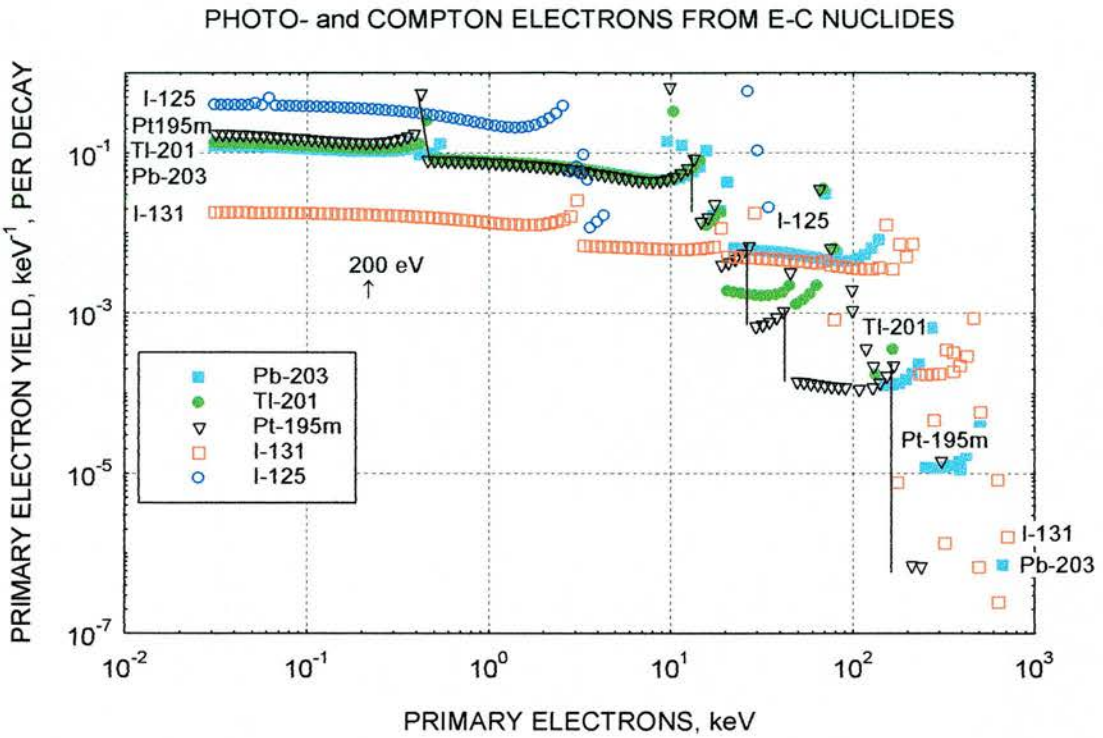

Fig 4.10 Graphs showing the primary electron yield from photo and Compton electrons the results having been extended down to 30eV.

In order to clarify the results in Fig 4.8-4.10, Auger emitting radionuclides, in particular the most commonly studied iodine and bromine are looked at in greater detail in Figure 4.11 for primary electron spectra of I-125 and Br-77 and in figure 4.12 for equilibrium spectra of Br-77 and I-125 respectively. The important observation here is that in Fig 4.11 the primary electron spectra for Br-77 is lower than the intensity of I-125, on the other hand, looking at Fig 4.12, it is seen that the equilibrium electron spectra from the photon decay, the order is reversed. This becomes important in the cyto-toxicity classification of these nuclides as will be discussed in chapter 5.

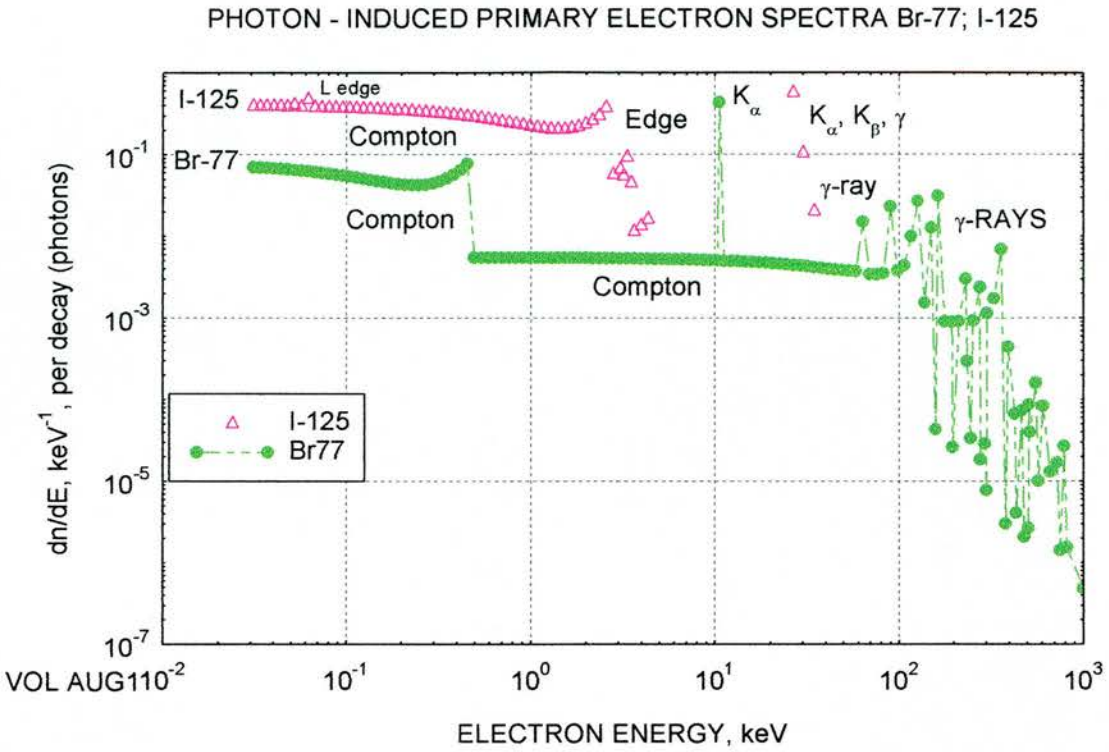

Fig 4.11 Graph showing the photon induced primary electron spectra for I-125 and Br-77.

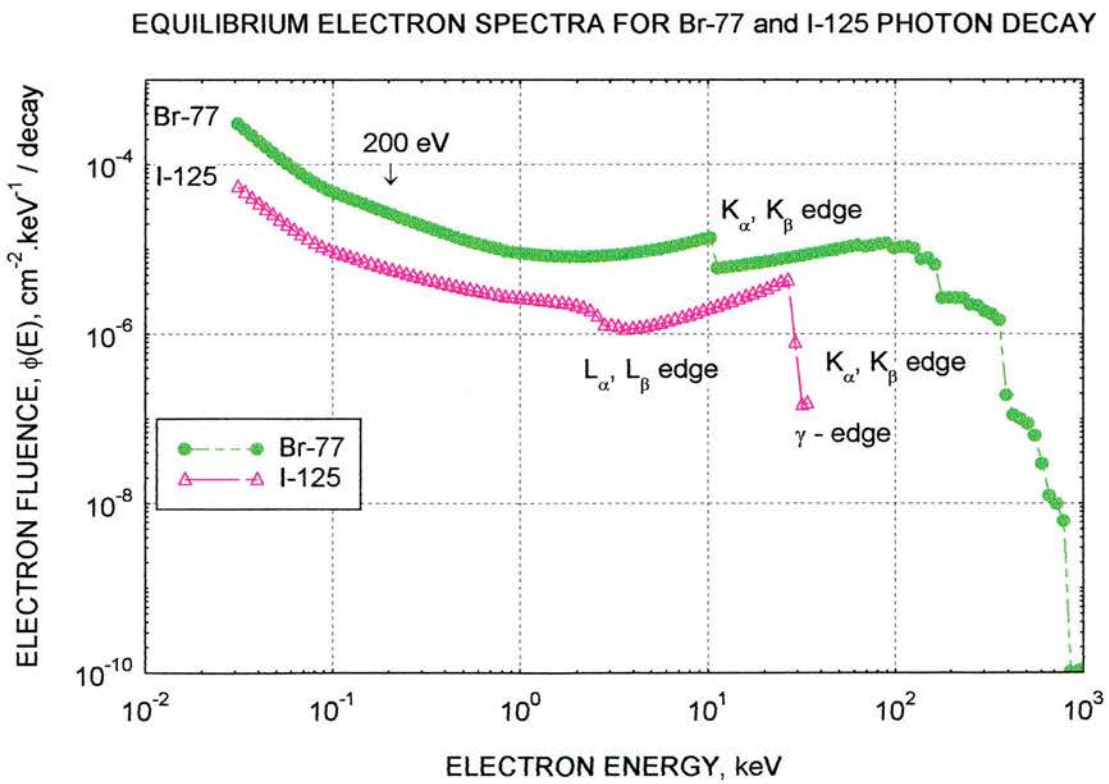

Fig 4.12 Graph of the equilibrium electron spectra for I-125 and Br-77.

Note that the equilibrium electron spectra in the lower energy region <500eV, have lost any sense of structure. The 200eV positron indicated represents the point at which the mean spacing is 2 nanometer in water. In principle this is the region of optimum damage.

The fact that the slowing down spectra of electron from beta emitters or Auger electrons calculated and compares well with established data, confirms several points including the fact that fluence per decay is not significantly different for the beta emitters compared to the Auger emitters. This hints at the idea that if the equilibrium spectrum is the important factor (which in biological terms is the case) the biological effect from beta and Auger emitters should be similar and vastly different. This is contrary to the ideas accepted presently.

The next step in the process is the analysis of the model with experimental data in particular the Hofer experiments.

4.15 Fitting experimental data with the Template model.

In chapter 2 the model showed that the 2nm mean free path, which correlates with the DNA double strand spacing, is an inflexion point of radiation action i.e. the effective cross-section changes significantly around that point regardless of whether it is heavy ions or electrons. Earlier in this chapter the model also demonstrated that the slowing down equilibrium spectra of both the established beta emitters and Auger electron emitters correlate very well and show similar trends. This is another important point, since it is this radiation fluence that is important in causing biological damage.

In the following sections the experimental data is applied to the Template model. This is carried out in several stages. First, the bio-effect cross section is looked at as a function of lambda for the different radiations and cell lines. Secondly, Hofer's experimental data is analysed with the model for radioprotector and synchronized cell effects.

4.15.1 Correlation between bio-effect cross section and lambda for calculated and experimental results.

The data collected in Table 4.1 is applied to the Template model. First the calculated (solid line) bio-effect cross section (σ) for heavy ions, beta, EC, characteristic x-rays along with the Auger electrons are plotted against the mean free path (λ). The experimental results are plotted on the same graph (see Fig 4.13). We can see from the Figure 4.14 that the results for the Auger emitters all 16 lie reasonably well in the curve and almost superimposed on the beta emitters. The results show that the values of the highest effective cross-sections have lambda greater than 1.8nm. This may suggest that the effectiveness of these Auger emitters in causing damage according to the model presented here may not be as high as generally thought. Looking at the correlation of effective cross section for the cells (V79) irradiated with various types of ionising radiation (heavy particles to electrons) against the mean free path lambda Fig 4.13, is shown to determine whether the Auger emitters (and other electrons) show consistency with the heavy ion experimental data. In figure 4.13 the heavy ions have an effective cross-section at the same lambda which is to the order of 10 times greater than that of the electrons. This difference is attributed to the multiplicity of targets along the charged particle chord. Electron tracks behave similarly to that of ions except that

1) electron tracks can produce interactions separated by ~2nm spacing only when their energy is about 200eV, and

2) at energies greater than ~200eV, there is a mis-match and the probability of causing a further match along the track decreases rapidly. Heavy particles, on the other hand, can sustain a match with 2nm spacing throughout the whole mean chord track.

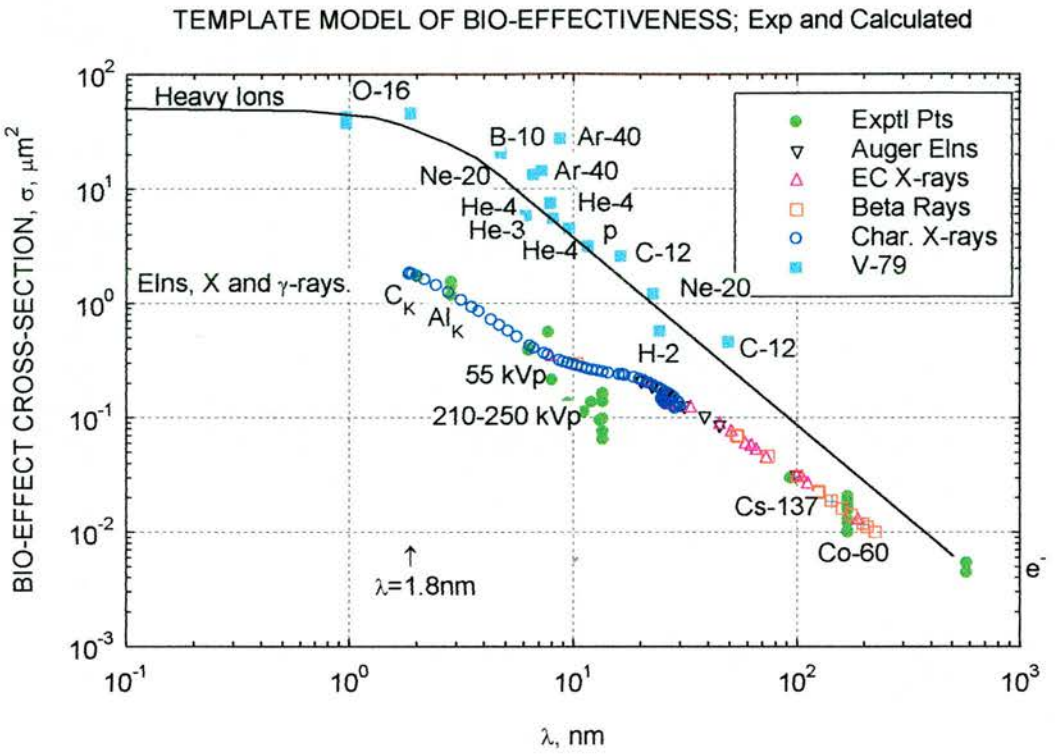

Fig 4.13 Plot of effective cross-section against lambda for V79 cells irradiated with heavy ions and the results of the Auger emitters (in pink triangles). Beta emitters are open red squares. Comparison can be made between the experimental data and the calculated data. In the lower graph, experimental points in external irradiations from C_k to Co-60 are indicated. Excellent agreement is obtained for both experimental and calculated, σ_B.

The results in Fig 4.13 are expanded and added too in Fig 4.14 which, shows the calculated bio-effect for sparsely ionizing radiations generated by the Template model for the Auger emitters. All 16, lie reasonably well on the curve and are superimposed on the beta emitters. The results show that the values of highest effective cross-section have lambda greater than 1.8nm. This may suggest that the effectiveness of these Auger emitters in causing damage according to the model presented here may not be as high as generally thought, for a dose based system.

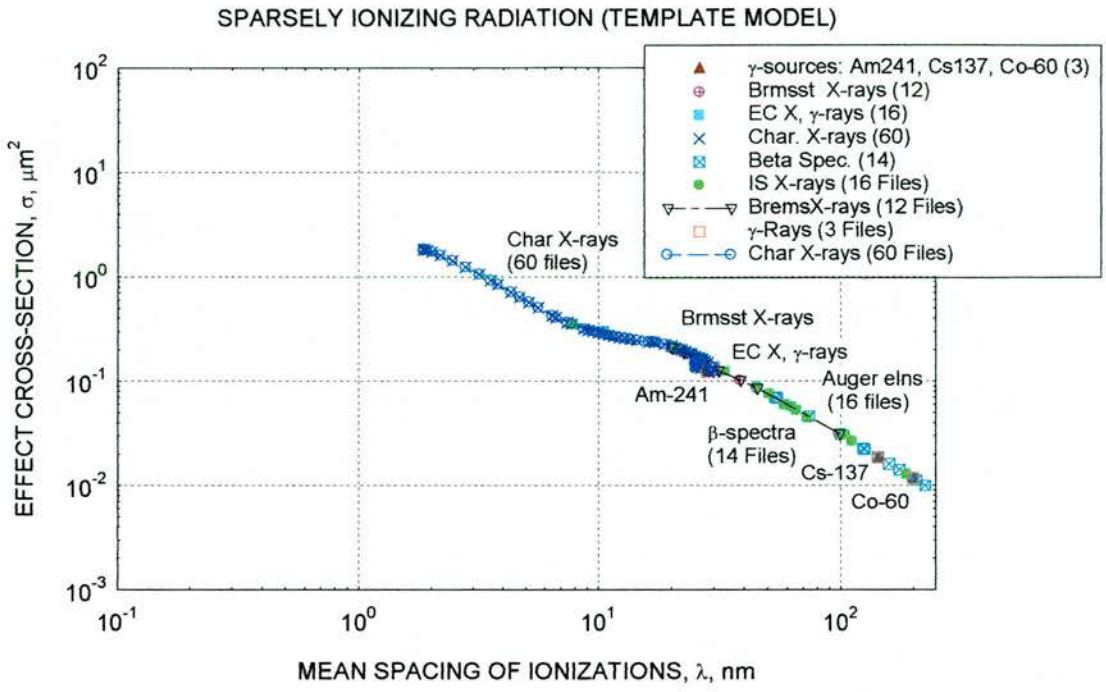

Fig 4.14 Graph of bio-effect cross-section for the calculated sparsely ionizing radiation along with the Auger electrons. Results for calculated and experimental effect cross-section are in very good agreement with the template model.

4.15.2 Assessment of radiation quality of different radiations on different cell lines from sparsely ionizing radiation.

The important point from Fig 4.14 is that, as the lambda increases the effect cross-section appears to decrease for V-79 cells. The peak lies around 2-5nm. This is in good agreement with the finding that it is the 2nm DNA spacing that is the important template requirement for maximum damage a segment of DNA is consistent as the critical target.

Having seen that the experimental data for three different cell lines (e.g. figure 4.16) show some form of trend with respect to the mean free path, the next step is to look at the experimental data on V-79 cells and the calculated curves of cross-section against lambda, Fig 4.15. We can see that the Figure 4.15 shows very good correlation for the different types of radiation and for the Auger electron emitters

(green). We can see that the results are within statistical tolerance limits considering that for biological systems the errors can be up to 30% whereas the errors in lambda being a physical parameter is often less than 2%. Fig 4.16 shows the effective cross-section for sparsely ionising radiation and different targets. We can see that for the wide range of radiation type the bio-effect appears to be on a nearly linear curve with respect to lambda. This graph also shows that human cells have about 5 times larger effect cross-sections than V79 cells.

One can conclude that the effect of radiation can in terms of effective cross-section be unified with respect to the mean free path of interaction of the radiation, in that all these lie on one trend line and the degree of damage in terms of effect cross-section has a direct correlation. With this correlation it is possible to assign the toxicity of a given radionuclide.

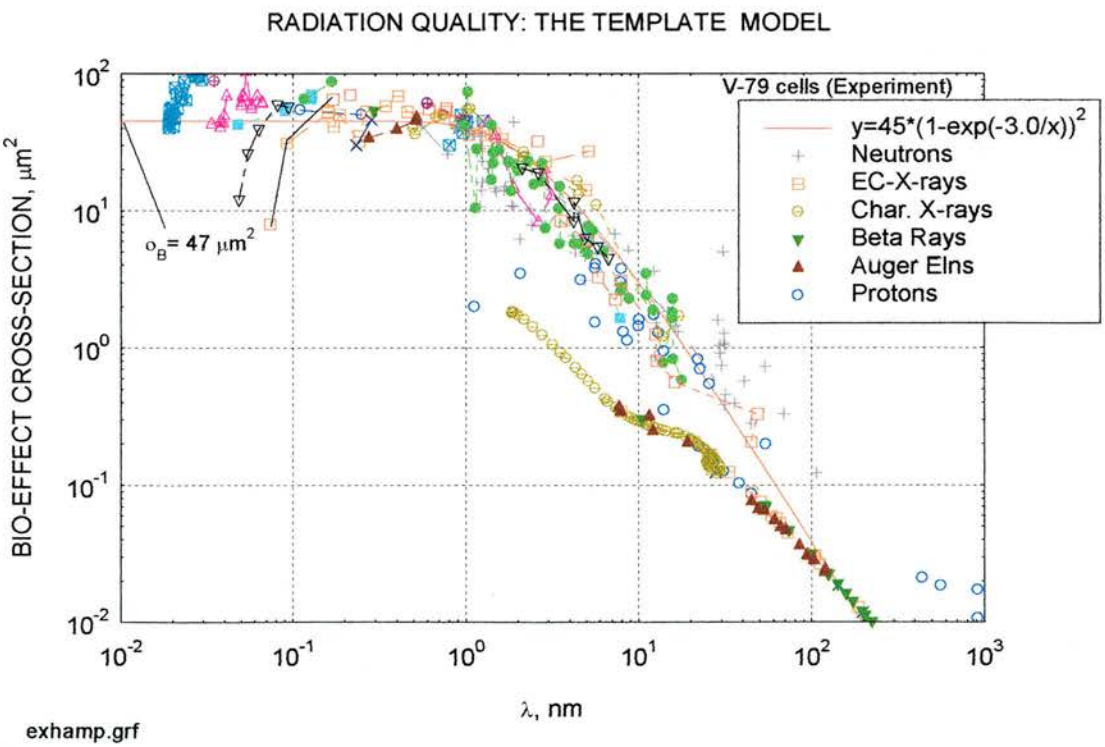

Fig 4.15 Plot of the effective cross-section against lambda including the experiments on V79 cells and the projected curves for the different ionising radiations.

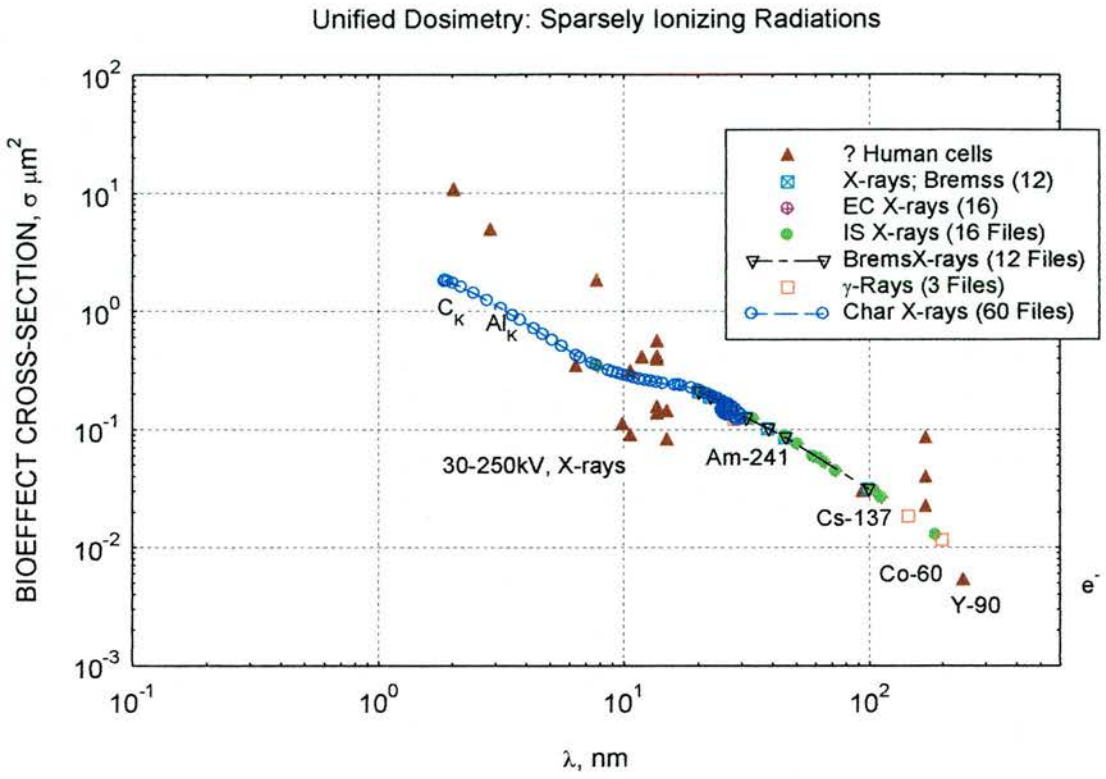

Fig 4.16 Plot of the effective cross-section against lambda for different sparsely ionising radiations and effect on human cells.

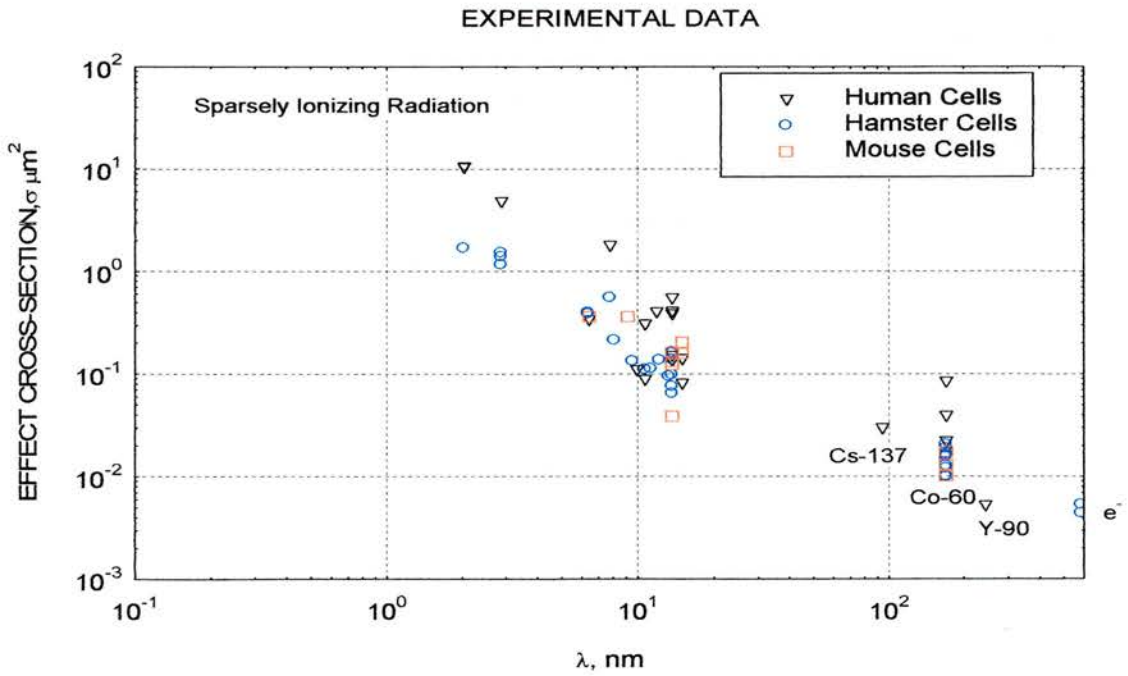

Fig 4.17 Plot of the effective cross-section against lambda for different sparsely ionising radiations and effect on human, hamster and mouse cells. Human cells have about 5 times larger effect cross-sections than V79 cells.

4.15.3 Hofer's experimental results.

4.15.3.1 General Trends.

Using the equations described in chapter two and the ones described earlier in this chapter, the Hofer data shown in the tables 4.1 is analysed further. The figure below contains plots of the survival fraction against the decay per cell, the points showing Hofer's experimental data and the solid lines showing the model calculations. The agreement is very good indeed, indicating that the timing element in the model is in good agreement with the experimental findings.

As a first step in the process of verification with the experimental results of Hofer et al some trends and correlations are shown to support the model with respect to cell lines.

The figures 4.18 and 4.19 below shows the correlation of inactivation probability against the mean free path at different temperatures.

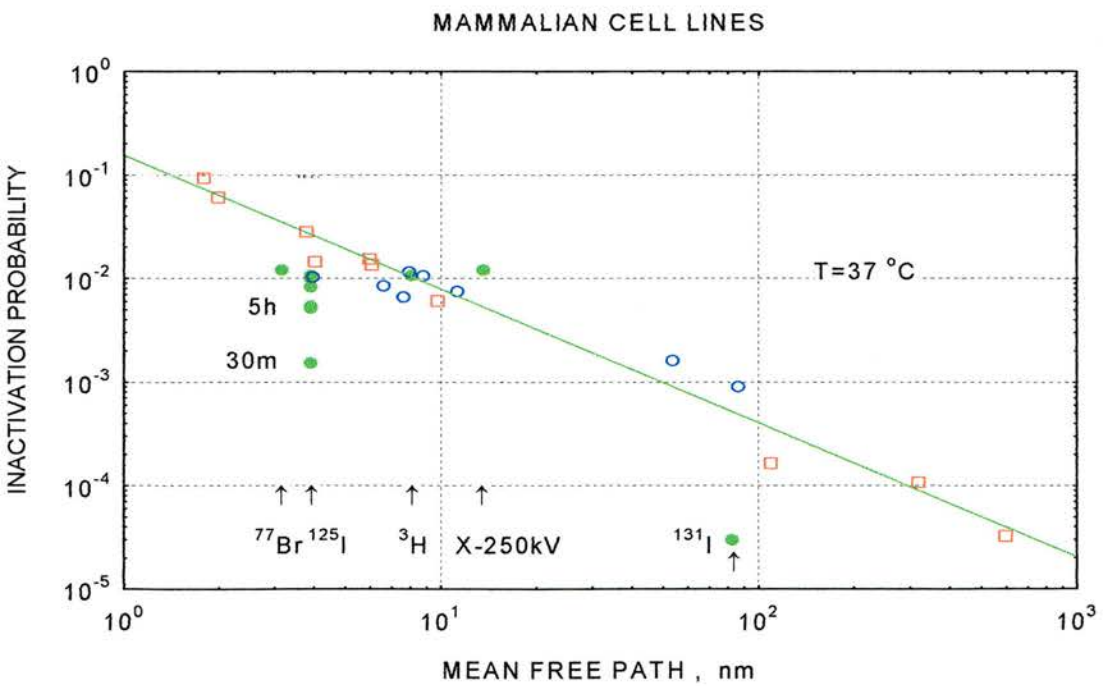

Fig 4.18 Graph of inactivation probability of mammalian cells correlated to the ionisation mean free path.

The figure 4.19 below shows the results obtained with the temperature at –196°C. The results in this case correlate better.

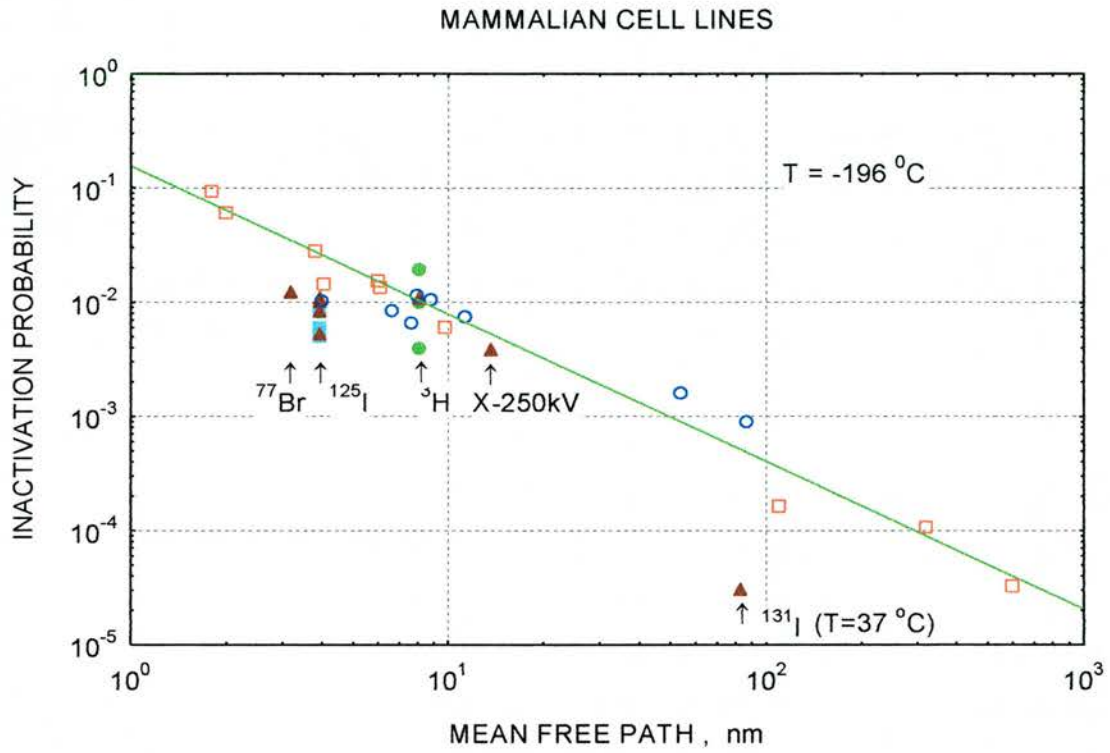

Fig 4.19 Graph of the inactivation against mean free path for an experimental temperature of –196C. The latter temperature is presumed to eliminate indirect action by diffusion.

These figures show that the model predictions correlate reasonably well taking into account the errors associated with biological systems and the different experimental methods used in ionising the cells and dose estimations.

As commented earlier, there are many end-points and cell types etc. Most of these are of limited value as they are not sufficiently specific to test against the model for Auger electron emitters. In order to improve the validity of the model and the assumption that single track action is the most critical and that the importance of duration of the irradiation time affecting the repair mechanism, the studies of Hofer et al (1992, 1995, 1997) are of great help.

These experiments were carried out in such a controlled fashion that the exposure of the Chinese hamster ovary cells (CHO) to radiation from an Auger electron emitting radionuclide, in this case I-125, was fixed not only for specific points in the cell cycle for these synchronised cells but also the experiments were performed at constant dose-rate. The dose was delivered by accumulating the decays at liquid nitrogen temperatures. This method of dose accumulation implies that, for synchronised cells, the U(z,t) function mentioned in chapter 2 can be applied.

4.15.3.2 Effect of radioprotectors.

Using the data from Hofer et al, for I-125 the effect of radioprotectors, in this case MEA, can be shown as a plot of decays per cell against survival fraction (Fig 4.20). A Comparison of synchronised cell data is made to test the model further. The calculations of the survival fractions, using the model, when plotted against decays per cell (Fig 4.20) give both slightly sigmoid curves and straight lines. Data are compared simultaneously for all six survival curves of Hofer et al. The correlation is seen to be very good, for all times into the cell cycle in the S-phase. The deviation of the experimental data from those calculated is only 9%, which is statistically significant.

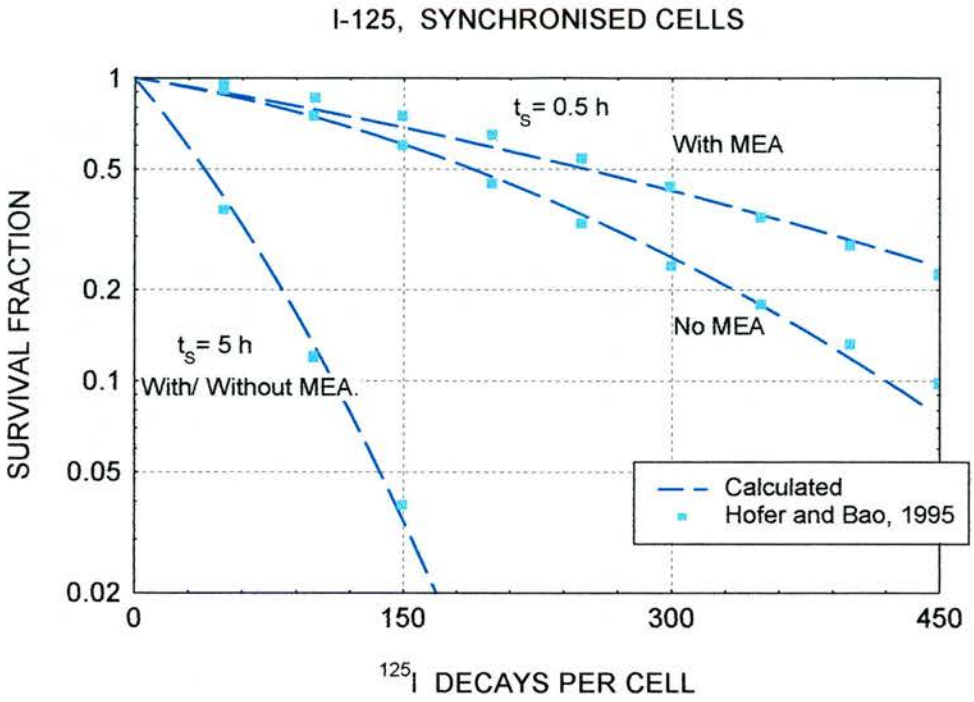

Figure 4.20 Plot of surviving fraction and decays per cell showing the effects of radioprotectors compared with Hofer and calculated data.

A very good correlation is obtained with the calculated data. However it should be noted that the radical diffusion constant (Λ) in the model was obtained by analysis of these data.

The relationship between the experimental surviving fraction versus the calculated surviving fraction for CHO cells with I-125 incorporation is shown in Figure 4.21. The linearity is seen to be very good, indicating that the models ability to predict the experimental results are very good indeed.

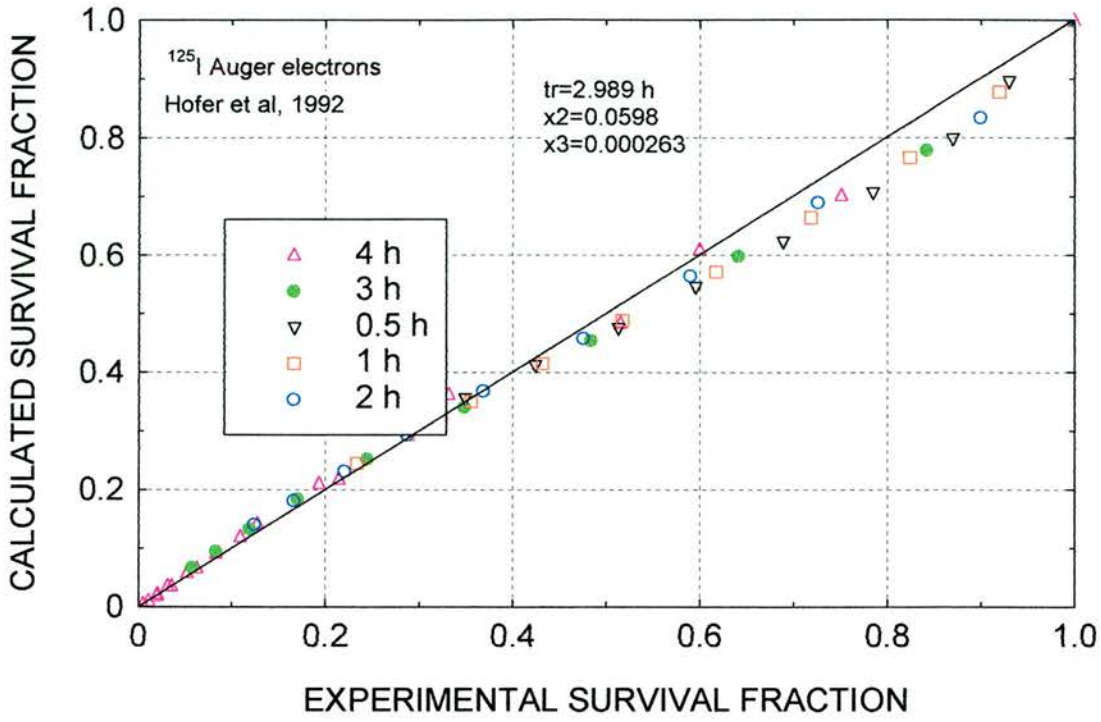

Figure 4.21 Plot of experimental and calculated survival fractions.

Figure 4.22 below shows that the results/collected data conform to the shoulder survival curve response, with the data falling in the model predicted pattern i.e. the solid lines. The calculated and experimental survival fraction as a function of decay indicates that the Auger electron emitters Br-77 and I-125 lie within acceptable error limits.

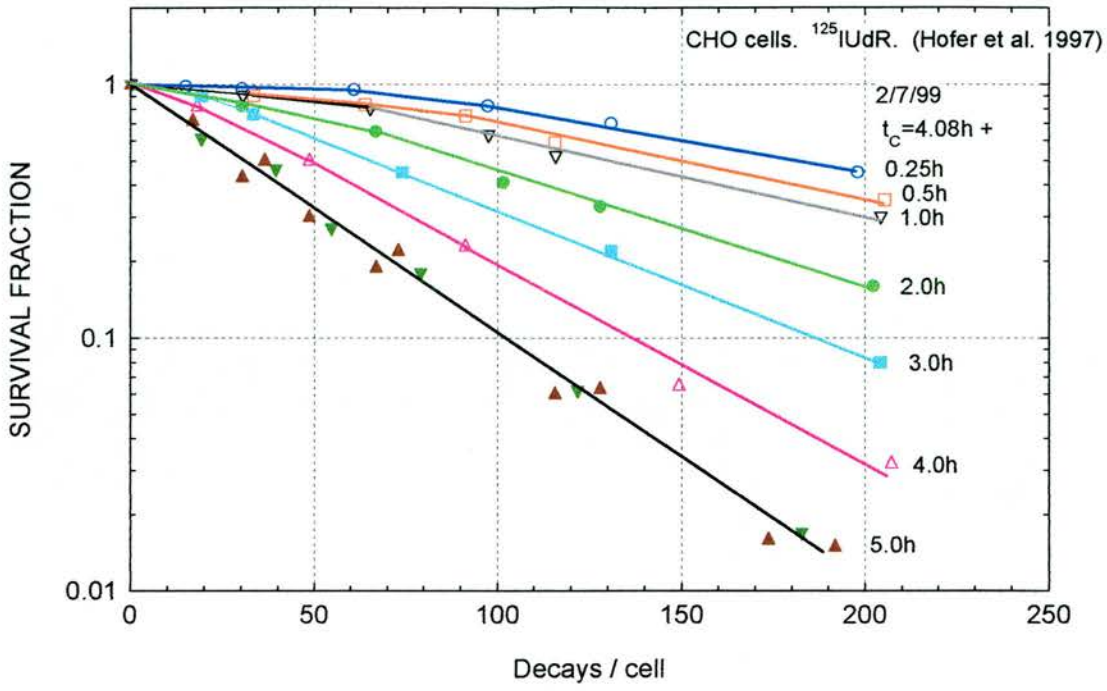

Fig 4.22 Graph of Hofer's experimental data with the model predicted curves in solid for all exposure durations.

We can see in the above figure that the experimental and calculated (solid lines) show very good coincidence. The results for synchronised CHO cells and the models prediction are shown in Fig 4.23. This a plot of the experimental mean number of dsb's in DNA per cell versus the calculated mean number of dsb's in DNA per cell using the Hofer 1995 data. The plot of DNA/cell for those calculated against the experimental data shows a straight line relationship with a deviation of less than 7% (see Fig 4.23).

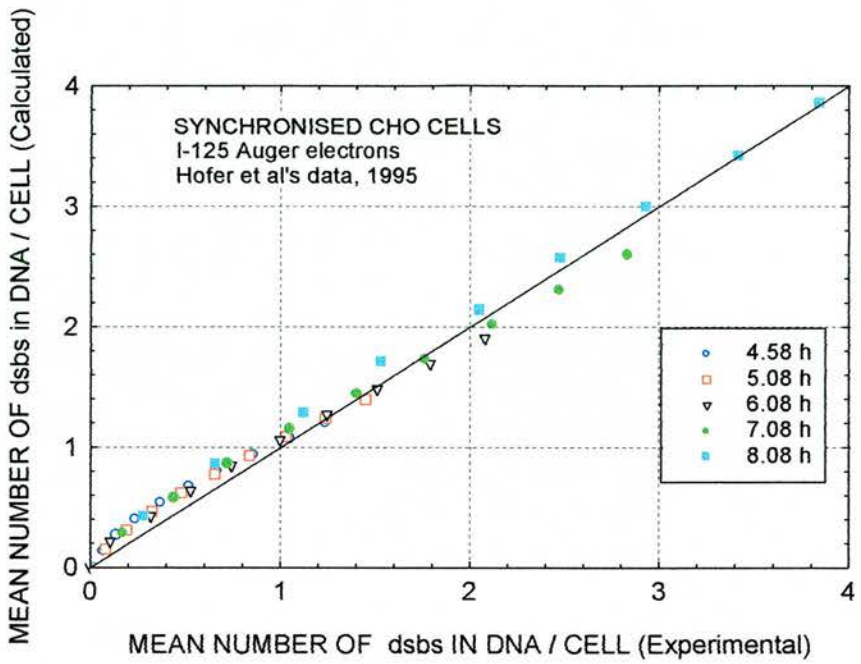

Figure 4.23 Plot of experimental mean number of dsb's in DNA per cell and calculated mean number of dsb's.

Looking at the results obtained by Hofer et al and comparing these with the model predictions we can come to several conclusions as follows.

The inactivation probability for mammalian cells correlates reasonably well with the predicted trend line the correlation being more statistically significant for experimental temperatures of -196°C. This is most likely due to the fact that the ionisation or the dose delivery is more likely to be localised in that state. Similar results are seen for E-coli and Phage cell lines.

The plot of model effect cross section and lambda for specific nuclides show that, although the cross section varies with nuclide, the value of lambda is relatively constant. It is not possible to conclude that the results lie within the 2nm specification mainly due to the wide methodologies used in the assessment of cell death in the different studies.

The test of the model for radioprotectors shows that the experimental results tally very well with the model predictions. The values are almost identical for decays per cell in the case of I-125. For the same nuclide the model predicts extremely well the survival fraction found in the experiments. For all the different timings that Hofer irradiated the cells at, the graphs also show that the results for synchronised CHO cells the experimental data lies within the model predicted values, not only for the survival fraction but also for the number of dsb's produced in the DNA per cell.

The experimental work, in particular the Hofer et al experiments and the calculated results are very consistent in predicting the actual survival fraction, number of dsb's, effect of radioprotectors and the effect of irradiation of the cells at different points in the cell cycle. It should be noted however that Hofer et al do not assume that the DNA dsb is the critical lesion for cell damage.

In order to relate the bio-effectiveness of the radiation with the mean free path of ionisation (lambda) further in a quantitative way with regards to physical damage, we need to look at the relationship of the dsb's in DNA to lambda. If we plot results of the number of dsb's in DNA for the different radiations we can see that the results from the Auger emitter (green) lie reasonably well within the pattern of the other radiation types, again within statistical acceptability with a few exceptions (see Fig 4.24).

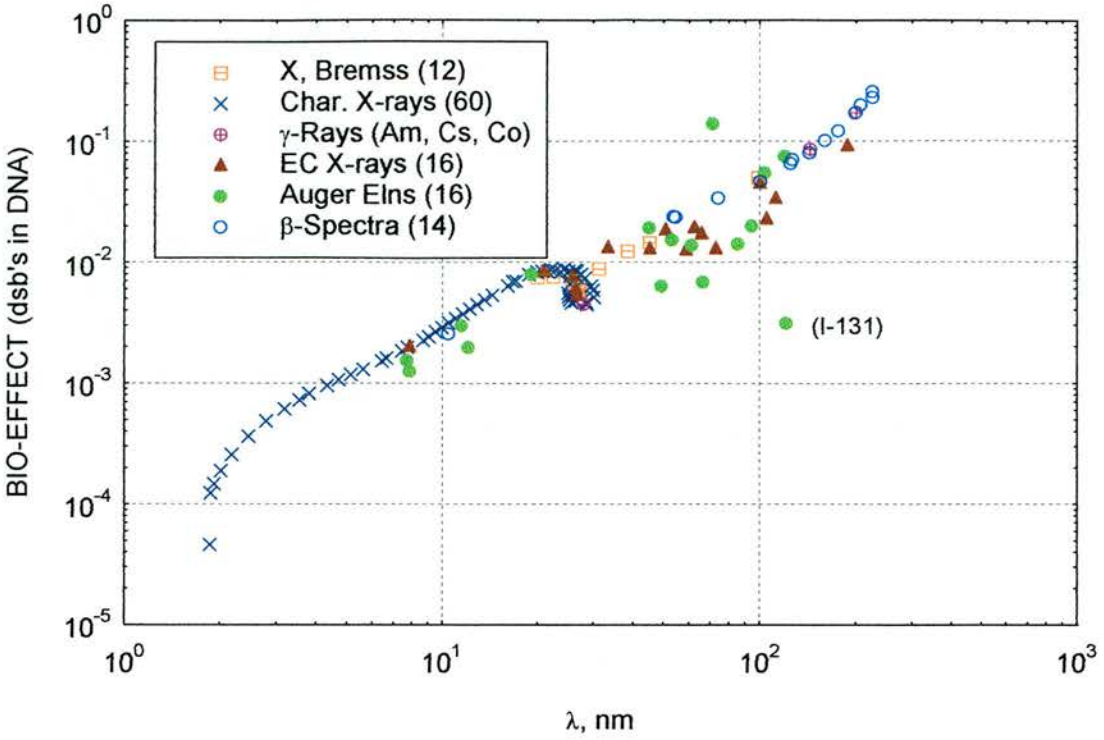

Fig 4.24 The relationship between the dsb's in DNA against lambda is shown for a wide number of radiation sources including 16 Auger electron emitters. It shows that Auger emitters generally tend to follow the pattern of the other established sources. [Only about 6% of the I-131 decays are by Auger processes, the remainder are mainly beta decay].

Having shown that the model has the ability to predict the experimental findings the next step is to determine the bio effect of the selected Auger electron emitters, and derive cyto-toxicity factors for these nuclides. This is done in the next chapter.

CHAPTER FIVE

Bio-effect and Cytotoxicity of Auger Electron Emitters

5.0 Introduction.

Taking the results from chapter 4 the aim here is to assign cyto-toxicity factors to the Auger electron emitters and β-emitters considered in this thesis.

5.1 Bio-effect of Auger Electron Emitters.

Looking at the effective cross-section for sparsely ionising radiation, Fig 4.19 onwards, we can see that for the wide range of radiation type the bio-effect appears to be on a linear curve with respect to lambda. One can conclude that the effect of radiation can in terms of effective cross-section be unified with respect to the mean free path of interaction of the radiation, in that all these lie on one trend line and the degree of damage in terms of effect cross-section has a direct correlation. With this correlation it is possible to assign the toxicity of a given radionuclide.

The correlation of experimental and model cross sections as a function of lambda the mean free path for ionisation, shown in the results above, shows that the model has the ability to predict the experimental data which corresponds very well with the predicted result.

However it should be noted that, in the present calculations no allowance is made for repair, these data also do not include a correction for the unrepair (U(Z,t) term but this latter is known to be approximately constant and independent of irradiation time for asynchronised cells. For an arbitrary 2 hour repair rate, the constant value of U(Z,t) is about 25%. This would act to further reduce, by a factor of 4, the calculated (model) cross-sections bringing them much more

closely into agreement with experiment. Results are within the statistical errors of the results for the external irradiations, indicating that a full unified theory may be attainable.

The model does seem to give values around the average for the experimental data. Considering the wide range of experimental parameters used, this is encouraging.

The results also suggest that I-125 can reach heavy ion damage purely due to the existence of the cascade electrons. The results also indicate that if the results are analysed in terms of unit fluence of electrons, then the effect is simply as expected from x-rays, within the limited accuracy of the experimental data.

Although the model predicts a radiation action that would result in pure exponential survival for doses of electrons less than several kilograys, the reason this is not the case is most likely due to the two main unknowns the mean time taken to repair of DNA dsb's and the radical diffusion length in the presence of natural scavengers. However for Auger electron emitters the increased number of highly localised electrons per decay may increase the number of coincident events as a result of the multiple tracks near the DNA of interest. An attempt is made in the next section to classify the Auger electron emitters taking into account the comments made above and in the previous chapters.

5.2 Cyto-toxicity factors for collected data and specific cases.

Having established that the bio-effect of these electron emitters is reasonably well predictable and this corresponds well with the experimental findings, an attempt is now made to assign cytotoxicity factors to the 16 Auger emitters concentrated here, also a comparison is made with the beta emitters.

First the beta nuclides are looked at and classified. Figure 5.1 shows the bio-effect cross-section (σ) as a function of the average linear primary ionization (λ), the tabulated figures are shown in Table 5.1. Figure 5.1 shows that the bio-effect lies on a linear trend line correlating to the primary ionization. Figure 5.2 shows the calculated cyto-toxicity for these emitters. What Fig 5.1, 5.2 and Table 5.1 show quite clearly is that, the cyto-toxicity is related to the primary/mean free path ionization.

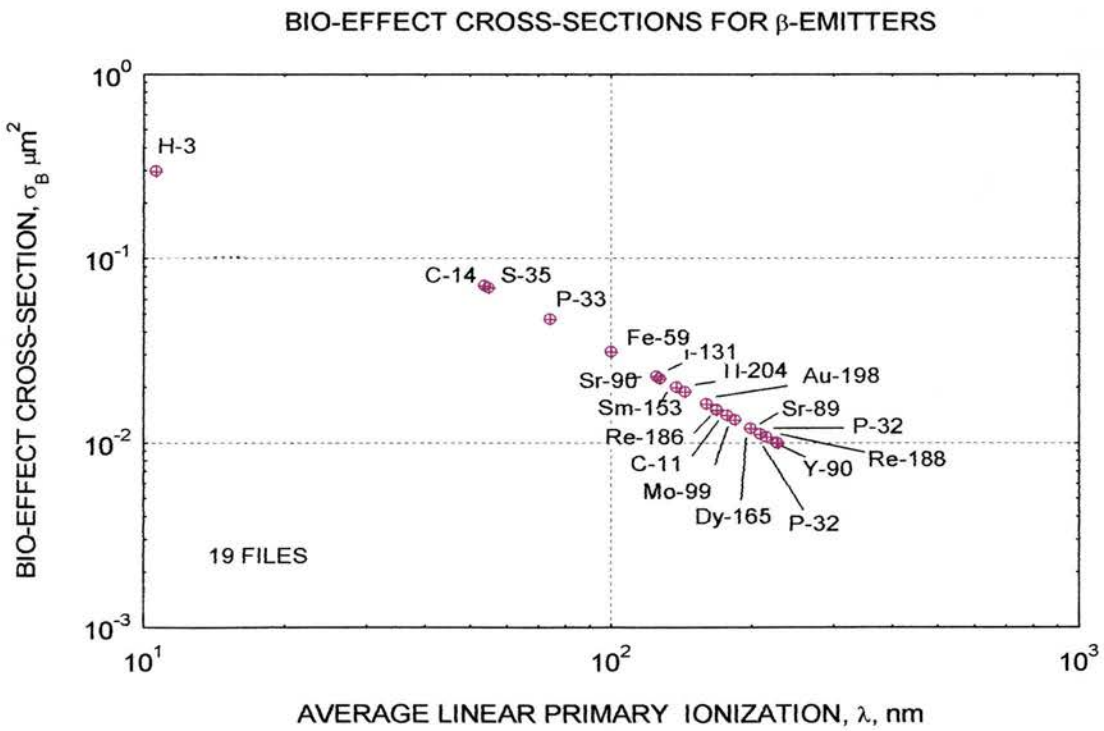

Fig 5.1 Graph of Bio-effect cross-section as a function of primary ionization for the beta emitters.

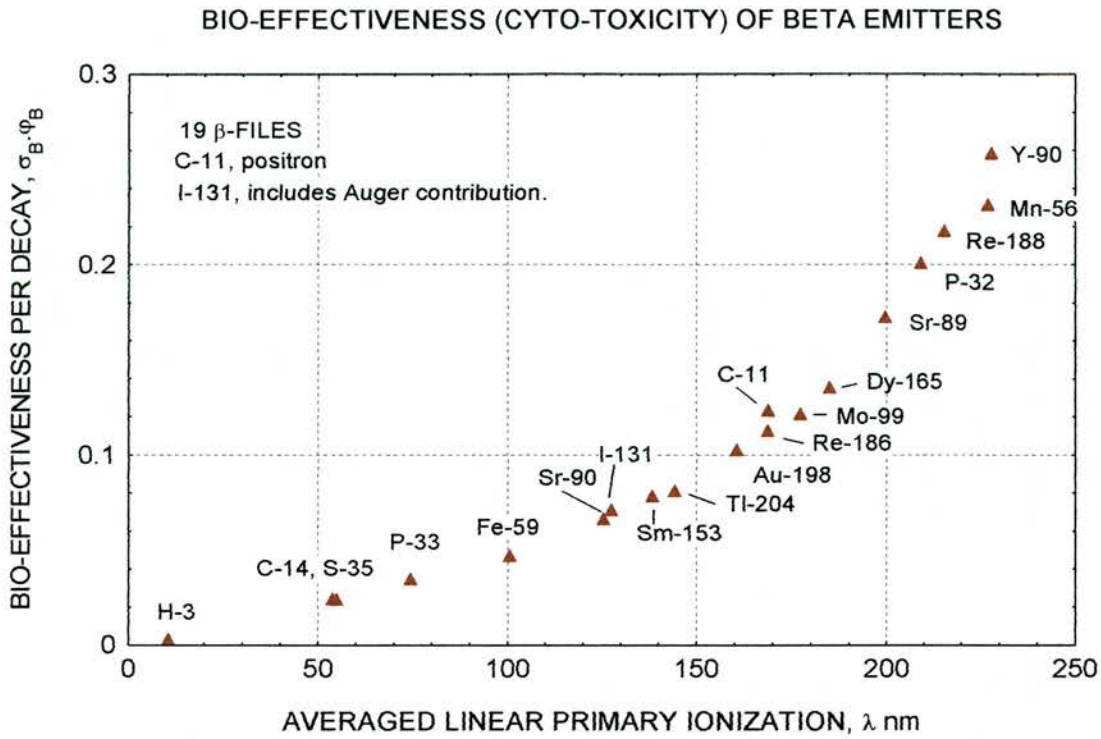

Fig 5.2 Calculated Cyto-toxicity factors for beta emitters (linear scales).

Table 5.1 Table of beta decay Bio-effect cross-sections, σ_B μm^2 , and Bio-effectiveness, $\sigma_B.\Phi_o$ (a pure number) for 19 β – decaying radionuclides. Φ_o is the intrinsic fluence at equilibrium for each β – decay. (Arranged in order of λ).

	(1) Radionuclide	(2) Mfp, λ nm	(3) σ_B μm^2	(4) Φ_o μm^{-2}	(5) $\sigma_B.\Phi_o$
1	**H-3**	10.66	2.965E-1	8.168E-3	2.442E-3
2	**C-14**	53.98	7.082E-2	3.351E-1	2.373E-2
3	**S-35**	55.04	6.891E-2	3.407E-1	2.348E-2
4	**P-33**	74.52	4.658E-2	7.321E-1	3.410E-2
5	**Fe-59**	100.7	3.105E-2	1.496E+0	4.645E-2
6	**I-131**	125.7	2.284E-2	2.884E+0	6.585E-2
7	**Sr-90**	127.7	2.222E-2	3.173E+0	7.053E-2
8	**Sm-153**	138.5	1.993E-2	3.908E+0	7.788E-2
9	**Tl-204**	144.4	1.882E-2	4.282E+0	8.060E-2
10	**Au-198**	160.7	1.617E-2	6.315E+0	1.021E-1
11	**Re-186**	168.8	1.507E-2	7.446E+0	1.122E-1
12	**C-11**	168.9	1.500E-2	8.202E+0	1.230E-1
13	**Mo-99**	177.9	1.404E-2	8.697E+0	1.221E-1
14	**Dy-165**	185.1	1.328E-2	1.016E+1	1.349E-1
15	**Sr-89**	199.7	1.193E-2	1.440E+1	1.719E-1
16	**P-32**	209.4	1.113E-2	1.801E+1	2.004E-1
17	**Re-188**	215.7	1.073E-2	2.024E+1	2.172E-1
18	**Mn-56**	227.2	1.001E-2	2.307E+1	2.309E-1
19	**Y-90**	228.1	9.910E-3	2.602E+1	2.579E-1

Having shown that the beta emitting nuclides show a relationship with lambda with respect to cyto-toxicity, we next look at the Auger electron emitters. Figure 5.3 shows the bio-effect cross-section of the Auger electron emitters as related to the average primary ionization, again as with the beta nuclides we can see that this lies on a linear trend line. This is confirmed further in Figure 5.4 which is a graph of the beta and Auger bio-effects. Plotted together the consistency is very good indeed. Figure 5.5 shows the cyto-toxicity factors for the Auger emitters as with the beta emitters we can see a reasonably good trend. However, this is not as consistent as shown by the beta data considering the variations in the experimental methods reported in Table 4.1, this is very encouraging. Some of these Auger electron emitting nuclides have complex spectra and there is a beta contribution which complicates the analysis. These results are also shown in tabulated form in Table 5.2 and 5.3.

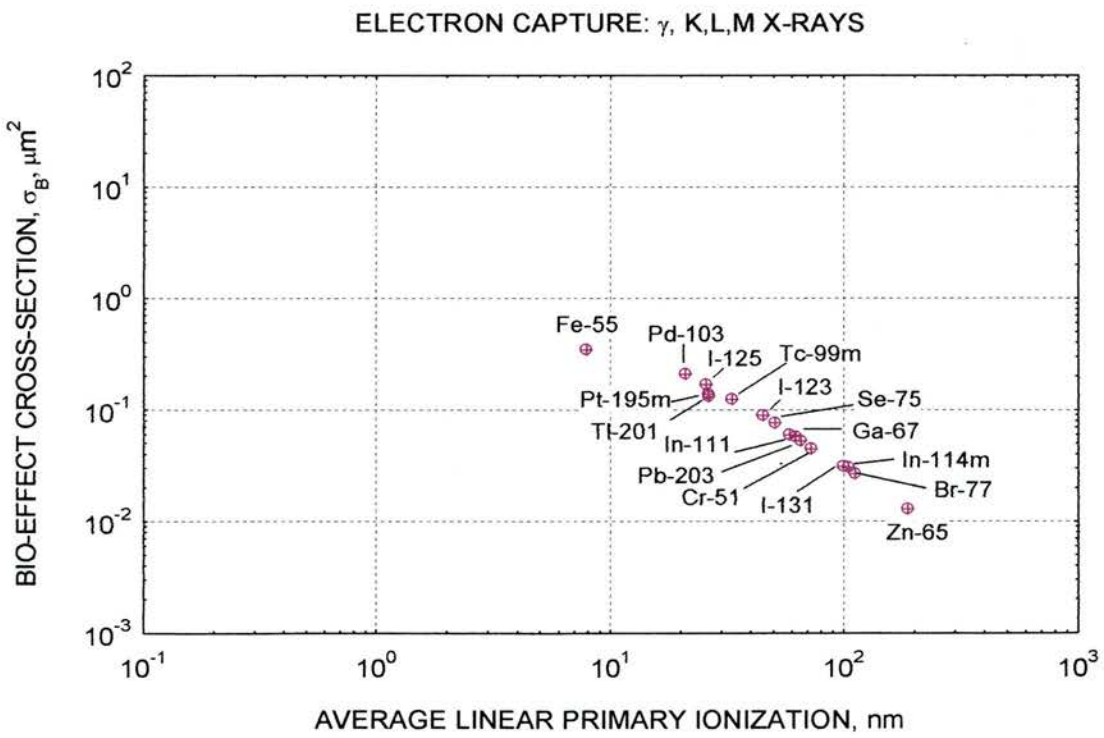

Fig 5.3 Graph of Bio-effect cross-section as a function of primary ionization for the photon components see table 5.2.

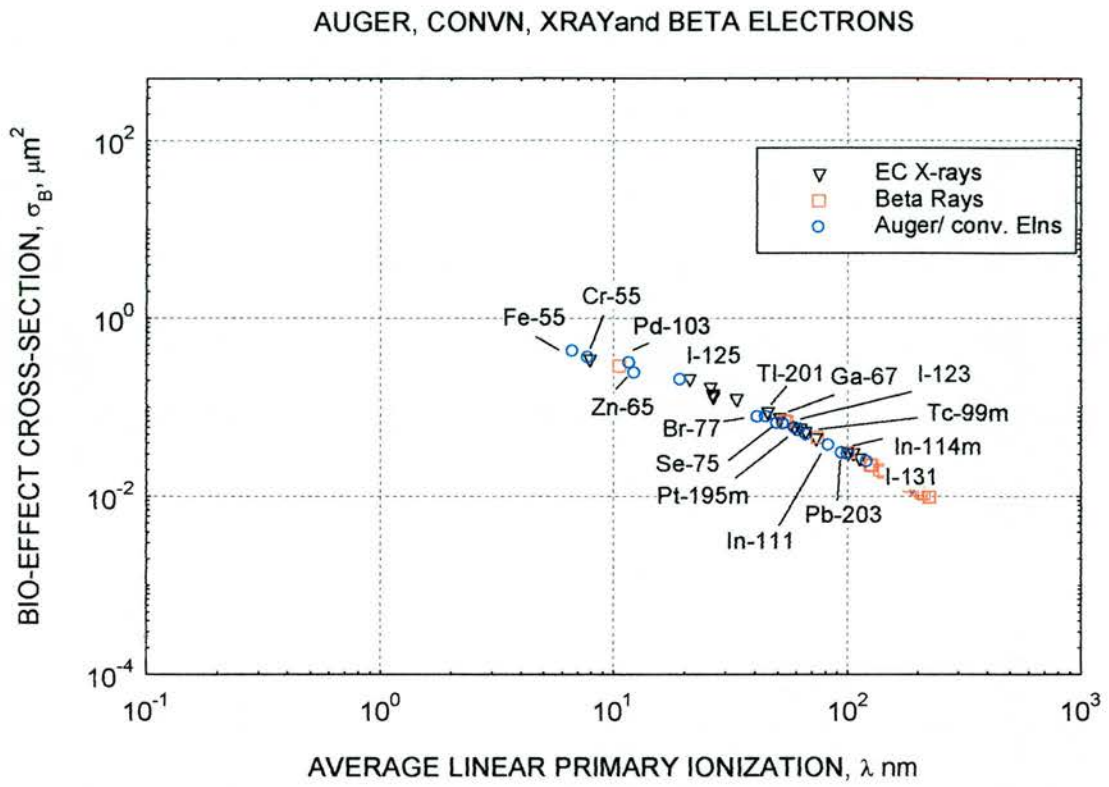

Fig 5.4 Composite graph of Bio-effect cross-section for EC, Auger and Beta nuclides as a function of lambda. See Tables 5.1, 5.2 and 5.3.

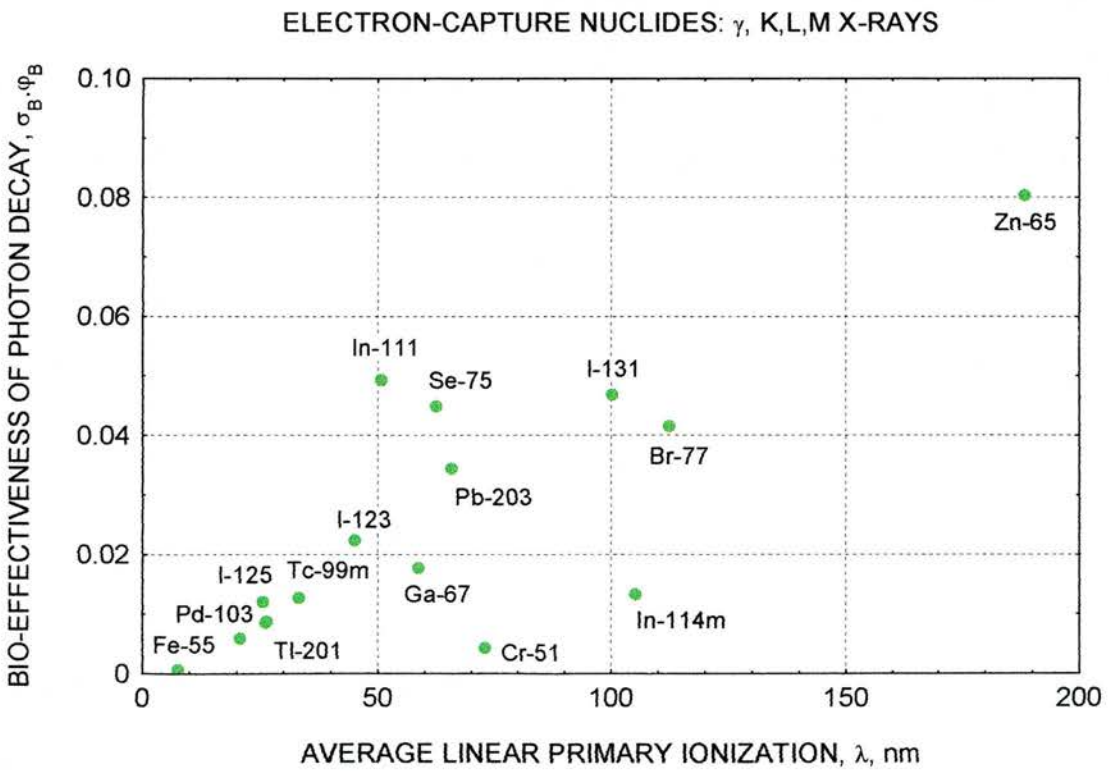

Fig 5.5 Calculated Cyto-toxicity factors for photon emitters. See data, Table 5.2 column 6.

Table 5.2 Shows the Bio-effect cross-section, σ_B cm^2 , and Bio-effectiveness, $\sigma_B.\Phi_0$, for various photon components of electron capture are determined for 16 radionuclides listed. The bio-effect cross-section, given by σ_B cm^2, is a measure of the absolute quality of the radiation field, determined by the 'template model. When multiplied by the charged particle fluence per decay at equilibrium, the partial product, σ_B, Φ_0 , yields a measure of the bio-effectiveness (col 6). For the total bio-effectiveness, where relevant, the summation in column 7 is applied. The asterisks in column 7, I-131, indicates that the beta rays present in the decay scheme should be added. Table 5.3 shows the same results for the Auger conversion electrons.

Table 5.2 Bio-effect cross section for 16 radionuclides
(Arranged in order of λ). * indicates beta-ray per decay has been added.

	(1) Radionuclide	(2) Photons /decay	(3) Mfp, λ nm	(4) σ_B μm^2	(5) Φ_o μm^{-2}	(6) $\sigma_B . \Phi_o$	(7) $\sum \sigma_B . \Phi_o$
1	**Fe-55**	0.2831	7.921	3.447E-1	1.638E-3	5.647E-4	2.236E-3
2	**Pd-103**	0.6916	21.09	2.084E-1	2.782E-2	5.796E-3	5.764E-3
3	**I-125**	1.561	25.97	1.681E-1	7.080E-2	1.190E-2	1.986E-2
4	**Tl-201**	1.406	26.56	1.385E-1	6.085E-2	8.430E-3	1.053E-1
5	**Pt-195m**	1.625	26.72	1.315E-1	6.580E-2	8.652E-3	8.567E-2
6	**Tc-99m**	0.9587	33.53	1.241E-1	1.014E-1	1.258E-2	1.941E-2
7	**I-123**	1.727	45.40	8.874E-2	2.508E-1	2.226E-2	3.61E-2
8	**In-111**	2.668	51.02	7.578E-2	6.495E-1	4.922E-2	6.324E-2
9	**Ga-67**	1.400	59.01	5.968E-2	2.952E-1	1.762E-2	3.291E-2
10	**Se-75**	2.329	62.72	5.728E-2	7.816E-1	4.477E-2	5.108E-2
11	**Pb-203**	2.003	66.03	5.275E-2	6.508E-1	3.433E-2	5.319E-2
12	**Cr-51**	0.3274	73.23	4.473E-2	9.438E-2	4.221E-3	5.764E-3
13	**I-131**	1.040	100.6	3.107E-2	1.503E0	4.669E-2	*1.16E-2
14	**In-114m**	0.5790	105.6	3.046E-2	4.324E-1	1.317E-2	6.743E-2
15	**Br-77**	1.231	112.7	2.665E-2	1.555E0	4.143E-2	4.483E-2
16	**Zn-65**	0.8763	188.7	1.288E-2	6.231E0	8.024E-2	8.216E-2

Table 5.3 Table for Auger conversion electrons
(Arranged in order of λ). * indicates beta-ray per decay has been added.

	(1) Radionuclide	(2) Photons/decay	(3) Mfp, λ nm	(4) σ_B μm^2	(5) Φ_o μm^{-2}	(6) $\sigma_B.\Phi_o$	(7) $\sum \sigma_B.\Phi_o$
1	**Fe-55**	5.068	6.699	4.317E-1	3.873E-3	1.672E-3	2.237E-3
2	**Cr-51**	5.396	7.804	3.660E-1	4.216E-3	1.543E-3	5.764E-3
3	**Pd-103**	2.804	11.79	3.187E-1	9.415E-3	3.001E-3	8.797E-3
4	**Zn-65**	4.408	12.38	2.444E-1	7.865E-3	1.922E-3	8.216E-2
5	**I-125**	4.160	19.33	2.057E-1	3.871E-2	7.963E-3	1.986E-2
6	**Br-77**	3.777	41.25	7.857E-2	4.330E-2	3.402E-3	4.483E-2
7	**Tl-201**	3.615	44.83	7.871E-2	2.493E-1	1.962E-2	1.053E-1
8	**Se-75**	4.580	50.14	6.630E-2	9.523E-2	6.314E-3	5.108E-2
9	**Ga-67**	6.047	53.20	6.574E-2	2.326E-1	1.529E-2	3.291E-2
10	**Pt-195m**	6.866	59.62	5.926E-2	1.301E-0	7.707E-2	8.567E-2
11	**I-123**	3.166	61.95	5.543E-2	2.498E-1	1.384E-2	3.61E-2
12	**Tc-99m**	2.327	66.92	4.945E-2	1.382E-1	6.833E-3	1.941E-2
13	**In-111**	3.242	83.41	3.793E-2	3.697E-1	1.402E-2	6.324E-2
14	**Pb-203**	2.203	95.05	3.098E-2	6.443E-1	1.886E-2	5.319E-2
15	**In-114m**	2.663	100.7	3.001E-2	1.808E-0	5.426E-2	6.743E-2
16	**I-131**	0.0629	121.5	2.457E-2	1.283E-1	3.153E-3	*1.16E-2

The results in Table 5.2 shows the Bio-effect cross-section, σ_B cm^2 , and Bio-effectiveness, $\sigma_B.\Phi_0$, for various photon components of electron capture, are determined for some radionuclides. Remember that the bio-effect cross-section, given by, σ_B cm2, is the intrinsic fluence per decay at equilibrium and the product of these, σ_B, Φ_0 , is a measure of the bio-effectiveness. Table 5.3, shows the results for various components of electron capture nuclides e.g. Auger and conversion electrons, (column 6) and total bio-effectiveness in column 7.

Note that the cyto-toxicity factor is a pure number (table 5.1 column 5; tables 5.2 and 5.3, columns 6 and 7) there is no direct relationship between the Atomic mass and the cyto-toxicity factor as derived here. In chapter 4 (also see Appendix 1) it was concluded that there was a large variations in the radiation output from different Auger electron emitting radionuclides.

The cyto-toxicity values shown in the Table 5.2 and 5.3 do not take in to account the repair function and are values determined from the initial slopes. The model and experimental cross section for one and two track mechanisms compared with experimental data need to be carried out.

It should be noted that the graphs also do not take repair into account. Thus the factor C_F represents the initial bio-effect per unit concentration of decays in the cell nuclear volume (see Equations in chapter 2 and 4). On the basis of Hofer's data, the diffusion length of radicals (Λ) is taken as 3nm. The U(Z,t) function is put equal to unity i.e. only the initial damage is considered, before there is time for repair. However, the repair function can be easily evaluated for a specified

irradiation time, t_i. The mean repair time for lesions is found to be almost exactly 2 hours. Note that these results are intended to apply to irradiations under equilibrium conditions, as for example when there is a uniform distribution of radionuclide throughout the tissue volumes of interest. There may be significant differences in the values of C_F if the radionuclide is used to 'tag' molecules within the cell nucleus. Then allowance must be made for the deviation from equilibrium - a problem yet to be solved in the foregoing method. From what we know about the decay schemes, equilibrium is probably much closer than generally believed. Tagged molecules should not be too different from 'untagged' and is revealed in the cross section analysis. Approximate results can be obtained using only those electron radiations from the decay that are absorbed within the cell nuclear dimensions.

Another way of looking at the results is in terms of yield of DNA lesions per decay, since the DNA is considered to be the critical target and the 2nm separation being the important factor in causing effective damage. The damage per decay related to the mean free path/ linear primary ionization would give an idea of the relative damage caused by the Auger electron emitting nuclides. Figure 5.6 shows the results for the Auger and conversion electrons, we can see that the results are much closer and the pattern is very comparable to the beta emitter shown earlier.

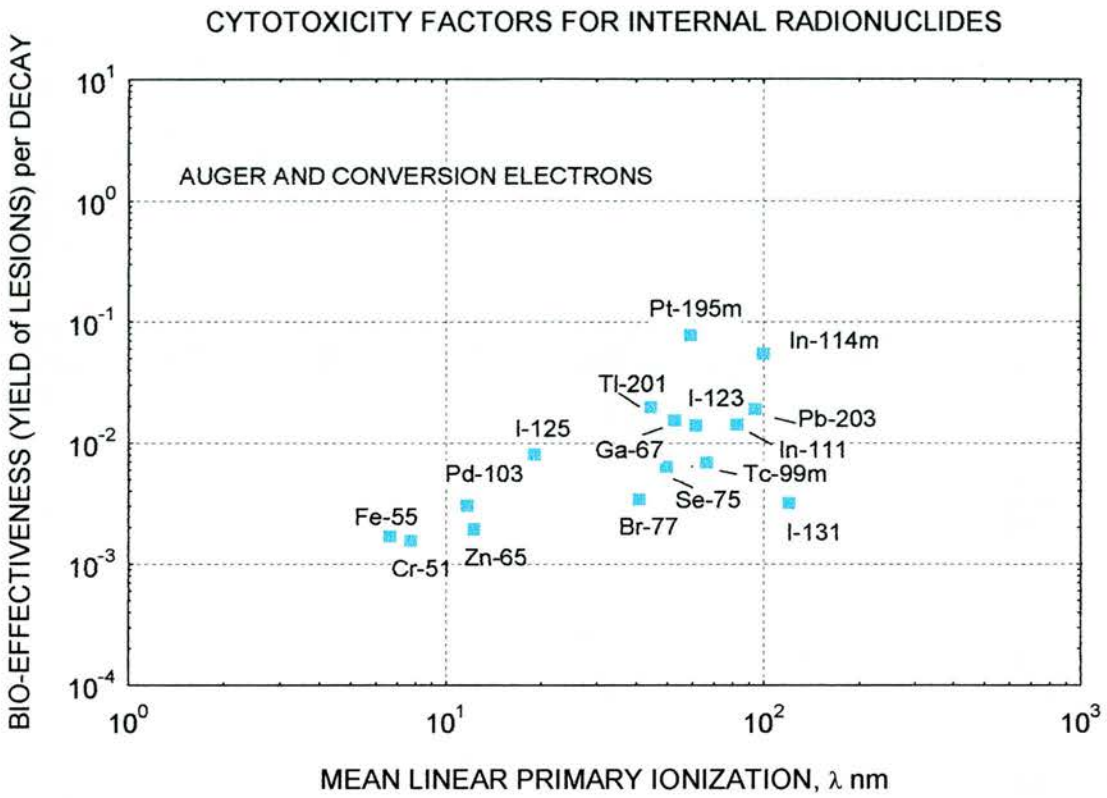

Fig 5.6 Graph of yield of lesions per decay as a function of lambda for Auger and conversion electrons. See Table 5.3 column 6 for data.

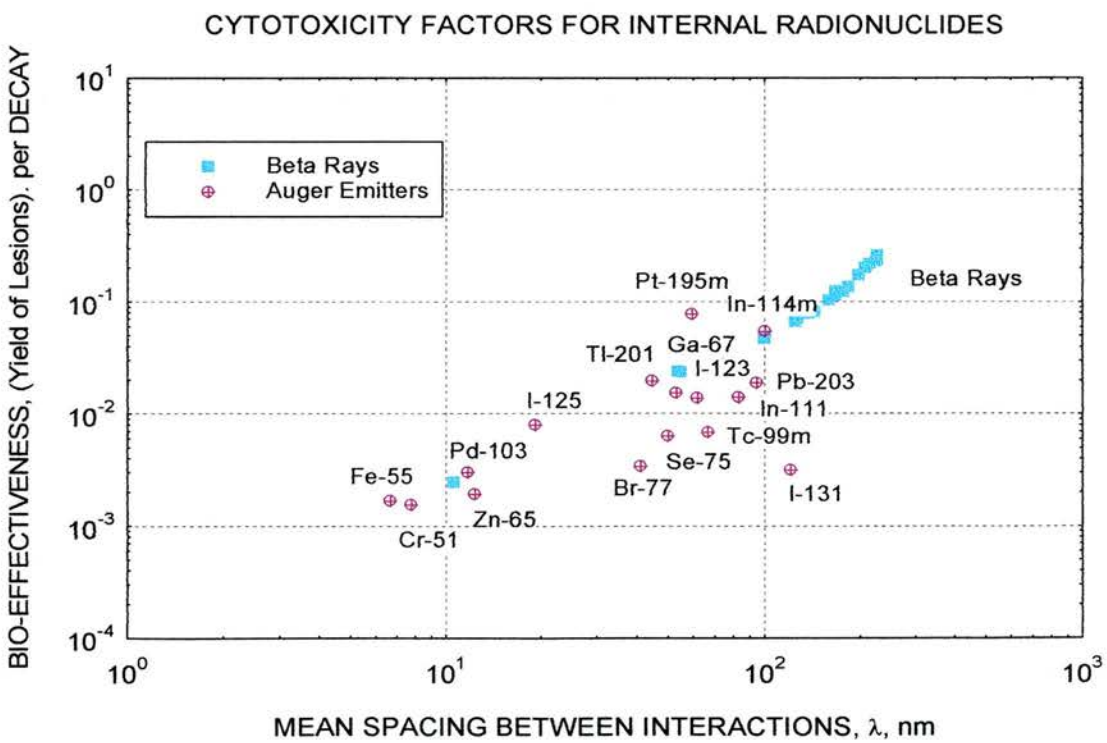

Fig 5.7 Composite graph of the beta and Auger emitter for the yield of lesions per decay against lambda.

Fig 5.6 and 5.7 also show that the Auger emitters (blue squares 5.6, and crosses in 5.7) tend to be 'less damaging' than the other radiations as shown by the scatter points, partially due to the averaging of 'λ' for the many discrete electron groups in the Auger decay.

Having derived the cytotoxicity values for the Auger electron emitters and shown that there is reasonably good correlation with the experimental data final conclusions are drawn below.

5.3 Conclusions.

Auger electron emitting radionuclides have been used extensively in nuclear medicine for both diagnostic and therapeutic purposes. They have gained wide use due to the good imaging characteristics offered by these radionuclides in dynamic studies as well as obtaining detailed pathological information. As the diagnostic and therapy application of radiopharmaceuticals have continued to grow, the general publics' awareness of the hazards of ionisation radiation has increased. With the current changes in radiation protection by the ICRP and NRPB the occupational and public limits have been reduced on a basis that may not be appropriate. The recommendations in the Ionising Radiations Regulations 99 (IRR99) are either very cautious or inappropriate with regard to limiting the risk to other individuals from patients who have undergone a nuclear medicine procedure. Basing radiation protection recommendations on a maximum value erring on the side of caution may result in unnecessary restrictions on clinical practice and on the behaviour of patients. This may have significant

consequences in particular with the application of radionuclides in medicine for diagnostic and therapeutic purposes.

The dosimetric quantities defined for protection purposes, since the discovery of x-rays and the first protection advice in 1896 which consisted of minimising the exposure time, were not directly measurable and caused concern in relation to measurable quantities. This has not changed significantly even in the light of findings of the Hiroshima and Nagasaki bombing where the sensitivity to low level radiation and its measurement was considered to be important. The concept of As Low As Reasonably Achievable (ALARA) and individual limits were introduced and widely accepted but with the same quantities and definitions.

The possible new ICRP recommendations uses the concept 'controllability of sources' and notes that the term 'dose' does not take into account the type or any other characteristics of the radiation and introduces the quantity 'absorbed dose at a point' which will be difficult to achieve. For this reason the commission uses the term 'average tissue dose' weighted for the radiation and tissue. This method has all the limitations outlined previously with the concept of 'dose'. The system of protection still relies on indirect quantities and therefore does not take into account the specific and stochastic nature of radiation action.

The assessment of risk to the patient from the administration of radioactivity as assessed by MIRD and ICRP have their limitations, including the fact that not all diseases are taken into account and in some cases values of organ absorbed dose are based on normal individuals or even animal data. The lack of biokinetic data, to describe the effects of age, sex, diet and drugs cause the biggest uncertainties.

The energy absorption is considered to be insignificant compared with the uncertainties in the biokinetic data and in the S-factor as derived by MIRD.

The use of Auger electron emitters in therapy has gained favour due to their cell killing ability through in vivo introduction into the site of interest and through tumour seeking ability, for example in the treatment of hyperactive thyroids with Iodine. There is hope that these Auger electron emitters can be used in performing targeted therapy as originally suggested by Fienendegen. This has been shown to be the case with limited success by Laster et al. The idea of binding the radionuclide to a compound, which is selectively taken up by a tumour, and the energy released at that site only, has the possibility of improved treatment and patient safety. Currently the radiation delivered to a site has a large component that is wasted, partly because it does not have the appropriate damaging characteristics, range, energy etc., but also because of the lack of appropriate dosimetry at the site of interest. Because the dosimetry is very difficult the activity given is in the higher range in order to ensure that some benefit is observed clinically.

The main characteristic of these Auger electron emitters that need to be considered when used medically, include the large variation in the dose to the individual cells and organ doses from the non-uniform distribution as shown by Makrigioros et al and the enhancement of the effectiveness when these radionuclides are located in or near the DNA of the cell as shown by Howell et al.

The selection of these radionuclides appears to be rather arbitrary either from the information gained through experience or, the imaging benefits for the camera in use. There does not appear to be a method of classification where the quality of

the radiation emitted by the radionuclide is taken into account when selecting the isotope. These radionuclides pose problems in dosimetry when they are incorporated into mammalian cells, as is sometimes the case in nuclear medicine but this does not seem to be taken into account in a much more rigorous fashion.

Due to the complex mechanisms involved and in order to simplify the method of assessment of the likely damage these radionuclides may cause, the ICRP and other scientific bodies have assigned the same quality factors to these i.e. a value of 20 (see chapter 1) as alpha emitters. Various authors including Sastry, Rao and Howell et al have subsequently argued against this value. However, it should be noted that the new modifications are still based on the modelling assumptions used previously (see chapter 1). The idea of classifying these radionuclides into one group seems rather odd, considering the huge variation in the radiations emitted by these radionuclides in terms of energy, number and range.

One of the aims of the model was to find a method of unifying the process by which the classification of Auger electron emitting radionuclides, into order of merits or quality of effectiveness. With the intention of improved selection of a radionuclide for diagnostic and therapeutic purposes in an analytical way that would produce the maximum damage to the sites of interest, rather than from experience, as is the case now. It was hoped that by being able to quantify the radionuclides, one could in effect reduce the ineffective dose that is generally delivered, with the view of improving the radiation protection to surrounding tissues and patient in general.

By specifying the nature of the radiation on the template basis it may be possible indirectly to reduce the overall 'dose' to the patient while maintaining the efficiency in meeting the end-point in terms of cell damage. That is, if the selection of radionuclide is such that the radiation quality will be such that at the point of interest the damage is likely to be a maximum. Currently the treatment of cancer by the use of radiation has the effect of delivering high radiation doses in order to cause cell death as the effective dose is determined by a method, which assumes an average over the target area as mentioned previously. The dose delivered to the patient generally is significantly higher in order to be effective but clinical work has shown that this is not the case and the damage is very localised with low efficiency. Assuming the model presented here is correct then by matching the radiation for the specific target, there will be no need to average out the delivered dose in order to reach the end-point of interest.

As a quality parameter Lambda (λ)-the linear primary ionisation is ideal in quantifying different radiation types without the need for indirect correlation. Lambda represents the mean free path between collisions. It excludes delta rays. It is not to be confused with the volume quantity, the *specific* primary ionisation used be Lea [2] and Harder [3] which includes the ionisation from secondary electrons. The benefits of lambda are presented in chapters 2 and 4. Clearly using a parameter that is fundamental to all types of radiations, the method of classification or unification becomes easier. This also gets away from the need to compare the quality of one type of radiation with respect to another type, as is the case with RBE.

The system proposed by Watt for heavy particles and sparsely ionising radiation expresses the cross-section for the induction of the effect, for a specified biological end-point as a function of lambda. The use of the effect cross-section allows the use of the primary charged particle track to be used as a probe to explore the target structure within the cell nucleus thereby allowing a physical quality parameter to be related to radiation damage. Also it allows for the correlation in general terms between biological targets and saturation cross-sections.

For heavy particles it has been shown previously that the mechanism initiating damage is due to the spatial correlation of two random interactions along single charged particle tracks, which is determined by λ, with the strands in the intranuclear DNA to produce dsb's. It has been shown in exposures of mammalian cells to external radiation fields that the biological mechanism of action is due to the correlated spacing of track events within the sites spaced at about 2nm in the DNA. Consequently absorbed dose is an invalid quantity. Even at the microscopic level the specification of radiation effect, is a template effect. Similar template interactions at other orientations are predicted to have negligible effect. This would imply energy imparted as being irrelevant. Since the radiation quality is defined by the zeroth moment of energy transfer, even at the sub-microscopic level, the absorbed dose and LET which involve the first moment of energy transfer cannot be physically relevant in the description of radiation effects in mammalian cells.

The problem of radionuclides decaying with Auger electron-emitting or internal conversion electrons incorporated into mammalian cells was addressed by

modelling the radiation action mechanisms which cause inactivation of mammalian cells to quantify the bio-effectiveness, concluding with a form of classification or cyto-toxicity factors.

The analysis in chapter 4 showed that even though there is a wide number of data present the experimental techniques with respect to control of radiation dose to cells and the subsequent calculation of the dose varies significantly. The number of isotopes used in analytical studies is restricted considering the wide variety available. This is mainly due to the concentration on the most commonly used isotopes in medicine and those that have had their theoretical and experimental decay schemes fully determined. The most common nuclides studied are I-125, I-123, Tc-99m, Br-77 and Pt-195m.

The fact that the useful experimental data is very limited has made the testing of the model extremely difficult. None-the-less, several conclusions can be drawn.

Using the modified program 'radnuc.for' to include Auger electron emitters with the equations developed in chapter 4, cross-sections of the tabulated data taken from the literature were determined both for experimental and model calculations.

Initial plots of effect cross-section per electron and per decay from experimental data along with the model calculations per electron as a function of lambda, shows that the correlation is reasonably good. The model values are around the average for the experimental data. This is promising considering the wide range of parameters used in each experiment. These plots excluded the repair function and with this applied in figure 2.1 (page 57 a comparison with heavy ion and electron damage) the results show that, the data with energy per electron relate

closely to the irradiation by external electrons confirming that the model is consistent in its approach and the data with energy per decay resembles that of heavy ions. This is most likely to be due to the Auger electron cascade.

The data used was reduced further to include only those that were well controlled experimentally with methods of irradiation that was helpful in the analysis of the model. This narrowed down to the experimental works of Hofer et al [ ].

The main objective of the research was to adopt the 'template' model, which was already available in unified form for external sparsely and densely ionising radiations, and to apply it to internal beta and Auger electron emitters as these are expected to be a critical test of the model because of two main reasons, (a) they are sources of low energy electrons and (b) they are sources of insider electron tracks which are sensitive to the target multiplicity.

There is no reason in the world to think that Auger electrons are different from any other electrons in their action unless the action of the Auger cascade has synergistic properties. Indeed, any electron ends its track with a cascade of soft electrons in the last few tens of nanometers of its track and doesn't differ all that much from the action of Auger electrons. Similarly for internal beta emitters. Indeed the figures (4.1 and 4.2) showing the SLD spectra of fluence as a function of electron energy for the 16 Auger electron emitters and the 19 beta spectra, without regard to any model, shows this very clearly.

Radiation quality can be expressed as the geometrical cross-sectional area $\sigma_{g,DNA}$, times the Possion probability $(1\text{-}exp\text{-}(2\Lambda+\sigma)/\lambda)^2$ that a dsb will be produced. The quality is obtained from the 'template' model and is expressed as the bio-effect cross-section σ_B. Whatever the decay scheme involved for Auger electrons, the quality is consistent with that obtained for other electrons having the same mean spacing between collisions, including internal beta emitters. In determining the quality the template model takes into account the target multiplicity, a mean number of sites of ~12-15 is known to occur across the mean chord, all 12 sites can be activated by fast heavy ions. We know that the fraction of cellular material which is insensitive occupies most of the track. The radiosensitive fraction across the sensitive section is ~2nm and the remainder wasted ~500nm i.e, ~6000nm/12nm ~500nm. From the projected range of e.g. an electron we can determine the approximate number of sensitive sites penetrated by the electron track. This seems to work quiet well. For heavy particles, the range is nearly always greater than the cell nuclear diameter and therefore all sites (~12-15) are at risk. For electrons, the 2nm spacing is only possible for electrons of range equivalent to 200eV ~6-7nm. For protons range for cell nucleus is ~6μm, the particle becomes less effective and proves that there is indeed a multiplicity of sites.

Whilst discussing the effect of Auger electrons it should be remembered that wherever there are Auger electrons there will be associated characteristic x-rays as in electron capture nuclides. These photon induced electrons are treated separately e.g. Table 5.2.

Within error limits, the system in indeed unified for radiation quality for all radiations whether internally or externally administered. This self-consistency implies validity of the theory. Direct validation is obtained by comparison of experimental data which, although sparse, is mainly due to the selection of radionuclides in research establishments i.e. Iodine and Bromine are favoured for various reasons.

From figure 5.6, showing the number of lesions per DNA dsb's versus Lambda, it can be concluded that Auger electrons tend to be less effective per decay per cell nucleus than other electrons at the same mean Lambda, but the reason is probably a result of averaging Lambda over the equilibrium electrons generated by several primary groups from electron-capture decays.

The derived Cyto-toxicity factors in Table 5.3 for the Auger emitters considered in the work here shows that it is possible to scale the nuclides in terms of effectiveness when looking at it from the point of view of cross-sections of interaction and fluence. However, is should be noted that these results do not take into account the repair capacity of the cell. This is for future work. Preliminary results indicate that the model predicts encouraging results as shown in Fig 5.5 and 5.6.

The model does show that it is suitable for radiobiological protection because it overestimates the effects of incorporated radionuclides. The reasons for this are: that no correction is made for the differences in the duration of the irradiations which will affect the repair of the cell; fluences are expressed as functions of energy whereas on the basis of the damage mechanism, fluence should be a

function of lambda and the cross sections extracted from survival curves, using D_0 decays per cell, are underestimated because of saturation effects.

The results also indicate that with respect to Auger electron emitters the single-track mechanisms relate reasonably well with the behaviour of external irradiation and allows the possibility of producing a unified model.

Future work is needed where more specific radiobiology experiments are required to address the problems of target multiplicity with better-controlled duration and rate of the applied radiation to get a more accurate unrepaired fraction.

On the basis of the present work, if a fluence based system of dosimetry is used, no abnormal effects are expected from Auger emitters. The derived fluence takes care of any extraordinary effects from the Auger electron cascade. Internal beta emitters behave exactly in the same way as Auger electron emitters. However, because the damage produced by the beta emitters occurs predominantly in the large electron cascade generated at the end of their tracks, the beta emitter's act under saturation conditions. Therefore all have the same effect as reflected in their cyto-toxicity factors, except for beta radiation from tritium, which has a mean electron range $\leq$ the cell nucleus.

The model is accurate enough in its present form to indicate that the highest bio-effectiveness per unit concentration of decays of Auger emitters is for the isotopes of Pt-195m, In-114m, Tl-201, Pb-203, Ga-67, In-111 and I-123, I-125, and Se-75 see Fig 5.6.

References:

1 Watt D.E, - 'On absolute biological effectiveness and unified dosimetry.' J of Rad protection 9 1 33-49 1989

2 Lea D.E – 'Actions of Radiations of Living Cells, 2nd edition.' Cambridge University press, New York 1955.

3 Harder D, Blohm R, Kessler M – 'Restricted LET remains a good parameter of radiation quality.' 6th sympo, on neutron dosimetry 23 (1/4) 79-82 1988.

4 Billen D., Spontaneous DNA damage and its significance for the "negligible dose" controversy in radiation protection, Radiation Research, 124, 242-245 (1990).)

5 Powers E.L, Ehret C.F and Bannon A - 'Applied Microbiology 5.' 61 1957.

6 Dertinger H Kinetics of regrowth of V79 spheroids after gamma- and pi--irradiation.
Strahlentherapie. 1979 Oct;155(10):722-5

7 Katz R. commentary on dose Rad. Res. 137 410-413 1994.

8 Bond V.P and Varma M.N – 'A stochastic weighted hit size theory of cellular radiobiological action.' 8th sympo in Microdosimetry Germany commission of the European communities 423-438 1981.

9 Simmons J.A – 'Absorbed dose an irrelevant concept for irradiation with heavy charged particles.' J Rad Prot. 12, 3, 173-179 1992.

10 ICRP report no 36 microdosimetry ICRU 7910 Woodmont Ave, Bethesda Maryland 20814 USA (1983).

11 Rossi H.H.- 'Specification of Radiation Quality.' Radiation Res. 10. 522-531 (1959).

12 ICRU Recommendations of the International Commission On Radiology units (cm 1950) Am. I. Roentg. Red. Thar. 65 , 99, 1951

13 Baverstock K.F, Charlton D.E, eds, - 'DNA damage by Auger emitters.' Taylor and Francis London 1988.

14 Humm J.L, Charlton D.E, - 'A new calculation method to assess the theraputic potential of Auger electron emission.' Int.J. Radiat. Oncol. Biol. Phys 17, 351-360 (1989)

15 Younis A.R.S, Watt D.E, - 'The quality of ionising radiations emitted by radionuclides incorporated into mammalian cells.' Phys. Med. Biol. 34, 821-834 (1989).

16 Goodhead D.T, - 'Spatial and temporal distribution of energy.' Health Phys. 55, 231-240 (1988).

17 Booz J, Paretzke H.G, Pomplun E, Olko P, - 'Auger-electron cascades, charge potential and microdosimetry of iodine-125.' Radiat. Environ. Biophys. 26, 151-162 (1987).

18 Halpern A, - 'Intra-and intermolecular energy transfer and super excitation in post Auger processes.' Radiochim. Acta 50, 129-134 (1990).

19 Kassis A.I, Fayad F, Kinsey B.M, Sastry K.S.R, Taube R.A, Adlestein S.J, - 'Radiotoxicity of 125I in mammalian cells.' Radiat. Res. 111, 305-318 (1987).

20 Link E.M, Brown I, Carpenter R.N, Mitchell S.J, - 'Uptake and therapeutic effectiveness of 125I and 211At-methlene blue for pigmented melanoma in an animal model system.' Cancer res. 49, 4332-4337 (1988).

21 Rao D.V, Sastry K.S.R, Grimmond H.E, Howell R.W, Govelitz G.F, Lanka V.K, Mylavarapu V.B, - 'Cytotoxicity of some indium radiopharmaceuticals in mouse testes.' J Nucl. Med. 29, 375-384 (1988).

22 Rao D.V, et al, - 'In vivo radiotoxcitity of DNA incorporated I-125 compared with that of densly ionising alpha-particles lancet II 650-653 1989

23 McLean J.R.N, Wilkinson D, - 'The radiation dose to cells in virto from intracellular indium-111.' Biochem. Cell biol 67, 661-665(1989).

24 McLean J.R.N, Blakey D.H, Douglas G.R, Bayley J, - 'The auger electron dosimetry of indium-111 in mammalian cells in vitro.' Radiat. Res. 119, 205-218 (1989).

25 Bialobrzeski J, Liniecki J, Greger J, Brykalski D, Zadrozna A, - 'Radiation doses from 51Cr-bleomycin.' Nuklearmedicin 26, 97-104 (1987).

26 Vezza M, Giuliani D, Roa D.V, Morse B.S, - '51-Cr dosimetry of lymphocytes labelled incidentally during nuclear medicine procedures.' Nucl. Med. Biol. 14, 75-77 (1987).

27 Makrigiorgos, S.J. Adelstein and A.I. Kassis, Limitations of conventional dosimetry at the cellular level. J Nuc. Med 30, 1856-1864 (1989)

28 Makrigiorgos G.M, Ito S, Baranowska-Kortylevwicz J, Vinter D.W, Iqbal A, Van Den Abbeele A.D, Adelstein S.J, Kassisi A.I, - 'Inhomogeneous deposition of radiopharmaceuticals at the cellular level: Experimental evidence and dosimetric implications.' J. Nuc Med 31, 1358-1363 (1900).

29 Makrigiorgos G.M, Adelstein S.J, Kassis A.I, - 'Cellular Radiation dosimetry and its implications for estimation of radiation risks. Illustrative results with technetium 99m-labeled microspheres and macroaggregates.' JAMA 264, 592-595 (1990)

30 Charlton D.E, Humm J.L, - 'A method of calculating initial DNA strand breakage following the decay of incorporated 125 I.' Int. J Radiat Bio. 53, 353-365 (1988).

31 Martin R.F, Haseltine W.A, *Sci.* 213 896 (1981)

32 Chadwick K.H, Leenhouts H.P, - 'The Molecular Theory of Radiation Biology.' Springer-Verlag Berlin 1981.

33 Unak P, Unak T, - 'Microscopic energy absorption of the DNA molecules from Auger electrons of iodine-125.' Appl. Radiat. Isot. 39, 1037-1949 (1988).

34 Wright H.A, Hamm R.N, Turner J.E, Howell R.W, Rao D.V, Sastry K.S.R, - 'Calculations of physical and chemical reactions with DNA in aqueous solution from Auger cascades.' Radiot. Prot. Dosim 31, 59-62 (1990).

35 Pomplun E, - 'A new DNA target model for track structure calculations and its first application to I-125 Auger cascades.' Int J. Radiat. Biol. 59, 625-642 (1991).

36 Makrigiorgos G.M, Berman R.M, Baranowska-Kortylevwicz J, Bump E, Humm J.L, Adelstein S.J, Kassis A.I, - 'DNA damage produced in V79 cells by DNA incorporated iodine-123: A comparison with iodine-125.' Radiat. Res. 129, 309-314 (1992).

37 Martin R.F, D'Cunha G, Pardee M, Allen B.J, - 'Induction of double-strand breaks following neutron capture by DNA-bound 157 Gd.' Int J. Radiat. Biol. 54, 205-208 (1988).

38 Nath R, Bongiorni P, Rockwell S, - 'Enhancement of IudR radiosensitisation by low energy photons.' Int. J. Radiat. Oncol. Bio. Phys.13, 1071-1079 (1987).

39 Miller R.W, DeGraff W, Kinsella T.J, Mitchell J.B, - 'Evaluation of incorporated iodondeoxyuridine cellular radiation sensitisation by photon activation therapy.' Int. J. Radiat. Oncol. Phys. 13, 1193-1197 (1987).

40 Larson D, Bodell W.J, Ling C, Phillips T.L, Schell M, Shrieve D, Troxel T, - 'Auger electron contribution to bromo-deoxyuridine cellular radiosensitisation.' Int. J. Radiat. Onco. Phys. 16, 171-176 (1989).

41 Takakura K, - 'Auger effects on bromo-deoxyuridine-monophosphate irradiated with monochromatix X-Rays around bromine K-absorption edge.' Radiat. Environ. Biophys. 28, 177-184 (1989).

42 Kassis A.I, Makrigiorgos G.M, Adelstein S.J, - 'Implications of radiobiologic and dosimetric studies of DNA-incorporated 123I: The use of the Auger effect as a biologic probe at the nanometre.' Radiat. Prof. Dosim 31, 333-338 (1990).

43 Pomplun E, Booz J, Dydejczhk A, Feinendegen L.E, - 'A microdosimetric interpretation of the radiobiologic effectiveness of 125I and the problem of quality factor.' Radiat, Environ. Biophys. 26, 181-188 (1987).

44 Rao D.V, Narra V.R, Howell R.W, Lanka V.K, SastryK.S.R, - 'Induction of spermhead abnormalities by incorporated radionuclides: Dependence on subcellular distribution, type of radiation, dose rate, and presence of radioprotectors.' Radiat. Res 125, 89-97 (1991).

45 Whaley J.M, Little J.B, - 'Efficient mutation induction by 125I and 131decays in DNA of human cells.' Radiat. Res. 123, 68-74 (1990).

46 Whaley J.M, Kassis A.I, Kinsey B.M, Adelstein S.J, Little J.B, - 'Mutation induction by 125Iodoacetylproflavine, a DNA-intercalating agent, in human cells.' Int. J. Radiat. Bio. 57, 108701193 (1990).

47 Humm J.L, Bagshawe K.D, Sharma S.K, Boxer G, - 'Tissue dose estimates following the selective uptake of 125IudR and other radiolabelled thymidine precursors in resistant tumours.' Br J. Radiol 64, 45-49 (1991).

48 Baranowska-Kortylevwicz J, Makrigiorgos G.M, Van Den Abbeele A.D, Berman R.M, Adelstein S.J, Kassisi A.I, - '5-[12I]Iodo-2'deoxyuridine in the radiotherapy of an early ascites tumor model.' Int. J. Radiat. Oncol. Biol. Phys. 21, 1541-1151 (1991).

49 Anderson R.E, Holt J.A, - 'Binding of radiolabelled estrogens by human cells in vitro: Implications to the development of a new diagnostic and therapeutic modality in the treatment of malignancies with estrogen receptors.' Gynecol. Oncol. 34, 80-83 (1989).

50 DeSombre E.R, Mease R.C, Hughes A, Harper P.V, DeJesus O.T, Friedman A.M, - 'Bromine-80m-labeled estrogens: Auger-electron-emitting, estrogen receptor-directed ligands with potential for therapy of estrogen receptor-positive cancers.' Caner Res. 48, 899-906 (1988).

51 DeSombre E.R, Harper P.V, Hughes A, Mease R.C, GatleyS.J, DeJesus O.T, Schwartz J.L, - 'Bromine-80m radiotoxicity and the potential for estrogen receptor-directed therapy with Auger electrons.' Cancer Res. 48, 5805-5809, (1988).

52 DeSombre E.R, Huges A, ChurchLandel C, Green G, Hanson R, Schwartz J.C, - 'Cellular and subcellular studies of the radiation effects of Auger electron-emitting Estrogens.' Acta Oncologica Vol 35 p7, pp 833-860 1996

53 HowellR.W, Rao D.V, Sastry K.S.R, - 'Macroscopic dosimetry for radiommunotheraphy: Nonuniform activity distributions in solid tumours.' Med Phys. 16, 66-74 (1989).

54 Woo D.V, Li D, Brady L.W, Emrich J, Mattis M, Steplewski Z, - 'Auger electron damage induced by radioiodinated iodine-125 monoclonal antibodies.' Front Radiat. Ther, Oncol. 24, 47-63 (1990).

55 Hou D, Maruyama Y, - 'Enhanced killing of human small cell lung cancer by hyperthermia and indium-111-bleomycin complex.' J Surg. Oncol. 44, 5-9 (1990).

56 Baranowska-Kortylevwicz J, Adelstein S.J, Kassisi A.I, - '5-Iodo-2'deoxyuridine protein conjugates: Synthesis and enzymatic degradation; Select.' Cancer Ther. 6, 1-13 (1990).

57 Goodman J.H, Gahbauer R.A, Kanellitsas C, Clendenon N.R, Laster B.H, Fairchild R.G, - 'Theoretical basis and clinical methodology for stereotactic interstitial brain tumour irradiation using iododeoxyuridine as a radiation sensitizer and 145Sm as a brachytheraphy source.' Sterotact. Funct. Neurosurg. 54055, 531-534 (1990).

58 Sastry K.S.R, Rao.D.V, - 'Dosimetry of Low energy electrons.' in Physics of Nuclear Medicine Recent Advances, ed Roa D.V, Chandra R, Graham M, (AAPM, Medical Physics Monographs No 10, American Institute of Physics pp 169-208 (1984)).

59 Sastry K.S.R, Howell.R.W, Rao.D.V, Lavarapu.V.B.M, Kassis.A.I, Adelstein.J.S, Write.H.A, Hamm R.N, Turner J.E, - 'Dosimetry of Auger Emitters: Physical and Phenomenological Approaches in DNA Damage by Auger Emitters.' ed Baverstock K.F, Charlton D.E, Taylor and Francis, London pp 27-38 (1988).

60 Sastry K.S.R, Rao.D.V, - 'Biological effects of Auger cascades.' The Lancet Vol I, 858-859 (1986).

61 Rao.D.V Sastry K.S.R, - 'Radiobiological Effects of Auger Emitters in vitro and in vivo.' Rad. Res Vol2 ed Fielden E.M, Fowler J.F, Hendry J.H, Scott D, Proc 8th ICRR, Edinbrough, Taylor and Francis London 1988, pp. 369-374 (1987).

62 Watt D.E, Khan S, - 'Cross section for the biological effectiveness of electrons in mammalian cells.' Presented at third international symposium on biophysical aspects of auger processes august 1995, university of Lund, Sweden.

63 Khan S, Watt D.E, - 'Physical specification of biological effectiveness of electrons from incorporated radionuclides.' Poster P01-15 at 10th ICRR Wurzburg Germany Sept 1995.

64 Watt D.E, Khan S, - 'Cytotoxicity factors for some radiopharmaceutical nuclides.' Presented at 12th symposium on microdosimetry, 29th Oxford, U.K. September 1996.

65 Watt D.E, Khan S, - 'Unified dosimetry: biological effectiveness of incorporated electron-emitting radionuclides.' 3rd international symposium of biophysical aspects of auger processes, submitted to Acta Oncologica.

66 Heavy particle track structure parameters for biophysical modelling. D.E.Watt. Nuclear Instruments and Methods in Physics Research B93 (1994) 215-221.

67 Charged Particle Track Structure Parameters for Application in Radiation Biology and Radiation Chemistry. Ali S. Alkharam and David E. Watt..

International Journal of Quantum Chemistry: Quantum Biology Symposium 21, 195-207 (1994).

68 Physical Quantification of the Biological Effectiveness of Ionizing Radiations. D.E. Watt and L.A. Kadiri. International Journal of Quantum Chemistry, Vol. xxxviii, 501-520 (1990).

69 Quantities for Dosimetry of Ionizing Radiations in Liquid Water. D.E. Watt. Taylor and Francis, 1 Gunpowder Square, London EC4A 3DE. 422 pages (1996).

70 A Radiobiological Data Base: Cellular Inactivation, Dicentrics, Mutations, Oncogenic Transformations and DNA Strand Breaks. Ali S. Alkharam and D.E.Watt. University Report, BIOPHYS/11/97, St. Andrews, U.K. (1997).

71 Watt D.E, - 'On absolute biological effectiveness and unified dosimetry.' J of Radiological Prot. 9 (1) 33-49 1989.

72 Weber D.A, - 'Radionuclide data and decay schemes.' The soc. Of nuc. Med, Inc. ISBN 0932004326.

73 McGinnies R.T, - 'Energy spectrum resulting from electron slowing down.' National bureau of standards circular 597 Feb 20 1959.

74 Sugiyamas H, - 'Energy loss and range of electrons below 10keV.' Jap Appl. Phys. 15 1979

75 Auger. P, - 'Sur les rayons β secondaries produit dans un gaz par des rayons X.' Comptes Rendus 180, 65-68 (1925).

76 Fink. R.W, Jopson R.C, Mark. H, Swift C.D, Rev. Med. Phys. 38 513-540 (1966).

77 Wentzel G. z.Phys 43 524-530 (1927).

78 Coster D, Kronig R, De L Physica 2 13-24 (1935).

79 Krause M.O, - Proc. 2nd Int. conf. Inner Shell Ionisation Phenomena ed. Mehlharn W, Brenn R, pp184-197 (1979).

80 Butt D.K, - 'Encyclopaedic dictionary of Physics Vol 6.' ed J Thearlis (Oxford Pergamon) pp 424-428 (1962).

81 Hedin L, Johannson A, - 'Physique' 32 1336.

82 Packer M.E, Wilson J.M, - 'Auger Transitions Between 0 and 1500eV for Elements up to Z=88.' London: Institute of Physics (1971).

83 Hornfeldt O, Fahlmann A, Nordling Ark Fys 23 155 (1965).

84 Burhop E.H.S, Assad W.N, in Adv. Med. Phys 8 163-284 (1974).

85 Larkins F.P, - 'Atomic Inner Shell Processes and transition probabilities, Vol VI.' ed Crasemann B, (New York: Academic) p377 (1975).

86 Chung M.F, Jenkins L.H, - 'Auger electron energies of the outer shell electrons.' Surf. Sci. 22 479-485 1970.

87 McGuire E.J, - 'M-shell Auger, CK and radiative matrix elements and Auger and CK transition rates in j-j coupling.' Res. Rep. SC-RA 710835 1972. 'N-shell Auger, CK and radiative matrix elements and Auger and CK transitions rates in j-j coupling.' Res. Rep. SAND 75-0443 1975.

88 Charlton D.E, Booz J, - 'A Monte Carlo treatment of decay of I-125.' Rad. Res. 87 10-23 1981.

89 Annals of the ICRP 'Radionuclide Transformations, energy and intensity of emissions' vol 11-13.

90 Howell R, 'Task group report No2: radiation spectra of radionuclides.' Med. Phys. 19 (6), nov/dec 1992.

91 Howell R.W, - 'Radiation Spectra for Auger-electron emitting radionuclides, Report No 2 of AAPM Nuclear Medicine Task Group No 6.' Med. Phys. 19 1371-1383 (1992).

92 Geard C.R, - 'Charged particle cytogenetics: effects of LET, fluence, and particle separation on chromosome aberrations.' Rad. Res. 104 S-112-S-121 1985.

93 Friedberg E.C, -'DNA Repair' Freeman, New York 1985.

94 Humm J.L, Charlton D.E, - 'A new calculation method to assess the theraputic potential of auger electron emission.' Int. J Radiat. Oncology Biol. Phys. 17 351-360 1989).

95 Markrigiogos G.M, et al, - 'DNA damage produced in V79 cells by DNA incorporated I-123, a comparison with I-125.' Radiat. Res. 129 309-314 1992).

96 Hofer K.G, et al, - 'The paradoxical nature of DNA damage and cell death induced by I-125 decay.' Radiat. Res. 130 121-124 1992.

97 Kassis A.I, et al, - 'Kinetics of uptake, retention and radiotoxicity of I-125 in mammalian cells, implications of localised energy deposition by auger processes.' Radiat. Res. 109 78-89 1987.

98 Hofer K.G, et al, - 'Radiotoxicity of intrnuclear tritium I-125 and I-131' Radiat. Res. 47 94-109 1971).

99 Kassis A.I, Howell R.W, Sastry.K.S.R, Adelstein.S.J, - 'Positional effects of Auger Decays in mammalian cells in culture in DNA Damage by Auger Emitters.' ed, Baverstock K.F, Charlton D.E, (Taylor and Francis, Lon.) (1988).

100 Loveninger R, Berman M, - 'A revised schema for calculating the absorbed dose for biologically distributed radionuclides.' MIRD Phamphlet No 1, revised (The society of nuclear medicine, New York (March 1976).

101 ICRU Report 32, - 'Methods of assessment of absorbed dose in clinical use of radionuclides.' International commission on radiation Units and Measurements, Washington, DC (1979).

102 Fienendegen L E, - Rad. Enviornm. Biophysics 12 85 1975.

103 Chen P.C, Lisco E, Lisco H, Adelstein S J. - Rad. Res. 64 332 1976.

104 Hofer K.G, Third Int. Radiopharmacutical Dosi Sympo. 371-389 1981.

105 Commerford S.L, Bond V.P, Cronkite E.P, Renike U, - Int. J Radiat. Biol. 37 547 1980.

106 Kassis A.I, Adelstein S.J, Haydock C, Sastry K.S.R, McElvay K.D, Welch M.J, - Radiat. Res. 90 362 1982.

107 Rao D.V, Govelitz G.F, Sastry K.S.R, - J Nucl. Med. 24 145 1983.

108 Adelstein S.J, Kassis A.I, Sastry K.S.R, - 'Cellular vs Organ Approaches to dose Estimates.' in Proc. 4th International Radiopharmaceutical Dosimetry Symposium, ed. Schlafke-Stelson A.T, Watson E.E, (Dept. of Energy, oak Ridge, TN) CONF 85-1113 pp 13-25 (1986).

109 Rao D.V, Goveltz G.F and Sastry K.S.R, - 'Radiotoxicity of Thallium-201 in mouse testies: Inadequacy of conventional dosimetry.' J.Nucl. Med. 24 145-153 (1983).

110 Makrigirogos G.M, Adelstein S.J and Kassis A.I, - 'Limitations of conventional internal dosimetry at the cellular level.' The J. of Nucl. Med 30 1856-1864, (1989).

111 Feinendgen L.E, - Rad. and Environm. Biophys. 12 85 (1975).

112 Chan. P.C, Lisco.E, and Adelstein S.J, - Radiat. Res 67 332 (1976).
113 Lomerford S.L, Bond V.P, Cronkite E.P, Reiwce - Int. J. Radiat. biol. 37 547 (1980).
114 Kassis A.I, Adelstein S.J, Haydock.C, Sastry K.S.R, Mcelvany, Welch M.J, - Radiat. Res 90 362 (1982).
115 Carlson T.A, White R.M, - 'Formation of fragment ions from $CH_3{}^{125}Te$ and $C_2H_5{}^{125}Te$ following the nuclear decays of $CH_3{}^{125}I$ and $C_2H_5{}^{125}I$.' J. Chem. Phys. 38 2930-2934 (1964).
116 Hofer K.G, - 'Radiation biology and potential therapeutic applications of radionuclides.' Cancer 67 343-353 1980.
117 Hofer K.G, - 'Toxicity of radionuclides as function of sub-cellular dose distribution.' Proc. Int. Radiopharm. Dosi. Symp. 3rd 371-389 1981).
118 Charlton D.E, Booz J, - 'A Monte Carlo treatment of decay of I-125.' Rad. Res. 87 10-23.
119 Moor F.D, Sastry K.S.R, - Proc. Natl. Acad. Sci. USA 7 1982.
120 Sastry K.S.R, Rao.D.V, -'Dosimetry of low energy electrons' in 'Physics of Nuclear Medicine: Recent Advances.' ed. Rao D.V, Chandra R, Graham M, (American Institute of Physics New York) pp. 169-208 (1984).
121 Kassis A.I, Howell R.W, Sastry.K.S.R, Adelstein.S.J, - 'Positional effects of Auger Decays in mammalian cells in culture in DNA Damage by Auger Emitters.' ed, Baverstock K.F, Charlton D.E, (Taylor and Francis, Lon.) (1988).
122 Fisher D.R, Frazier M.E, Andrews T.K Jr, - 'Energy distribution and the relative biological effects of internal alpha emitter, Radiat. Prot. Dosim.' 13 223-227 1985.
123 Rao D.V, Govelitz G.F, Sastry K.S.R, - 'Radiotoxicity of thallium-201 in mouse testes: inadequacy of conventional dosimetry.' J. Nucl. Med. 24 145-153 1983.
124 Kassis A.I, et al, - 'Kinetics of uptake, retention and radiotoxicity of I-125 in mammalian cells, implications of localised energy deposition by auger processes.' Radiat. Res. 109 78-89 1987.
125 Rao D.V, et al, 'In vivo radiotoxicity of DNA incorporated I-125 compared with that of densly ionising alpha-particles.' Lancet II 650-653 1989).
126 Rao D.V, Sastry K.S.R, Grimmand H.E, Howell R.W, Govelitz G.F, Larka V.U Malavarapu V.B, - 'Cytotoxicity of some indium radiopharmaceuticals in mouse testis." J.NUcl. Med. 29 375-384 (1988).
127 Goodhead D.T, Nikjoo H, - 'Track structure analysis of ultra-soft x-rays compared to high-and-low-LET radiations.' Int. J Radiat. Biol. 55 513-529 1989).
128 Weber D.A, Eckerman K.F, Dillman L. J, Ryman J. C, - MIRD radionuclide data and decay schemes, Soc. Nucl. Med. NY 1989.
129 Howell R.W, et al, - 'The question of relative biological effectiveness and quality factor for auger emitters incorporated into proliferating mammalian cells.' Radiat. Res. 128 282-292 1991.
130 Charlton D.E, Booz J, - 'A Monte Carlo treatment of decay of I-125.' Rad. Res. 87 10-23 1981.
131 Pomplun E, Booz J, Charlton D.E, - 'A Monte Carlo simulation of Auger cascades.' Rad. Res. 111 533-552 1987).
132 Cole A, - 'Absorption of 20-50000eV electron beams in air and plastic.' Rad. Res. 38 7-33 1969.

133 Booz J, Humm J.L, Charlton D.E, Pomplun E, Feinendegen L.E, - 'Microdosimetry of the Auger effect: the biological significance of Auger electron cascades of phosphorus after low energy photon interaction with DNA.' Proceedings of the 8th Symposium on microdosimetry Eds. Booz J, Ebart H.G, 625-638 1983.

134 Paretzke H.G, - 'Radiation track structure theory kinetics of inhomogeneous processes.' Ed. Freemann G.R, Wiley 1987.

135 Terrisol M, Patan J.P, Endaldo T, Proceeding 6th symposium on microdosimetry Ed. Booz J, Ebart H.G, Smith B.G.R, Harwood Academic Lon 169-181 1978.

136 Wright H.A, Haman R.N, Turner J.E, Howell R.W, Rao D.V, Sastry K.S. R, - 'Calculations of physical and chemical reactions with DNA in aqueous solutions from Auger cascades.' Radiat. Prot. Dosi. 31 59-62 1990.

137 ICRP PUB 36.

138 ICRP recommendations of the ICRP Report 26, international commission on radiological protection. Pergamon oxford 1977.

139 Howell R.W, Narra V.R, Sastry K.S.R, Rao D.V, - Rad. Res. 134 71-78 1993.

140 Paschoa A.S, Nogueira C.A, Lourenco M.C, Malamut C, Wrenn M.E, - 'Local Auger electron dosimetry of K-40.' Radiat. Prot. Dosi. 45 677-679 1992.

141 Nettleton J.S, Lawson R, - 'Cellular dosimetry of In-111 for spherical and ellipsoidal geometry.' presented at Lund 3rd symposium on biophysical aspects of auger emitter.

142 McLaughlin W.H, Pillai K.M.R, Edasery J.P, Blumenthal R.D, Bloomer W.D, - 'Cytotoxicity of receptor-mediated 16alpha I-125 iodo-estradiol in cultured (MCF-7) breast cancer cells.' J. Natl. Cancer Inst. 81 437-440 1989.

143 DeSombre E.R, Shafii B, Hanson R.N, Kuivanen P.C, Hughes A, - 'Estrogen receptor-directed radiotoxicity with auger electrons: specificity and mean lethal dose.' 5752-5758.

144 Cox R, Masson W.K, - 'Mutation and inactivation of cultured mammalian cells exposed to beams of accelerated heavy ions III. Human diploid fibroblasts.' Int. J. Radiat. Biol. 36 149-160 1979.

145 Thacker J, Stretch A, Stephen M.A, - 'Mutation and inactivation of cultured mammalian cells exposed to beams of accelerated heavy ions II, Chinese hampster V79 cells.' Int J Radiat. Biol. 36 137-148 1979.

146 Wulf H, Kraft-Weyrather W, Miltenburger H.G, Blakely E.A, Tobias C.A, Kraft G, - 'Heavy ion effects on mammalian cells: inactivation measurements with different cell lines.' Radiat. Res. 104 s-122-s134 1985.

147 Simmons and Watt radiation protection dosimetry, medical physics publishing (1999).

148 Grafstrom G, Strand S.E, Tennuall J, Jonsson Bo-Anderson, Lindquist H, - 'Radiological effects of In-110 Vs In-111 in Rat testes.'

149 Redford I.R, Hodgson G.S, - 'Cell killing and DNA dsb by DNA associated I-125 decay or X-irradiation: implication for radiation action models.' in 'DNA damage by Auger emitter', ed. Baverstock K. Taylor & Francis 1988.

150 Fujiwara Y, Miyazaki N, - 'Lethal, Mutagenic and DNA breaking effects of decays of I-125 unifilarly incorporated into DNA of mammalian cells.' In

'DNA damage by Auger emitter', ed. Baverstock K, Taylor & Francis 1988.

151 Ehrfeld A, Plamers Bohue F, Lucke-Huhle C, - 'Gene amplification in Chinese hamster embryo cells by the decay of incorporated I-125.' Rad Res 108 43.

152 Scheiderman M.H, Hofer K.G, - Rad Res 84 462.

153 Kassis A.I, Howell R.W, Sastry K.S.R, Adelstein S.J, - 'Positional effects of auger decays in mammalian cell in culture.' In 'DNA damage by Auger emitter', ed. Baverstock K,. Taylor & Francis1988.

154 Rao D.V, Mylavarpu V.P, Sastry K.S.R, Howell R.W, - 'Internal Auger emitters: effects on spermatogenesis and oogenesis in mice.' In 'DNA damage by Auger emitter', ed. Baverstock K, Tayler and Francis 1988.

155 Howell R.W, Rao D.V, Hou De-Yan, Narra V.R, Sastry K.S.R, - 'The question of relative biological effectiveness and quality factor for auger emitters incorporated into proliferating mammalian cells.' Rad. Res. 128 282-292 1991.

156 Narra V.R, Sastry K.S.R, Goddu S.M, Howell R.W, Strand S.E, Rao D.V, - 'Relative biological effectiveness of Tc-99m radiopharmaceuticals.' Med Phys 21 1921-1927 1994.

157 Howell R.W, Rao D.V, De-Yan Hou, Narra V.R, Sastry K.S.R, - 'The question of relative biological effectiveness and quality factor for auger emitters incorporated into proliferating mammalian cells.' Rad. Res 128 282-292 1991.

158 Narra V.R, Harapanhalli R.S, Howell R.W, Sastry K.S.R, Rao D.V, - 'Chemical protection against radionuclides in vivo: implications to the mechanisms of the auger effect.' In Biophysical Aspects of Auger processes.

159 Hofer K.G, Loon N.V, Schneiderman M.H, Charlton D.E, - 'The paradoxical nature of DNA damage and cell death induced by I-125 decay.' Rad Res 130 121-124 1992.

160 Howell R.W, Kassis A.I, Adelstein S.J, Rao D.V, Wright H.A, Hamm R.N, Turner J.E, Sastry K.S.R, - 'Radiotoxicity of Platinum-195m-labeled trans-Platinum (II) in mamalinam cells.' Rad Res 140 55-62 1994.

161 Narra V.R, Howell R.W, Sastry K.S.R, Rao D.V, - 'Auger electron emitters as tools for elucidating the localisation of primary radioactive targets.' Rad. Prot. Dosi. Vol 52 229-232 1994.

162 Krisch R.E, - 'Comparison of the lethal effects of P-32 and P-33 decay in E Coli and in Bacteriophages.' Int. J. Rad. Biol. 18 259-266 1970.

163 Miyazaki N, Fujiwara Y, - 'Mutagenic and lethal effects of [5-I-125] iodo-2-deoxyuridine incorporated into DNA of mammalian cells and their RBE's.' Rad. Res. 88 456-465 1981.

164 Liber H.L, LeMotte P.K, Little J.B, - 'Toxicity and mutagenicity of x-rays and I-125 dUrd or H-3 TdR incorporated in the DNA of human lymphoblast cells.' Mutation Res 111 387-407 1983.

165 Kassis A.I, Adelstein S.J, Haydock C, Sastry K.S.R, Mcelvany K.D, Welch M.J, - 'Lethality of Auger electrons from the decay of Br-77 in the DNA of mammalian cells.' Rad. Res. 90 362-373.

Appendix 1

The following tables contain the calculated (a) Conversion and Auger electron data and (b) Characteristic X-Ray and γ-Ray decay energies and yields. The groups are determined using the MIRD data. Fractions represent the number of particles per transitions. The tabulated conversional Auger electron data were converted to slowing down spectra using program PELSLD.FOR. The tabulated data for characteristic x-rays and γ-ray decay energies ad yields were converted to primary electron using XSECL.FOR. then the primary electron data were converted to slowing down electron spectra suing PELSLD.FOR. see the relevant programs in CD ROM. The data in these tables were used by programs (see CD ROM) 'XSCEL.FOR' to derive the relevant fluence and range for the electron distributions.

RADIONUCLIDES DECAYING BY ELECTRON CAPTURE:

ELECTRON COMPONENT.

51-CHROMIUM-24 (FILE 1)

(a) CONVERSION and AUGER ELECTRONS (6 groups)

Group	E (keV)	Fraction, f	f.E (keV)	$f_{Av.}$	E_{Av} keV
Group 1					
Ce K,L	314.6	1.69E-4	5.317E-2	-	-
	319.5	1.52E-5	4.8564E-3	1.842E-4	315.0
Group 2					
Auger KXY	5.386	8.59E-3		8.59E-3	5.386
Group 3					
	4.796	3.24E-2	0.1554	-	-
Auger KL,X	4.903	2.85E-2	0.1397	-	-
"	4.911	5.19E-2	0.2549	0.1128	4.876
Group 4					
	4.168	3.03E-2	0.1263	-	-
Auger KLL	4.259	0.117	0.4983	-	-
	4.293	2.66E-2	0.1142	-	-
	4.362	3.59E-2	0.1566	-	-
	4.381	0.323	1.4151	-	-
	4.397	2.53E-2	0.1112	0.5581	4.339
Group 5					
Auger LM	0.5986	1.71E-2	1.024E-2	-	-
	0.4909	2.59E-1	0.1271	-	-
	0.5183	1.05E-2	5.4422E-3	-	-
	0.4833	1.24	0.5993	1.5266	0.4861
Group 6					
Auger M	1.603E-2	3.19		3.19	1.603E-2

Mean number of primary electrons / decay = 5.3963

RADIONUCLIDES DECAYING BY ELECTRON CAPTURE.

51-CHROMIUM-24

(b) CHARACTERISTIC X-RAY and GAMMA RAY DECAYS (3groups)

Group	E (keV)	Fraction, f	f.E (keV)	f_{Av}. photons	E_{Av} keV	$N.\sigma_{el}$ cm^2/g
Group 1						
γ–Rays	320.1	0.101	32.33	0.101	320.1	0.1152
Group 2						
K_β X-rays	5.427	1.76E-2	9.55E-2	-	-	-
	5.427	8.8E-3	4.776E-2	2.64E-2	5.4265	32.42
Group 3						
K_α X-rays	4.952	0.1330	0.6586	-	-	-
	4.945	0.067	0.3313	0.200	4.952	42.84

Number of photons per decay: 0.3274
(Derive the fluence and range of the electron distribution. See program **xscel.for**).

Total number of electrons per decay = 5.3963 + 0.3274 = **5.7237**

RADIONUCLIDES DECAYING BY ELECTRON CAPTURE: ELECTRON COMPONENT.

55 - IRON –26, (FILE 2)

(a) CONVERSION and AUGER ELECTRONS (5 groups)

Group	E (keV)	Fraction, f	f.E (keV)	Σf yield.	E_{AV} (keV)
Group 1					
Auger KLX	6.438	9.51E-3	0.06123	0.00951	6.438
Group 2					
Auger KLX	5.717	0.0327	0.1869	-	-
	5.835	0.0282	0.16455	-	-
	5.846	0.0515	0.3011	0.1124	5.806
Group 3					
Auger KL	4.956	0.027	0.1338		
	5.056	0.103	0.5208		
	5.094	0.024	0.1223		
	5.164	0.0295	0.15234		
	5.191	0.280	1.45348		
	5.211	0.0321	0.1673	0.4956	5.1453
Group 4					
Auger LM	0.73	0.0143	1.0439E-2		
	0.6124	0.233	0.1427		
	0.6481	0.0132	8.555E-3		
	0.6013	1.14	0.6855		
	0.637	0.0496	3.1595E-2	1.4501	0.606
Group 5					
Auger MXY	0.021	3.00	0.063	3.00	0.021

Mean number of primary electrons / decay = 5.0676

RADIONUCLIDES DECAYING BY ELECTRON CAPTURE.

55 - IRON – 26 (continued)

(b) CHARACTERISTIC X-RAY and GAMMA RAY DECAYS (2 groups)

Group	E (keV)	Fraction, f	f.E (keV)	Σf yield	E_{AV} (keV)	$N.\sigma_{el}$ cm^2/g
Group 1						
K_β X-rays	6.49	0.0222	0.14408			
	6.49	0.0113	0.07334	0.0335	6.49	18.78
Group 2						
K_α X-rays	5.899	0.166	0.9792			
	5.888	0.0836	0.4922	0.2496	5.8952	25.19

Number of photon induced primary electrons/decay: 0.2831
(Derive the fluence and range for the electron distribution. See program **xscel.for**).

Total number of electrons per decay = 5.06761 + 0.2831 = **5.3507**

RADIONUCLIDES DECAYING BY ELECTRON CAPTURE:

ELECTRON COMPONENT.

65 - ZINC - 30 (FILE 3)

(a) CONVERSION and AUGER ELECTRONS (5 groups)

Group	E (keV)	Fraction, f	f.E (keV)	Σf yield.	E_{AV} (keV)
Group 1					
Ce-K	1107.0	8.43E-5	9.332E-2		
	1114.0	8.17E-6	9.101E-3	9.247E-5	1107.6
Group 2					
Auger KLX	7.799	3.04E-2	0.2371		
	7.945	2.52E-2	0.2002		
	7.964	4.59E-2	0.3655		
	8.822	9.74E-3	8.593E-2	0.11124	7.9893
Group 3					
Auger KL	6.732	2.32E-2	0.1562		
	6.865	6.99E-2	0.4799		
	6.911	2.48E-2	0.1714		
	7.000	1.43E-2	0.1001		
	7.030	0.211	1.4833		
	7.055	2.72E-2	0.1919	0.3704	6.973
Group 4					
Auger LM	1.032	0.0142	1.465E-2		
	0.8863	0.179	0.1586		
	0.9494	1.4E-2	1.33E-2		
	0.8664	0.993	0.8603		
	0.9295	7.65E-2	7.11E-2	1.2767	0.8756
Group 5					
Auger MXY	0.03464	2.65	0.0918	2.65	3.46E-2

Mean number of primary electrons / decay = 4.4084

RADIONUCLIDES DECAYING BY ELECTRON CAPTURE.

65 – ZINC – 30

(b) CHARACTERISTIC X-RAY and GAMMA RAY DECAYS (3 groups)

Group	E (keV)	Fraction, f	f.E (keV)	Σf yield photons	E_{AV} (keV)	$N.\sigma_{el}$ cm^2/g
Group 1						
γ-Rays	1115.6	0.507	565.61	0.507	1115.6	6.686E-2
Group 2						
γ-ray,β+	511.0	2.83E-2	14.461	2.83E-2	511.0	9.58E-2
Group 3						
K_α X-rays	8.048	0.226	1.81885			
	8.028	0.115	0.9232	0.341	8.041	9.749

Number of photon events per decay: 0.8763
(Derive the fluence and range for the electron distribution. See program **xscel.for**).

Total number of electrons per decay = 4.4084 + 0.8763 = **5.2847**

RADIONUCLIDES DECAYING BY ELECTRON CAPTURE:

ELECTRON COMPONENT.

67 - GALLIUM - 31, (FILE 4)

(a) CONVERSION and AUGER ELECTRONS (10 groups)

Group	E (keV)	Fraction, f	f.E (keV)	Σf yield.	E_{AV} (keV)
Group 1					
Ce-K, g5	290.6	5.43E-4	0.1578	5.43E-4	290.6
Group 2					
Ce-K, g4	199.3	1.87E-4	3.7269E-2	1.87E-4	199.3
Group 3					
Ce-KL	174.9	3.28E-3	0.5737		
	183.4	3.15E-4	0.0578	3.595E-3	175.65
Group 4					
Ce-KM	83.65	0.278	23.255		
	92.12	0.0246	2.2662		
	92.27	3.85E-3	0.35524		
	92.29	5.62E-3	0.51867		
	93.22	5.0E-3	0.4661	0.3171	84.72
Group 5					
Ce-K, g1	81.61	2.07E-3	0.1689	2.07E-3	81.61
Group 6					
Auger KXY	9.47	0.013		0.013	9.47
Group 7					
Auger KLX	8.366	0.0393	0.32878		
	8.517	0.0329	0.28021		
	8.54	0.0592	0.50557	0.1314	8.48
Group 8					
Auger KLL	7.214	2.96E-2	0.21353		
	7.353	8.48E-2	0.62353		
	7.40	3.29E-2	0.24346		
	7.493	1.75E-2	0.13113		
	7.526	0.258	1.9417		
	7.554	4.03E-2	0.30443	0.4631	7.467
Group 9					
Auger LMX	0.956	0.623	0.59559		
	1.035	5.44E-2	0.0563		
	0.9329	0.892	0.83215		
	1.012	0.0869	0.08794	1.6563	0.9491
Group 10					
Auger MXY	0.04566	3.46	0.1580	3.46	0.04566

Mean number of primary electrons / decay = 6.0473

RADIONUCLIDES DECAYING BY ELECTRON CAPTURE.

67 – GALLIUM - 31

(b) CHARACTERISTIC X-RAY and GAMMA RAY DECAYS (11 groups)

Group	E (keV)	Fraction, f	f.E (keV)	Σf yield photons	E_{AV} (keV)	$N.\sigma_{el}$ cm^2/g
Group 1						
γ-rays g11	887.7	1.44E-3		1.44E-3	887.7	0.07478
Group 2						
γ-rays g9	794.4	5.09E-4		5.09E-4	794.4	0.07881
Group 3						
γ-rays g7	494.2	6.8E-4		6.8E-4	494.2	0.09715
Group 4						
γ-rays g6	393.5	4.64E-2		4.64E-2	393.5	0.1065
Group 5						
γ-rays g5	300.0	0.166		0.166	300.0	0.1180
Group 6						
γ-rays g4	209.0	2.33E-2		2.33E-2	209.0	0.1337
Group 7						
γ-rays g3	184.6	0.204		0.204	184.6	0.1391
Group 8						
γ-rays g2	93.31	0.370		0.370	93.31	0.1699
Group 9						
γ-rays g1	91.27	0.0296		0.0296	91.27	0.1708
Group 10						
K_β X-rays	9.572	0.0228	0.2182			
	9.572	0.0445	0.4260	0.0673	9.572	5.712
Group 11						
K_α X-rays	8.639	0.325	2.8077			
	8.616	0.166	1.4303	0.491	8.6312	7.837

Number of photon events per decay: 1.4002
(Derive the fluence and range for the electron distribution. See program **xscel.for**).

Total number of electrons per decay = 6.0473 + 1.4002 = **7.4475**

RADIONUCLIDES DECAYING BY ELECTRON CAPTURE:

ELECTRON COMPONENT.

75 - SELENIUM - 34, (FILE 5)

(a) CONVERSION and AUGER ELECTRONS (16 groups)

Group	E (keV)	Fraction, f	f.E (keV)	Σf yield.	E_{AV} (keV)
Group 1					
Ce-K; g 13	388.8	1.39E-4	0.0540	1.39E-4	388.8
Group 2					
Ce-KL; g11	292.1	6.31E-4	0.1843		
	302.4	6.03E-5	0.01823	6.913E-4	292.98
Group 3					
Ce-LK; g 9	252.8	3.77E-3	0.95306		
Ce-LM; g9	263.1	3.81E-4	0.10024		
	264.5	5.79E-5	0.01532		
	267.7	1.79E-3	0.47918		
	278.0	1.79E-4	0.049762	6.178E-3	258.6
Group 4					
Ce-K; g7	186.7	2.98E-4	0.05564	2.98E-4	186.7
Group 5					
Ce-KM; g6	135.9	2.48E-4	0.0337		
	134.5	1.47E-3	0.1977		
	124.1	1.55E-2	1.9236	1.722E-2	125.15
Group 6					
Ce-KL, g5	109.3	6.45E-3	0.7050		
	119.6	6.07E-4	7.26E-2	7.057E-3	110.18
Group 7					
Ce-KLM,g4	95.21	2.41E-3	0.2295		
	95.38	5.02E-4	4.7881E-2		
	95.41	7.13E-4	6.803E-2		
	96.59	5.56E-4	5.3704E-2	4.18E-3	95.48
Group 8					
Ce-K, g4	84.87	2.70E-2	2.2915	0.027	84.87
Group 9					
Ce-L, g2	64.53	3.55E-4	2.2908E-2	3.55E-4	64.53
Group 10					
Ce-K, g2	54.19	3.60E-3	0.1951	3.60E-3	54.19
Group 11					
Ce-LM, g1	23.07	7.62E-3	0.1758		
	23.24	1.29E-3	2.998E-2		
	23.28	2.82E-3	6.565E-2		
	24.46	1.88E-3	4.559E-2	0.01361	23.32

75 - SELENIUM - 34, (FILE 5) Continued.

(a) CONVERSION and AUGER ELECTRONS (16 groups)

Group	E (keV)	Fraction, f	f.E (keV)	Σf yield.	E_{AV} (keV)
Group 12					
Ce-K, g 1	12.73	5.32E-2	0.6772	5.32E-2	12.73
Group 13	**Continued**				
GROUPS (contd)	**E (keV)**	**Fraction, f**	**f.E (keV)**	**Σf yield.**	**E_{AV} (keV)**
Group 13					
Auger KL	8.749	0.0218	0.19073		
	8.908	0.0539	0.48014		
	8.964	0.0263	0.23575		
	9.063	0.0115	0.10422		
	9.107	0.166	1.5118		
	9.148	0.038	0.34762	0.3175	9.040
Group 14					
Auger, KL	10.18	0.0302	0.30744		
	10.35	0.0248	0.25668		
	10.39	0.0448	0.46547		
	11.57	0.0105	0.12149	0.1103	10.436
Group 15					
Auger LMZ	1.349	0.0382	0.05153		
	1.181	0.417	0.49428		
	1.317	0.066	0.08692		
	1.145	0.690	0.79005		
	1.282	0.108	0.13846	1.3192	1.182
Group 16					
Auger MXY	0.0908	2.70	0.2452	2.7	0.0908

Mean number of primary electrons / decay = 4.5805

RADIONUCLIDES DECAYING BY ELECTRON CAPTURE.

75 - SELENIUM - 34

(b) CHARACTERISTIC X-RAY and GAMMA RAY DECAYS (11 groups)

Group	E (keV)	Fraction, f	f.E (keV)	Σf yield photons	E_{AV} (keV)	$N.\sigma_{el}$ cm^2/g
Group 1						
g-13	400.7	0.116		0.116	400.7	0.1057
Group 2						
g-11	303.9	1.34E-2		1.34E-2	303.9	0.1174
Group 3						
g-10	279.5	0.252		0.252	279.5	0.1210
Group 4						
g-9	264.7	0.591		0.591	264.7	0.1234
Group 5						
g-7	198.6	1.47E-2		1.47E-2	198.6	0.1345
Group 6						
g 6	136.0	0.59		0.59	136.0	0.1550
Group 7						
g 5	121.1	0.173		0.173	121.1	0.1599
Group 8						
	96.73	3.48E-2		0.0348	96.73	0.1686
Group 9						
	66.06	1.14E-2		1.14E-2	66.06	0.1846
Group 10						
K_β X-rays	11.73	0.0472	0.5536	0.0472	11.73	3.087
Group 11						
K_α X-rays	10.54	0.321	3.3833			
	10.51	0.165	1.7342	0.486	10.53	4.273

Number of photon events per decay: 2.3295
(Derive the fluence and range for the electron distribution. See program **xscel.for**).

Total number of electrons per decay = 4.5805 + 2.3295 = **6.9100**

RADIONUCLIDES DECAYING BY ELECTRON CAPTURE:

ELECTRON COMPONENT.

77-BROMINE-35, (FILE 6)

(a) CONVERSION and AUGER ELECTRONS (8 groups)

Group	E (keV)	Fraction, f	f.E (keV)	Σf yield.	E_{Av} keV
Group 1					
Ce-Kg37	508.0	3.32E-4	0.1687	3.32E-4	508.0
Group 2					
Ce-KLa	226.3	2.27E-3	0.5137	-	-
"	237.3	2.30E-4	0.05458	-	-
	237.1	7.74E-4	0.18257	-	-
	269.0	1.47E-4	0.03954	-	-
	284.6	2.39E-4	0.06802	3.66E-3	234.5
Group 3					
Ce KLb	149.2	8.43E-3	1.2578	-	-
"	160.2	7.70E-4	0.1234	-	-
	160.4	3.15E-4	0.05053	-	-
	160.4	3.48E-4	0.05582	9.863E-3	150.86
Group 4					
Ce-Kg3	74.93	1.68E-3	0.12588	1.68E-3	74.93
Group 5					
Auger KLX	10.83	2.58E-2	0.2794	-	-
	11.00	2.13E-2	0.2343	-	-
	11.05	3.79E-2	0.4188		
	12.32	9.14E-3	0.1126	9.414E-2	11.11
Group 6					
Auger KLL	9.283	1.85E-2	0.17174	-	-
	9.452	4.38E-2	0.4140	-	-
	9.511	2.27E-2	0.2159	-	-
	9.616	9.4E-3	0.0904	-	-
	9.665	0.135	1.3048	-	-
	9.711	3.37E-2	0.3273	0.2631	9.59
Group 7					
Auger KLX	1.269	0.34	0.4315	-	-
	1.419	0.0706	0.10018	-	-
	1.228	0.580	0.71224	-	-
	1.379	0.124	0.1710	1.1146	1.269
Group 8					
Auger MXY	0.1056	2.29	0.2418	2.29	0.1056

Mean number of primary electrons / decay = 3.7774

RADIONUCLIDES DECAYING BY ELECTRON CAPTURE.

77-BROMINE-35

(b) CHARACTERISTIC X-RAY and GAMMA RAY DECAYS (17 groups)

Group	E (keV)	Fraction, f	f.E (keV)	Σf yield.	E_{AV} keV	$N.\sigma_{el}$ cm^2/g
Group 1						
γ-1 Rays	1005.0	9.56E-3	9.6078	9.56E-3	1005.0	7.042E-2
Group 2						
γ–2 Rays	817.8	2.15E-3	1.7583	2.15E-3	817.8	7.774E-2
Group 3						
γ–3 Rays	755.3	1.72E-3	1.299	1.72E-3	755.3	8.067E-2
Group 4						
γ–4 Rays	565.9	4.42E-3	2.5013	-	-	-
	567.9	8.89E-3	5.0316	-	-	-
	574.6	1.23E-2	7.0676	-	-	-
	578.9	3.06E-2	17.7143	-	-	-
	585.5	1.62E-2	9.4851	0.07238	577.51	9.094E-2
Group 5						
γ–5 Rays	520.7	0.232	120.80	0.232	520.7	9.505E-2
Group 6						
β^+; γ–6 Rays	511.0	1.48E-2	7.5628	1.48E-02	511.0	9.58E-2
Group 7						
γ-7 Rays	484.6	1.03E-2	4.9914	1.03E-2	484.6	9.794E-2
Group 8						
γ-8 Rays	439.5	1.62E-2	7.850	1.62E-2	439.5	0.1019
Group 9						
γ–9 Rays	385.0	8.65E-3	3.3302	8.65E-3	385.0	0.1074

77-BROMINE-35 Continued.

(b) CHARACTERISTIC X-RAY and GAMMA RAY DECAYS (17 groups)

Group	E (keV)	Fraction, f	f.E (keV)	Σf yield.	E_{AV} keV	$N.\sigma_{el}$ cm^2/g
Group 10						
γ-10 Rays	303.8	1.22E-2	3.7064	1.22E-2	303.8	0.1174
Group 11						
γ-11 Rays	297.2	4.30E-2	12.78	4.30E-2	297.2	0.1184
Group 12						
γ-12 Rays	281.6	2.37E-2	6.6739	2.37E-2	281.6	0.1207
Group 13						
γ-13 Rays	249.8	3.08E-2	7.6938	3.08E-2	249.8	0.1259
Group 14						
γ-14 Rays	239.0	0.239	57.121	0.239	239.0	0.1278
Group 15						
γ-15 Rays	200.4	1.25E-2	2.505	1.25E-2	200.4	0.1355
Group 16						
γ-16 Rays	161.8	1.14E-2	1.8445	1.14E-2	161.8	0.1465
Group 17						
$K_{\alpha 1}$ X-rays	11.22	0.301	3.3772	-	-	-
$K_{\alpha 2}$ X-rays	11.18	0.155	1.7329	0.456	11.206	3.547

Number of photon events per decay: 1.2312
(Derive the fluence and range for the electron distribution. See program **xscel.for**).

Total number of electrons per decay = 3.7774 + 1.2312 = **5.0086**

RADIONUCLIDES DECAYING BY ELECTRON CAPTURE:

ELECTRON COMPONENT.

99m - TECHNETIUM – 43, (FILE 7)

(a) CONVERSION and AUGER ELECTRONS (9 groups)

Group	E (keV)	Fraction, f	f.E (keV)	Σf yield.	E_{AV} (keV)
Group 1					
Ce-LMN	137.5	9.72E-3	1.3365		
g2,g3	137.7	6.32E-4	8.7026E-2		
	137.8	3.29E-4	4.5336E-2		
	140.1	1.94E-3	0.27179		
	140.5	3.74E-4	5.2547E-2		
	139.6	9.34E-4	0.13039		
	139.8	1.94E-4	2.712E-2		
	140.0	5.92E-4	8.288E-2		
	142.2	3.35E-4	4.7637E-2	1.505E-2	138.29
Group 2					
Ce-K, g3	121.6	5.53E-3	0.6725	5.53E-3	121.6
Group 3					
Ce-K, g2	119.5	8.84E-2	10.5638	8.84E-2	119.5
Group 4					
Auger KLX	17.55	1.80E-3	3.159E-2		
	17.80	1.42E-3	2.5276E-2		
	17.92	2.49E-3	4.4621E-2	5.71E-3	17.774
Group 5					
Auger KLL	14.87	1.23E-3	1.829E-2		
	15.12	2.14E-3	3.2357E-2		
	15.24	1.64E-3	2.4994E-2		
	15.47	6.44E-3	9.9627E-2		
	15.59	2.43E-3	3.7884E-2	1.388E-2	15.36
Group 6					
Auger LM	2.125	1.98E-2	4.2075E-2		
	2.538	8.37E-3	2.1243E-2		
	2.009	4.81E-2	9.6633E-2		
	2.442	2.07E-2	5.055E-2	9.697E-2	2.171
Group 7					
Ce-N, g1	2.173	7.58E-2	0.1647	7.58E-2	2.173
Group 8					
Ce-M, g1	1.748	0.916	1.6012	0.916	1.748
Group 9					
Auger MXY	0.4092	1.11	0.4542	1.11	0.4092

Mean number of primary electrons / decay = 2.3273

RADIONUCLIDES DECAYING BY ELECTRON CAPTURE.

99m - TECHNETIUM - 43

(b) CHARACTERISTIC X-RAY and GAMMA RAY DECAYS (3 groups)

Group	E (keV)	Fraction, f	f.E (keV)	Σf yield photons	E_{AV} (keV)	$N.\sigma_{el}$ cm^2/g
Group 1						
γ-Rays, g2	140.5	0.891		0.891	140.5	0.1535
Group 2						
K_β X-rays	20.62	6.82E-3		6.82E-3	20.62	0.6584
Group 3						
K_α X-rays	18.37	3.99E-2	0.7330			
	18.25	2.10E-2	0.3833	6.09E-2	18.33	0.8781

Number of photon events per decay: 0.9587
(Derive the fluence and range of the electron distribution. See program **xscel.for**).

Total number of electrons per decay = 2.3273 + 0.9587 = **3.2860**

RADIONUCLIDES DECAYING BY ELECTRON CAPTURE:

ELECTRON COMPONENT.

103 - PALLADIUM - 46 (FILE 8)

(a) CONVERSION and AUGER ELECTRONS (4 groups)

Group	E (keV)	Fraction, f	f.E (keV)	Σf yield.	E_{AV} (keV)
Group 1					
Auger	19.29	1.47E-2	0.2836		
KLX	19.55	1.17E-2	0.2287		
	19.69	2.01E-2	0.3958		
	22.2	5.8E-3	0.1288	0.0523	19.83
Group 2					
Auger KLL	16.3	1.02E-2	0.16626		
	16.56	1.68E-2	0.2782		
	16.71	1.35E-2	0.2256		
	16.81	3.68E-3	6.1861E-2		
	16.95	4.95E-2	0.8390		
	17.10	1.95E-2	0.33345	0.11318	16.83
Group 3					
Auger LMX	2.622	2.74E-2	7.184E-2		
	3.103	1.38E-2	4.282E-2		
	2.356	0.163	0.3840		
	2.838	6.99E-2	0.1984		
	3.142	8.81E-3	2.7681E-2		
	2.214	0.4271	0.9456		
	2.695	0.1860	0.5013		
	3.00	2.21E-2	6.63E-2	0.9181	2.4376
Group 4					
Auger MX	0.397	1.72	0.6828	1.72	0.397

Mean number of primary electrons / decay = 2.8036

RADIONUCLIDES DECAYING BY ELECTRON CAPTURE.

103 - PALLADIUM - 46

(b) CHARACTERISTIC X-RAY and GAMMA RAY DECAYS (5 groups)

Group	E (keV)	Fraction, f	f.E (keV)	Σf yield photons	E_{AV} (keV)	$N.\sigma_{el}$ cm^2/g
Group 1						
γ-Rays,g7	497.1	3.96E-4		3.96E-4	497.1	0.09691
Group 2						
γ-Rays,g9	357.4	2.21E-4		2.21E-4	357.4	0.1105
Group 3						
K_β X-rays	22.72	6.6E-2	1.4995			
	23.17	1.74E-2	0.4032			
	22.70	3.49E-2	0.7922	0.1183	22.78	0.5273
Group 4						
K_α X-rays	20.22	0.375	7.5825			
	20.07	0.198	3.9739	0.573	20.07	0.6937
Group 5						
$L_{\alpha\,\beta}$ Xrays	2.697	0.0201	0.0542			
	2.834	0.0125	0.0354	0.0326	2.7485	246.7 (?)

Number of photons per decay: 0.7245
(Derive the fluence and range for the electron distribution. See program **xscel.for**).

Total number of electrons per decay = 2.8036 + 07245 = **3.5281**

RADIONUCLIDES DECAYING BY ELECTRON CAPTURE:

ELECTRON COMPONENT.

111 - INDIUM - 49 (FILE 9)

(a) CONVERSION and AUGER ELECTRONS (9 groups)

Group	E (keV)	Fraction, f	f.E (keV)	Σf yield.	E_{AV} (keV)
Group 1					
Ce-LMN,g3	241.3	5.15E-3	1.2427		
	241.6	1.38E-3	0.3334		
	241.8	1.32E-3	0.3192		
	244.7	1.52E-3	0.3719		
	245.3	3.01E-4	7.383E-2	9.671E-3	242.06
Group 2					
Ce-K, g3	218.6	5.04E-2	11.017	5.04E-2	218.6
Group 3					
Ce-LMN,g2	167.3	9.62E-3	1.60943		
	167.6	6.55E-4	0.10978		
	167.7	2.90E-4	4.863E-2		
	170.7	2.03E-3	0.3465		
	171.3	4.22E-4	7.229E-2	0.01302	170.2
Group 4					
Ce-K, g2	144.6	8.41E-2	12.1609	8.41E-2	144.6
Group 5					
Auger L	25.44	5.86E-3	0.1491	5.86E-3	25.44
Group 6					
Auger KLX	22.04	1.46E-2	0.3218		
	22.33	1.13E-2	0.2523		
	22.52	1.96E-2	0.4414	0.0455	22.32

111 - INDIUM - 49 (FILE 9) Continued.

(a) CONVERSION and AUGER ELECTRONS (9 groups)

Group	E (keV)	Fraction, f	f.E (keV)	Σf yield.	E_{AV} (keV)
Group 7					
Auger KLL	18.57	1.01E-2	0.1876		
	18.86	1.57E-2	0.2961		
	19.05	1.34E-2	0.2553		
	19.12	3.39E-3	0.0648		
	19.32	4.48E-2	0.8655		
	19.52	1.85E-2	0.3611	0.1059	19.173
Group 8					
Auger LMX	3.003	2.52E-2	7.568E-2		
	3.598	1.31E-2	0.1228		
	2.712	0.178	0.4827		
	3.307	7.94E-2	0.2625		
	3.701	1.03E-2	3.812E-2		
	2.522	0.471	1.4686		
	3.118	0.214	0.6673		
	3.512	2.68E-2	9.412E-2	1.0178	2.8057
Group 9	**continued**				
Auger MXY	0.5104	1.91	0.9749	1.91	0.5104

Mean number of primary electrons / decay = 3.2423

RADIONUCLIDES DECAYING BY ELECTRON CAPTURE.

111 - INDIUM - 49

(b) CHARACTERISTIC X-RAY and GAMMA RAY DECAYS (4 groups)

Group	E (keV)	Fraction, f	f.E (keV)	Σf yield photons	E_{AV} (keV)	$N.\sigma_{el}$ cm^2/g
Group 1						
γ-Rays, g3	245.3	0.94	233.82	0.94	245.3	0.1267
Group 2						
γ-Rays, g2	171.3	0.902	154.5	0.902	171.3	0.1434
Group 3						
K_β X-rays	26.09	8.08E-2	2.1081			
	26.64	2.35E-2	0.6260			
	26.06	4.15E-2	1.0815	0.1458	26.17	0.4023
Group 4						
K_α X-rays	23.17	0.444	10.287			
	22.98	0.236	5.4232	0.68	23.10	0.5119

Number of photons per decay: 2.6678
(Derive the fluence and range for the electron distribution. See program **xscel.for**).

Total number of electrons per decay = 3.2423 + 2.6678 = **5.9101**

RADIONUCLIDES DECAYING BY ELECTRON CAPTURE:

ELECTRON COMPONENT.

114m - INDIUM - 49, (FILE 10)

(a) CONVERSION and AUGER ELECTRONS (5 groups)

Group	E (keV)	Fraction, f	f.E (keV)	Σf yield.	E_{AV} (keV)
Group 1					
Ce-K	162.3	0.398	64.595	0.398	162.3
Group 2					
Ce-KL	186.0	3.67E-2	6.8262		
	186.3	0.156	29.0628		
	186.5	0.124	23.126		
	189.6	6.63E-2	12.5705		
	190.3	1.34E-2	2.5500	0.3964	187.0
Group 3					
Auger K	20.14	1.67E-2	0.3363		
	23.51	7.48E-3	0.1759	2.418E-2	21.18
Group 4					
Auger L	2.835	0.150	0.4253		
	3.471	6.85E-2	0.2378		
	2.627	0.270	0.7093		
	3.263	0.126	0.4111	0.6145	2.9024
Group 5					
Auger MXY	0.5509	1.23	0.6676	1.23	0.5509

Mean number of primary electrons / decay = 2.6631

RADIONUCLIDES DECAYING BY ELECTRON CAPTURE.

114m – INDIUM - 49

(b) CHARACTERISTIC X-RAY and GAMMA RAY DECAYS (5 groups)

Group	E (keV)	Fraction, f	f.E (keV)	Σf yield photons	E_{AV} (keV)	$N.\sigma_{el}$ cm^2/g
Group 1						
γ-Rays,g2	725.2	4.33E-2	31.40	4.33E-2	725.2	8.219E-2
Group 2						
γ-Rays,g1	558.4	4.39E-2	24.51	4.39E-2	558.4	9.22E-2
Group 3						
γRays,g11	190.3	0.154	29.306	0.154	190,3	0.1372
Group						
K_α-X-rays	27.28	3.32E-2	0.9057			
	27.86	9.8E-3	0.2730			
	27.24	1.71E-2	0.4658	0.0601	27.36	0.3725
Group 5						
K_α-X-rays	24.21	0.181	4.3820			
	24.00	9.67E-2	2.3208	0.2777	24.137	0.4683

Number of photons per decay: 0.579
(Derive the fluence and range for the electron distribution. See program **xscel.for**).

Total number of electrons per decay = 2.6631 + 0.579 = **3.2421**

RADIONUCLIDES DECAYING BY ELECTRON CAPTURE:

ELECTRON COMPONENT.

123 – IODINE - 53, (FILE 11)

(a) CONVERSION and AUGER ELECTRONS (7 groups)

Group	E (keV)	Fraction, f	f.E (keV)	Σf yield.	E_{Av} (keV)
Group 1					
Ce-K	497.1	9.97E-5	4.956E-2	9.97E-5	497.1
Group 2					
Ce-LMN	154.0	1.61E-2	2.4794		
g 2	154.4	1.17E-3	0.1806		
	154.6	4.2E-4	6.4932E-2		
	158.2	3.52E-3	0.5569	2.121E-2	154.49
Group 3					
Ce-K g2	127.2	0.136	17.299	0.136	127.2
Group 4					
Auger KLX	26.01	1.19E-2	0.3095		
	26.34	9.3E-3	0.2450		
	26.61	1.57E-2	0.4178		
	30.13	4.93E-3	0.1485	4.183E-2	26.79
Group 5					
Auger, KL	21.81	8.47E-3	0.1847		
	22.15	1.24E-2	0.27466		
	22.41	1.10E-2	0.24651		
	22.44	2.57E-3	0.05767		
	22.72	3.3E-2	0.7498		
	23.00	0.142	3.266	0.20944	22.82
Group 6					
Auger LM	3.553	5.05E-2	0.17943		
	4.317	3.02E-2	0.1304		
	3.226	0.168	0.5420		
	3.990	8.19E-2	0.32678		
	4.523	1.16E-2	5.247E-2		
	2.955	0.388	1.14654		
	3.720	0.199	0.74028		
	4.252	2.83E-2	0.12033	0.9575	3.382
Group 7					
Auger MXY	0.6991	1.8	1.2584	1.8	0.6991

Mean number of primary electrons / decay = 3.1661

RADIONUCLIDES DECAYING BY ELECTRON CAPTURE.

123 - IODINE - 53

(b) CHARACTERISTIC X-RAY and GAMMA RAY DECAYS (14 groups)

Group	E (keV)	Fraction, f	f.E (keV)	Σf yield photons	E_{AV} (keV)	$N.\sigma_{el}$ cm^2/g
Group 1						
γ-Rays, g1	783.6	5.94E-4	0.4655	5.94E-4	783.6	7.931E-2
Group 2						
γ-Rays	735.8	6.16E-4	0.4533	6.16E-4	735.8	8.165E-2
Group 3						
K_α X-rays	687.9	2.67E-4	0.1837	2.67E-4	687.9	8.418E-2
Group 4						
γ-Rays	624.6	8.33E-4	0.5203	8.33E-4	624.6	8.788E-2
Group 5						
γ-Rays	538.5	3.82E-3	2.0571	3.82E-3	538.5	9.371E-2
Group 6						
γ-Rays	529.0	1.39E-2	7.3531	1.39E-2	529.0	9.441E-2
Group 7						
γ-Rays	505.3	3.16E-3	1.5967	3.16E-3	505.3	9.625E-2
Group 8						
γ-Rays	440.0	4.28E-3	1.8832	4.28E-3	440.0	0.1019
Group 9						
γ-Rays	346.4	1.26E-3	0.4365	1.26E-3	346.4	0.1119
Group 10						
γ-Rays	281.0	7.91E-4	0.1962	7.91E-4	281.0	0.1208
Group 11						
γ-Rays	248.0	7.11E-4	0.1763	7.11E-4	248.0	0.1262
Group 12						
g2	159.0	0.833	132.44	0.833	159.0	0.1474
Group 13						
K_β X-rays	31.0	8.68E-2	2.6908			
	31.71	2.66E-2	0.9233			
	30.94	4.46E-2	1.3799	0.158	31.61	0.3073
Group 14						
K_α X-rays	27.47	0.459	12.608			
	27.20	0.247	6.7184	0.706	27.37	0.3726

Number of photon events per decay: 1.7273
(Derive the fluence and range of the electron distribution. See program **xscel.for**).

Total number of electrons per decay = 3.1661 + 1.7273 = **4.8934**

RADIONUCLIDES DECAYING BY ELECTRON CAPTURE:

ELECTRON COMPONENT.

125 - IODINE – 53, (FILE 12)

(a) CONVERSION and AUGER ELECTRONS (5 groups)

Group	E (keV)	Fraction, f	f.E (keV)	Σf yield.	E_{AV} (keV)
Group 1					
Ce- LMN	30.55	9.49E-2	2.8992	-	-
	30.88	8.61E-3	0.2659	-	-
	31.15	3.32E-3	0.1034	-	-
	34.67	2.13E-2	0.7385	-	-
	35.49	5.05E-3	0.1792	0.1332	31.43
Group 2					
Auger KX	26.01	1.92E-2	0.4994		
	26.34	1.50E-2	0.3951		
	26.61	2.54E-2	0.6757		
	30.13	7.94E-3	0.2392	0.06754	26.79
Group 3					
Auger KL	23.0	2.28E-2	0.5244	-	-
	22.72	5.31E-2	1.2054	-	-
	22.44	4.14E-2	0.9290	-	-
	22.41	1.78E-2	0.3989	-	-
	22.15	2.00E-2	0.443	-	-
	21.81	1.37E-2	0.2988	0.1688	22.51
Group 4					
Ce-K	3.678	0.8	2.9424	0.8	3.678
Group 5					
Auger MXY	0.6988	2.99	2.0894	2.99	0.6988

Mean number of primary electrons / decay = 4.1595

RADIONUCLIDES DECAYING BY ELECTRON CAPTURE.

125 - IODINE - 53

(b) CHARACTERISTIC X-RAY and GAMMA RAY DECAYS (5 groups)

Group	E (keV)	Fraction, f	f.E (keV)	Σf yield photons	E_{AV} (keV)	$N.\sigma_{el}$ cm^2/g
Group 1						
γ-Rays	35.49	0.0665	2.3601	0.0665	35.49	0.2627
Group 2						
K_β X-rays	31.00	0.140	4.34	-	-	
	31.71	0.0429	1.3604	-	-	
	30.94	0.0719	2.2246	-	-	
	31.24	0.00144	0.04499	0.25724	30.98	0.3089
Group 3						
K_α X-rays	27.47	0.739	20.30	-	-	
	27.20	0.397	19.80	1.136	27.377	0.3722
Group 4						
L_β X-rays	4.029	0.0358	0.1442	-	-	
	4.302	0.00994	0.0428	0.04574	4.0883	0.7619
Group 5						
L_α X-rays	3.769	0.0552	0.2080	0.0552	3.769	97.13

Number of photon events per decay: 1.5607
(Derive the fluence and range for the electron distribution. See program **xscel.for**).

Total number of electrons per decay = 4.1595 + 1.5607 = **5.7202**

RADIONUCLIDES DECAYING BY ELECTRON CAPTURE:

ELECTRON COMPONENT.

131 – IODINE - 53, (FILE 13)

(a) CONVERSION and AUGER ELECTRONS (4 groups)
(Beta spectra excluded)

Group	E (keV)	Fraction, f	f.E (keV)	Σf yield.	E_{AV} (keV)
Group 1					
Ce-KL g14	329.9	1.55E-2	5.1134		
	359.0	1.71E-3	0.6139	1.721E-2	332.8
Group 2					
Ce-K g7	249.7	2.48E-3	0.6193	2.48E-3	249.7
Group 3					
Ce-L g1	74.73	4.3E-3	0.3213	4.3E-3	74.73
Group 4					
Ce-K g1	45.62	3.63E-2	1.6560	3.63E-2	45.62

Mean number of primary electrons / decay = 0.06029. Beta decay (89.4%) excluded.

RADIONUCLIDES DECAYING BY ELECTRON CAPTURE.

131 - *IODINE* - 53

(b) CHARACTERISTIC X-RAY and GAMMA RAY DECAYS (10 groups)

Group	E (keV)	Fraction, f	f.E (keV)	Σf yield photons	E_{AV} (keV)	$N.\sigma_{el}$ cm^2/g
Group 1						
γ-Rays	722.9	1.8E-2	13.0122	1.8E-2	722.9	8.231E-2
Group 2						
	642.7	2.2E-3	1.4139	2.2E-3	642.7	8.678E-2
Group3						
	637.0	7.27E-2	46.3099	7.27E-2	637.0	8.712E-2
Group 4						
	503.0	3.61E-3	1.8158	3.61E-3	503.0	9.643E-2
Group 5						
	364.5	0.812	297.78	0.812	364.5	0.1097
Group 6						
	325.8	2.51E-3	0.8178	2.51E-3	325.8	0.1145
Group 7						
	284.3	6.06E-2	17.2286	6.06E-2	284.3	0.1203
Group 8						
	177.2	2.65E-3	0.4696	2.65E-3	177.2	0.1415
Group 9						
	80.18	2.62E-2	2.1007	2.62E-2	80.18	0.1758
Group 10						
K_α X-rays	29.78	2.59E-2	0.7713			
	29.46	1.40E-2	0.4124	3.99E-2	29.67	0.3281

Number of photons per decay: 1.0404
(Derive the fluence and range of the electron distribution. See program **xscel.for**).

Total number of electrons per decay = 0.06029 + 1.0404 = **1.10069**

RADIONUCLIDES DECAYING BY ELECTRON CAPTURE:

ELECTRON COMPONENT.

195m - PLATINUM – 78, (FILE 14)

(a) CONVERSION and AUGER ELECTRONS (16 groups)

Group	E (keV)	Fraction, f	f.E (keV)	Σf yield.	E_{AV} (keV)
Group 1					
Ce-MN,g6	127.1	6.98E-3	0.8872	-	-
"	129.8	2.14E-3	0.27778	9.12E-3	127.74
Group 2					
Ce-Mn, g5	126.9	0.192	24.3648	-	-
	129.5	6.47E-2	8.3787	0.2567	127.56
Group 3					
Ce-L, g6	115.9	1.62E-3	0.1878	-	-
	116.5	1.44E-2	1.6776	-	-
"	118.2	1.11E-2	1.3120	2.712E-2	117.19
Group 4					
Ce-L. g5	115.6	0.174	20.114	-	-
	116.2	0.0389	4.5202	-	-
	117.9	0.397	46.806	0.6099	117.13
Group 5					
Ce-MN	96.25	2.69E-2	2.5891	-	-
	98.90	8.52E-3	0.84263	3.542E-2	96.89
Group 6					
Ce-L; g4	85.0	9.9E-2	8.415	-	-
	85.63	1.31E-2	1.1218	-	-
	87.34	3.77E-3	0.3293	0.11587	85.15
Group 7					
Auger KLX	62.88	0.0101	0.6351	0.0101	62.88
Group 8					
Auger KLL	52.36	0.0183	0.9581	0.0183	52.36
Group 9					
Ce-K, g 6	51.40	0.0134	0.6888	0.0134	51.4
Group 10					
Ce-K, g5	51.11	0.135	6.900	0.135	51.11

195m - PLATINUM – 78, (FILE 14) Continued.

(a) CONVERSION and AUGER ELECTRONS (16 groups)

Group	E (keV)	Fraction, f	f.E (keV)	Σf yield.	E_{AV} (keV)
Group 11					
Ce-MN, g3	28.24	0.159	4.4902	-	-
	30.89	0.055	1.6990	0.214	28.92
Group 12					
Ce-K, g4	20.51	0.66	13.5366	0.66	20.51
Group 13					
Ce-L_3, g3	19.33	0.0116	0.22423	0.0116	19.33
Group 14					
Ce-L; g3	17.01	0.611	10.488	-	-
	17.62	0.0654	1.1523	0.6764	17.325
Group 15					
AugerLMM	7.396	0.809	5.9834	-	-
Auger LMX	9.715	0.521	5.0615	-	-
"	11.52	0.0863	0.9942	1.4163	8.5
Group 16					
Auger MXY	2.417	3.22	7.7827	3.22	2.417

Mean number of primary electrons / decay = 6.8659

195m - ELEMENT - 78

(b) CHARACTERISTIC X-RAY and GAMMA RAY DECAYS (8 groups)

Group	E (keV)	Fraction, f	f.E (keV)	Σf yield	E_{AV} (keV)	$N.\sigma_{el}$ cm^2/g
Group 1						
γ-Ray 3	308.9	0.0229	7.0738	0.0229	308.9	0.1167
Group 2						
γ-Ray 9	239.5	5.42E-4	0.1298	5.42E-4	239.5	0.1277
Group 3						
γ-Ray 8	211.3	3.88E-4	0.0820	3.88E-4	211.3	0.1332
Group 4						
γ-Ray 5	129.5	8.49E-4	0.10995	-	-	-
γ-Ray 6	129.8	0.0283	3.6733	0.02915	129.8	0.1570
Group 5						
γ-Ray 4	98.9	0.114	11.2746	0.114	98.9	0.1678
Group 6						
K_β X-rays	75.7	8.7E-2	6.5859	-	-	-
	77.92	3.5E-2	2.7272	-	-	-
	75.37	4.54E-2	3.4218	-	-	-
	76.24	2.25E-3	0.17154	0.16965	76.08	0.1779
Group 7						
K_α X-rays	66.83	0.385	25.729	-	-	-
	65.12	0.224	14.586	0.609	66.20	0.1844
Group 8						
L-X-rays	9.434	0.318	3.0000	-	-	-
	11.12	0.294	3.26928	-	-	-
	13.13	0.0557	0.73134	-	-	-
	8.268	0.0120	9.9216E-2	0.6797	10.446	4.383

Number of photons per /decay: 0.3274
(Derive the fluence and range for the electron distribution. See program **xscel.for**).

Total number of electrons per decay = 6.8659 + 0.3274 = **7.1933**

RADIONUCLIDES DECAYING BY ELECTRON CAPTURE:

ELECTRON COMPONENT.

201 – THALLIUM - 81, (FILE 15)

(a) CONVERSION and AUGER ELECTRONS (17 groups)

Group	E (kcV)	Fraction, f	f.E (keV)	Σf yield.	E_{AV} (keV)
Group 1					
Ce-KLM	152.6	2.35E-2	3.5861		
g8	153.2	2.48E-3	0.37994		
	164.6	6.1E-3	1.0041		
	167.4	1.96E-3	0.3281	3.404E-2	155.64
Group 2					
Ce-MN, g6	132.5	2.97E-3	0.39353		
	135.3	9.58E-4	0.12962	3.928E-3	133.18
Group 3					
Ce-L g6	120.5	1.14E-2	1.3737		
	121.1	1.20E-3	0.14532	0.0126	120.56
Group 4					
Auger KXY	77.33	1.80E-3	0.1392	1.80E-3	77.33
Group 5					
Auger KLX	66.59	1.121E-2	0.7577	1.121E-2	66.59
Group 6					
Ce-K, g7,8	82.78	2.26E-3	0.1871		
	84.33	0.154	12.97	0.15626	84.20
Group 7					
Auger KLL	53.14	3.28E-3	0.1743		
	53.81	5.15E-3	0.2771		
	55.71	2.90E-3	0.1616		
	56.33	5.69E-3	0.3205		
	58.27	2.52E-3	0.1468	1.954E-2	55.29
Group 8					
Ce-K g6	52.24	7.47E-2	3.9023	7.47E-2	52.24
Ce-L g4	15.76	0.073	1.1505		
	16.39	7.55E-3	0.1237	0.08055	15.82

201 – THALLIUM – 81 Continued.

(a) CONVERSION and AUGER ELECTRONS (17 groups)

Group	E (keV)	Fraction, f	f.E (keV)	Σf yield.	E_{AV} (keV)
Group 9					
Ce-MN g5	29.3	1.63E-2	0.4776		
	32.2	5.74E-3	0.1848	0.02204	30.054
Group 10					
Ce-MN,g4	27.75	1.90E-2	0.5273		
	30.6	6.78E-3	0.2075	0.02578	28.50
Group 11					
Ce-L, g5	17.35	6.28E-2	1.0896		
	17.98	6.53E-3	0.1174	0.06933	17.409
Group 12					
Ce-L g4	15.76	0.073	1.1505		
	16.39	7.55E-3	0.1237	0.08055	15.82
Group 13					
Auger LXY	11.52	3.23E-2	0.3721	3.23E–2	11.52
Group 14					
Auger LM	9.679	0.0217	0.2100		
	12.14	0.0155	0.1882		
	9.049	0.112	1.0135		
	11.51	0.0709	0.8161		
	13.44	0.0114	0.1532		
	9.582	0.192	1.8397	0.4235	9.97
Group 15					
AugerLMM	7.124	0.297	2.1158	0.297	7.124
Group 16					
Auger MXY	2.673	1.74	4.1290	1.74	2.673
Group 17					
Ce-N, g2	1.57	0.610	0.9577	0.610	1.57

Mean number of primary electrons / decay = 3.6146

RADIONUCLIDES DECAYING BY ELECTRON CAPTURE.

201 - THALLIUM - 81

(b) CHARACTERISTIC X-RAY and GAMMA RAY DECAYS (5 groups)

Group	E (keV)	Fraction, f	f.E (keV)	Σf yield photons	E_{AV} (keV)	$N.\sigma_{el}$ cm^2/g
Group 1						
g7	165.9	1.6E-3	0.2654			
g8	167.4	0.100	13.74	0.1016	167.38	0.1447
Group 2						
γ-Rays, g6	135.3	2.65E-2	3.6871	2.65E-2	135.3	0.1552
Group 3						
K_β X-rays	80.26	0.105	8.6314			
	82.58	4.43E-2	3.6583			
	79.82	5.48E-2	4.3741	0.2041	80.645	0.1755
Group 4						
K_α X-rays	70.82	0.462	32.7188			
	68.89	0.272	18.73808	0.734	70.105	0.1816
Group 5						
L X-rays	9.989	0.171	1.7081			
	11.820	0.105	1.2411			
	11.920	4.19E-2	0.4994			
	13.83	2.15E-2	0.2973	0.3394	11.037	3.707

Number of photons per decay: 1.4056. (Derive the fluence and range for the electron distribution. See program **xscel.for**).

Total number of electrons per decay = 3.6146 + 1.4056 = **5.0202**

RADIONUCLIDES DECAYING BY ELECTRON CAPTURE:

ELECTRON COMPONENT.

203 – LEAD – 82, (FILE 16)

(a) CONVERSION and AUGER ELECTRONS (7 groups)

Group	E (keV)	Fraction, f	f.E (keV)	Σf yield.	E_{AV} (keV)
Group 1					
Ce-KLM g2	315.8	5.28E-3	1.6674		
	386.0	8.05E-4	0.31034		
	398.4	2.07E-4	0.08247	6.292E-3	327.43
Group 2					
Ce-LMN	263.9	2.04E-2	5.3836		
	264.5	1.09E-2	2.88305		
	266.5	4.91E-3	1.3085		
	276.2	8.85E-3	2.44437		
	279.2	2.82E-3	0.78734	4.788E-2	267.48
Group 3					
Ce-K g1	193.7	0.136	26.3432	0.136	193.7
Group 4					
Auger KLX	67.14	3.54E-3	0.23768		
KXY	67.79	2.59E-3	0.17558		
	69.83	4.07E-3	0.28421		
	79.53	1.65E-3	0.13122	1.185E-2	69.93
Group 5					
Auger KLL	54.54	3.02E-3	0.16471		
	55.23	4.79E-3	0.26455		
	57.24	2.60E-3	0.148824		
	57.89	5.09E-3	0.29466		
	59.94	2.25E-3	0.134865	1.775E-2	56.767
Group 6					
Auger LMX	9.98	1.14E-2	0.113772		
LMM	12.52	8.18E-3	0.2162		
LXY	9.33	9.11E-2	0.850		
	11.87	5.81E-2	0.6896		
	13.88	9.39E-3	0.1303		
	7.29	0.236	1.7204		
	9.83	0.153	1.504		
	11.84	2.60E-2	0.3078	0.59317	9.33
Group 7					
Auger MXY	2.803	1.39	3.8962	1.39	2.803

Mean number of primary electrons / decay = 2.2029

RADIONUCLIDES DECAYING BY ELECTRON CAPTURE.

203 – LEAD – 82

(b) CHARACTERISTIC X-RAY and GAMMA RAY DECAYS (7 groups)

Group	E (keV)	Fraction, f	f.E (keV)	Σf yield photons	E_{AV} (keV)	$N.\sigma_{el}$ cm^2/g
Group 1						
γ-Rays, g3	680.5	7.03E-3	4.7839	7.03E-3	680.5	8.459E-2
Group 2						
g2	401.3	3.47E-2	13.9251	3.47E-2	401.3	0.1057
Group 3						
g1	279.2	0.808	225.594	0.808	279.2	0.1211
Group 4						
K_β X-rays	82.57	9.85E-2	8.1331			
	84.97	4.28E-2	3.6367			
	82.11	5.13E-2	4.2122	0.1926	82.98	0.1744
Group 5						
K_α X-rays	72.87	0.432	31.4798			
	70.83	0.255	18.06165	0.687	72.113	0.1803
Group 6						
L_β X-rays	12.21	9.6E-2	1.17216			
	12.27	3.52E-2	0.431904	0.1312	12.23	2.729
Group 7						
L_α X-rays	10.27	0.143	1.4686	0.143	10.27	4.610

Number of photons per decay: 2.00353
(Derive the fluence and range for the electron distribution. See program **xscel.for**).

Total number of electrons per decay = 2.2029 + 2.00353 = **4.20643**

Summary of the number of electrons produced by the Auger electron emitting radionuclides per decay.

Nuclide	Number of electrons per decay
Cr-51	5.7237
Fe-55	5.3507
Zn-65	5.2847
Ga-67	7.4475
Se-75	6.9100
Br-77	5.0086
Tc-99m	3.2860
Pd-103	3.5281
In-111	5.9101
In-114m	3.2421
I-123	4.8934
I-125	4.4869
I-131	1.10069
Pt-195m	8.4917
Tl-201	5.0202
Pb-203	4.20643